TECH LIBRARY KAFB, NM
0060831

NASA CONTRACTOR REPORT

NASA CR-15

NASA CR-1542

LOAN COPY: RETURN TO
AFWL (WLOL)
KIRTLAND AFB, N MEX

RESPONSE AND OPTIMIZATION OF AN ISOLATION SYSTEM WITH RELAXATION TYPE DAMPING

by Thomas F. Derby and Peter C. Calcaterra

Prepared by
BARRY WRIGHT CORPORATION
Watertown, Mass.
for Langley Research Center

NATIONAL AERONAUTICS AND SPACE ADMINISTRATION • WASHINGTON, D. C. • MAY 1970

call no.
NASA CR-1542
TECH LIBRARY KAFB, NM
0060831

RESPONSE AND OPTIMIZATION OF AN ISOLATION SYSTEM WITH RELAXATION TYPE DAMPING

By Thomas F. Derby and Peter C. Calcaterra

may 70

Prepared under Contract No. NAS 1-8465 by
omit
m.e. BARRY CONTROLS
~~Division of Barry Wright Corporation~~
Watertown, Mass.

for Langley Research Center

NATIONAL AERONAUTICS AND SPACE ADMINISTRATION

For sale by the Clearinghouse for Federal Scientific and Technical Information
Springfield, Virginia 22151 – CFSTI price $3.00

CONTENTS

	Page
SUMMARY	1
INTRODUCTION	2
DEFINITIONS OF SYMBOLS	3
EQUATIONS OF MOTION	5
FREE VIBRATION	7
IMPULSE RESPONSE	9
Optimization of Parameters	12
Design Example	14
RANDOM VIBRATION RESPONSE	16
Optimization of Parameters	18
Design Example	19
RESPONSE TO VARIOUS PULSE SHAPES	21
Half-Cycle Sine Pulse	24
Rectangular Pulse	26
Versed-Sine Pulse	28
Terminal-Peak Saw-Tooth Pulse	31
Symmetrical Triangular Pulse	33
Initial-Peak Saw-Tooth Pulse	36
Graphical Presentation of Results	38
Numerical Procedures	39
Comparison to Impulse Response	41
RESULTS AND CONCLUSIONS	43
REFERENCES	47
FIGURES	49

RESPONSE AND OPTIMIZATION OF AN ISOLATION SYSTEM WITH RELAXATION TYPE DAMPING

by

Thomas F. Derby and Peter C. Calcaterra

Barry Controls
Division of Barry Wright Corporation
Watertown, Massachusetts

SUMMARY

The scope of the investigation reported herein deals with the effect of damping on the free vibration, impulse, random vibration, and shock pulse response of mechanical isolation systems which incorporate elastically coupled damping elements. The response quantities considered are the acceleration of the mass and the deflection of the isolator, with the acceleration of the base as the input.

The nature of the free vibration is investigated first by considering the roots of the characteristic equation. The regions in which the system is underdamped, critically damped, and overdamped are established as functions of dimensionless combinations of the system parameters.

The impulse response is considered next. The excitation in this case is an acceleration of the base equivalent to an impulse of area V (i.e., a velocity step of magnitude V). Computer solutions are obtained for the peak values of the acceleration and displacement. The results are presented graphically in dimensionless form as functions of dimensionless parameters of the system. The parameters for this system are optimized according to a shock isolator optimization criteria which states: "For a given input and maximum deflection of the isolator, find the isolator parameters that will minimize the peak acceleration of the isolated mass." Trade-off limit curves (i.e., a plot of the minimum acceleration expressed in g's versus a dimensionless parameter containing the deflection of the isolator and the level of the input) are also presented and compared to the best possible trade-off limit curve independent of the isolator configuration.

The response to random vibration is then investigated. The random excitation is taken to be white noise acceleration of the base. The response quantities are the RMS values of the acceleration of the mass and the deflection of the isolator. Results are presented graphically, and the system is optimized in much the same manner as for the impulse response.

Finally, the responses to various shock pulses are presented and compared to the impulse responses.

INTRODUCTION

A recent study of the vibration transmission and resonance characteristics of vibration isolation systems [Ref. 1] has shown that the mathematical models employing directly coupled damping elements most frequently used by vibration engineers provide a poor representation of many of the dynamic response characteristics of mechanical systems as observed in practice. Mathematical models employing elastically coupled damping elements (also referred to as relaxation type damping) were shown to provide a substantially improved representation.

A literature search was conducted to find material on the response of an isolation system using relaxation type damping to random vibration and shock excitation. Reference 2 is one of the first papers about this system. It gives the equation of motion but does not give any responses to specific inputs. Reference 3 is a more detailed mathematical description of this system and gives the impulse response for various values of the parameters. Reference 4 uses this system to model an isolation system using an elastomer as the resilient element and concludes that this system is a better model than the standard model which uses a spring and damper in parallel. Reference 5 presents some optimum values of damping for this system and also presents some time history responses to two types of shock input. Reference 6 compares the response of the relaxation system to the standard isolation system (i.e., spring and damper in parallel) for two particular shock inputs.

This report presents analyses and graphical results for free vibration, impulse response, response to random vibration, and response to various pulse shapes for an isolation system using relaxation type damping. Optimum values of the system parameters are defined for each case. Recommendations are made for selecting values of parameters other than those optimized according to the chosen performance criteria.

DEFINITION OF SYMBOLS

There are no dimensions given in the definitions since the quantities are always used as dimensionless ratios. Quantities that are defined in the text and used only immediately afterward are not defined here.

a	=	absolute displacement of the foundation (Figure 1)
$\ddot{a}_o$	=	maximum acceleration of the foundation
c , c'	=	viscous damping coefficients (Figure 1)
F	=	force transmitted to the foundation or magnitude of a constant force device
f	=	frequency
f_o	=	$\omega_o/2\pi$ = undamped natural frequency
f_e	=	expected frequency
g	=	acceleration of gravity
k , k'	=	spring constants (Figure 1)
$\mathcal{L}$	=	Laplace transform operator
m	=	mass (Figure 1)
N	=	stiffness ratio (Figure 1)
P	=	force applied to mass (Figure 1)
s	=	Laplace transform variable
T	=	$1/f_o = 2\pi/\omega_o$ = undamped natural period
t	=	time
t_1	=	time duration of pulse
V	=	magnitude of velocity step (area of acceleration impulse)
W_o	=	magnitude of acceleration spectral density

x	=	absolute displacement of mass (Figure 1)
$\ddot{x}_o$	=	maximum acceleration of the mass
y	=	s/ω_o = nondimensional Laplace transform variable
α, β, γ	=	real roots or real and imaginary parts of complex roots (Equations 9 and 13)
δ	=	$x - a$ = deflection of the isolator
δ_o	=	maximum deflection of the isolator
ζ	=	$c/2\sqrt{km}$ = viscous damping ratio
ζ_m	=	optimum damping ratio to minimize either mass acceleration or isolation deflection
ζ_{op}	=	optimum damping ratio to minimize parameters $\frac{\delta_o \ddot{x}_o}{V^2}$ or $\frac{\delta_{RMS}\, \ddot{x}^3_{RMS}}{W_o^2}$
τ	=	$\omega_o t$ = nondimensional time
τ_1	=	$\omega_o t_1$ = nondimensional time duration of pulse
ω_o	=	$\sqrt{\frac{k}{m}}$ = undamped natural frequency

EQUATIONS OF MOTION

The equations of motion for the vibration isolation systems with elastically coupled viscous damping shown in Figure 1(a) and 1(b) respectively are

$$\left(\frac{mc}{Nk}\right) \dddot{x} + m\ddot{x} + c\left(\frac{N+1}{N}\right)\dot{\delta} + k\delta = P + \frac{c}{Nk}\dot{P} \tag{1}$$

$$\left[\frac{m\,\frac{c'}{k'}}{N+1}\right]\dddot{x} + m\ddot{x} + c'\left(\frac{N}{N+1}\right)\dot{\delta} + k'\left(\frac{N}{N+1}\right)\delta = P + \left[\frac{c'}{(N+1)k'}\right]\dot{P} \tag{2}$$

where $\delta = x-a$.

The form of the differential equation of motion is the same for these two systems. Therefore they can be made dynamically equivalent by equating coefficients of like terms, namely

$$k = \left(\frac{N}{N+1}\right) k' \tag{3}$$

$$c = \left(\frac{N}{N+1}\right)^2 c' \tag{4}$$

Because of this equivalence, only the unprimed system shown in Figure 1 (a) and described by Equation (1) will be considered. The results are presented in terms of the undamped natural frequency $\omega_o = \sqrt{k/m}$, the viscous damping ratio $\zeta = c/2\sqrt{km}$, and the stiffness ratio N.

Two types of excitation are considered: (1) acceleration of the base $\ddot{a}$; and (2) force on the mass P. When the excitation is the acceleration of the base, the system response is characterized by acceleration of the mass $\ddot{x}$ and the relative deflection across the isolator δ. Taking the Laplace transform of Equation (1), with $P = \dot{P} = 0$, the following transfer functions

are obtained

$$\frac{\ddot{x}(s)}{\ddot{a}(s)} = (N + 1)\omega_o^2 \frac{s + \frac{N}{2\zeta(N + 1)}\omega_o}{s^3 + \frac{N}{2\zeta}\omega_o s^2 + (N + 1)\omega_o^2 s + \frac{N}{2\zeta}\omega_o^3} \tag{5}$$

$$\frac{\delta(s)}{\ddot{a}(s)} = - \frac{s + \frac{N}{2\zeta}\omega_o}{s^3 + \frac{N}{2\zeta}\omega_o s^2 + (N + 1)\omega_o^2 s + \frac{N}{2\zeta}\omega_o^3} \tag{6}$$

When the excitation is a force on the mass, the system response is characterized by the force F transmitted to the base through the isolator and the deflection of the isolator x. The following equivalent relations between transfer functions were obtained:

$$\frac{F(s)}{P(s)} = \frac{\ddot{x}(s)}{\ddot{a}(s)} \tag{7}$$

$$\frac{\delta(s)}{P(s)/m} = \frac{\delta(s)}{\ddot{a}(s)} \tag{8}$$

Therefore, only the responses to an acceleration of the base need be considered, and the results obtained from these analyses will be applicable to the responses to a force on the mass.

FREE VIBRATION

The characteristic equation for this system is obtained by setting the denominator in Equations (5) and (6) equal to zero. The roots of the characteristic equation determine the form of the time history of free vibration. The time history is oscillatory if there is one real root and a pair of complex conjugate roots, and is non-oscillatory if there are three real roots. If at least two of the three real roots are equal, the time history is on the border line between being oscillatory (underdamped) and non-oscillatory (overdamped) and the system is said to be critically damped. The roots of the characterisitic equation are all proportional to the undamped natural frequency ω_o (i.e., if the characteristic equation is divided by ω_o^3 the roots of s/ω_o can be determined as functions of ζ and N). Therefore, for a given value of N, a value of ζ that causes the system to be critically damped will be designated as ζ_{cr}. Values of ζ_{cr} are found by equating the modified characteristic polynomial to a solution containing at least two equal roots:

$$\left(\frac{s}{\omega_o}\right)^3 + \frac{N}{2\zeta}\left(\frac{s}{\omega_o}\right)^2 + (N+1)\left(\frac{s}{\omega_o}\right) + \frac{N}{2\zeta} = \left(\frac{s}{\omega_o} + \alpha\right)\left(\frac{s}{\omega_o} + \beta\right)^2 \tag{9}$$

Expanding the right hand side of Equation (9) and setting the coefficients of s/ω_o equal to those on the left hand side results in:

$$2\beta + \alpha = \alpha\beta^2 = \frac{N}{2\zeta} \tag{10}$$

$$\beta^2 + 2\beta\alpha = N + 1 \tag{11}$$

For $N < 8$, there is no value of ζ that will satisfy Equations (10) and (11) and therefore, the time history of free vibration is always oscillatory. For $N = 8$, there is a triple root of the characteristic equation (i.e., $\alpha = \beta = \sqrt{3}$) and there is only one value of the damping ratio, $\zeta_{cr} = 4/3\sqrt{3}$, that satisfies Equations (10) and (11). These values of ζ_{cr} are displayed graphically in Figure 2. To more fully illustrate the nature of the roots of the characteristic equation, the root locus plots are shown in Figures 3, 4, and 5 for values of N equal to 3, 8, and 15, respectively. From the root locus plots it is easily seen that the dividing line between oscillatory and non-oscillatory motion occurs when there are at least two equal real roots. The pair of complex conjugate roots must reach the real axis at the same point, as ζ is increased from zero, and must leave the real axis at the same point, as ζ is further increased.

The free vibration time histories, when the initial condition is a negative velocity of the mass of magnitude V, are identical to the time history responses to an acceleration of the base in the form of an impulse of area V. These responses will be considered in the next section of the report.

IMPULSE RESPONSE

The excitation in this case is an acceleration of the base equivalent to an impulse of area V (i.e., a velocity step of magnitude V or a displacement ramp of slope V). The Laplace transform of base acceleration $\ddot{a}$ is

$$\ddot{a}(s) = V \tag{12}$$

and the acceleration and displacement responses are obtained by taking the inverse Laplace transform of Equations (5) and (6), respectively, and multiplying by V. The roots of the characteristic equation are found by letting $y = s/\omega_o$ and solving for the roots of:

$$y^3 + \frac{N}{2\zeta} y^2 + (N+1)\ y + \frac{N}{2\zeta} = 0 \tag{13}$$

Defining a nondimensional time as

$$\tau = \omega_o t \tag{14}$$

and using the roots obtained from Equation (13), Equations (5) and (6) can be inverted to give the impulse responses. These are presented in Table I. In order to solve for the peak values of the nondimensional impulse responses Q it is not necessary to specify an undamped natural frequency ω_o but just a stiffness ratio N and a viscous damping ratio ζ.

TABLE I

ROOTS	IMPULSE RESPONSE	Q	ρ	A	B	C
$y_1 = -\alpha + i\beta$ $y_2 = -\alpha - i\beta$ $y_3 = -\gamma$	$Q = Ae^{-\alpha\tau}\sin(\beta\tau+B)+Ce^{-\gamma\tau}$	$\frac{\ddot{x}}{\omega_o V}$	$\frac{N}{2\zeta(N+1)}$	$\frac{N+1}{\beta}\sqrt{\frac{(\rho-\alpha)^2+\beta^2}{(\gamma-\alpha)^2+\beta^2}}$	$\tan^{-1}\frac{\beta}{\rho-\alpha} - \tan^{-1}\frac{\beta}{\gamma-\alpha}$	$\frac{(N+1(\rho-\gamma)}{(\gamma-\alpha)^2+\beta^2}$
		$\frac{\delta\omega_o}{V}$	$\frac{N}{2\zeta}$	$\frac{1}{\beta}\sqrt{\frac{(\rho-\alpha)^2+\beta^2}{(\gamma-\alpha)^2+\beta^2}}$	$\tan^{-1}\frac{\beta}{\rho-\alpha} - \tan^{-1}\frac{\beta}{\gamma-\alpha}$	$\frac{\rho-\gamma}{(\gamma-\alpha)^2+\beta^2}$
$y_1 = -\alpha$ $y_2 = -\beta$ $y_3 = -\gamma$	$Q = Ae^{-\alpha\tau}+Be^{-\beta\tau}+Ce^{-\gamma\tau}$	$\frac{\ddot{x}}{\omega_o V}$	$\frac{N}{2\zeta(N+1)}$	$\frac{(N+1)(\rho-\alpha)}{(\beta-\alpha)(\gamma-\alpha)}$	$\frac{(N+1)(\rho-\beta)}{(\alpha-\beta)(\gamma-\beta)}$	$\frac{(N+1)(\rho-\gamma)}{(\alpha-\gamma)(\beta-\gamma)}$
		$\frac{\delta\omega_o}{V}$	$\frac{N}{2\zeta}$	$\frac{\rho-\alpha}{(\beta-\alpha)(\gamma-\alpha)}$	$\frac{\rho-\beta}{(\alpha-\beta)(\gamma-\beta)}$	$\frac{\rho-\gamma}{(\alpha-\gamma)(\beta-\gamma)}$
$y_1 = -\alpha$ $y_2 = -\alpha$ $y_3 = -\gamma$	$Q = (A\tau-C)e^{-\alpha\tau}+Ce^{-\gamma\tau}$	$\frac{\ddot{x}}{\omega_o V}$	$\frac{N}{2\zeta(N+1)}$	$\frac{(N+1)(\rho-\alpha)}{\gamma-\alpha}$	———	$\frac{(N+1)(\rho-\gamma)}{(\gamma-\alpha)^2}$
		$\frac{\delta\omega_o}{V}$	$\frac{N}{2\zeta}$	$\frac{\rho-\alpha}{\gamma-\alpha}$	———	$\frac{\rho-\alpha}{(\gamma-\alpha)^2}$
$y_1 = -\alpha$ $y_2 = -\alpha$ $y_3 = -\alpha$	$Q = (A\tau+B)\tau e^{-\alpha\tau}$	$\frac{\ddot{x}}{\omega_o V}$	$\frac{N}{2\zeta(N+1)}$	$\frac{1}{2}(N+1)(\rho-\alpha)$	N+1	———
		$\frac{\delta\omega_o}{V}$	$\frac{N}{2\zeta}$	$\frac{1}{2}(\rho-\alpha)$	1	———

For the special case of $N = \infty$ (i.e., convential spring and damper in parallel), the viscous damping ratio ζ is also the fraction of critical damping and the impulse response solutions are somewhat simplified as shown below.

$N = \infty;\ \zeta < 1$

$$\frac{\ddot{x}}{\omega_o V} = \frac{e^{-\zeta\tau}}{\sqrt{1-\zeta^2}} \sin\left[\sqrt{1-\zeta^2}\,\tau + \tan^{-1}\frac{2\zeta\sqrt{1-\zeta^2}}{1-2\zeta^2}\right] \tag{15}$$

$$\frac{\delta\dot{\omega}_o}{V} = \frac{e^{-\zeta\tau}}{\sqrt{1-\zeta^2}} \sin\left(\sqrt{1-\zeta^2}\,\tau\right) \tag{16}$$

$N = \infty;\ \zeta = 1$

$$\frac{\ddot{x}}{\omega_o V} = (2 - \tau)\, e^{-\tau} \tag{17}$$

$$\frac{\delta\omega_o}{V} = \tau\, e^{-\tau} \tag{18}$$

$N = \infty;\ \zeta > 1$

$$\frac{\ddot{x}}{\omega_o V} = \frac{\zeta}{\sqrt{\zeta^2-1}} \left[\left(\frac{1}{2\zeta} - \zeta + \sqrt{\zeta^2-1}\right) e^{-\left(\zeta - \sqrt{\zeta^2-1}\right)\tau} - \left(\frac{1}{2\zeta} - \zeta - \sqrt{\zeta^2-1}\right) e^{-\left(\zeta + \sqrt{\zeta^2-1}\right)\tau}\right] \tag{19}$$

$$\frac{\delta\omega_o}{V} = \frac{1}{2\sqrt{\zeta^2-1}}\left[e^{-(\zeta-\sqrt{\zeta^2-1})\tau} \quad -e^{-(\zeta+\sqrt{\zeta^2-1})\tau}\right] \tag{20}$$

Because of the importance of the peak values of acceleration and displacement, the maximum values of the dimensionless acceleration $\ddot{x}_o/\omega_o V$ and the dimensionless displacement $\delta_o\omega_o/V$ were obtained for various values of the stiffness ratio N and the viscous damping ratio ζ. These results are displayed graphically in Figures 6 through 9. The curves in Figure 7, each for a particular value of stiffness ratio N, all have a minimum at some value of ζ. These values of ζ will be designated as ζ_m and are shown plotted versus the stiffness ratio N in Figure 10. The significance of ζ_m is that for given values of mass m, stiffness k, and stiffness ratio N, the damping c determined from ζ_m will minimize the peak acceleration $\ddot{x}_o$. In Figure 8 it can be observed that for any stiffness ratio N, the higher the value of the viscous damping ratio ζ, the lower is the value of the dimensionless displacement $\delta_o\omega_o/V$, and as ζ approaches infinity, $\delta_o\omega_o/V$ approaches $1/\sqrt{N+1}$.

Optimization of Parameters

The parameters for this system have been optimized according to the shock isolator optimization criteria which states: "For a given input and maximum deflection of the isolator, find the isolator parameters that will minimize the peak acceleration of the isolated mass". In general, solutions to this problem are difficult to obtain because the expressions for the maximum values can not be written analytically and numerical search techniques must be employed. However, for the system under consideration, the influence of the three parameters ω_o, ζ, and N on the optimum impulse response can be effectively separated. The undamped natural frequency ω_o can be eliminated from the search procedure, since letting

$$\frac{\ddot{x}_o}{\omega_o V} = Q_1 \tag{21}$$

and

$$\frac{\delta_o \omega_o}{V} = Q_2 \tag{22}$$

results in

$$\frac{\delta_o \ddot{x}_o}{V^2} = Q_1 \; Q_2 \tag{23}$$

Figure 11 shows a plot of Equation (23) obtained as the product of values of $\ddot{x}_o/\omega_o V$ from Figure 6 and values of $\delta_o\omega_o/V$ from Figure 8. The minimum value of $\delta_o\ddot{x}_o/V^2$ represents the minimum value of the acceleration $\ddot{x}_o$, given the input V and the isolator deflection δ_o. It can be seen from Figure 11 that the minimum value of $\delta_o\ddot{x}_o/V^2$ is 0.52 and the values of the parameters are $N=\infty$ and $\zeta=0.4$. Since there may be other criteria that require a finite value of N, it was decided to keep N as a given parameter and then optimize ω_o and ζ for certain values of N.

The values of ζ that minimize the curves in Figure 11 are designated as the optimum viscous damping ratio ζ_{op} and are plotted in Figure 12 versus the stiffness ratio N. Associated with each value of ζ_{op} are values of Q_1 and Q_2 from which the optimum undamped natural frequency $(\omega_o)_{op}$ can be obtained from Equation (21) or (22) for a given value of V, and either a given maximum acceleration $\ddot{x}_o$ or a given maximum displacement δ_o, respectively. The value of Q_2 corresponding to ζ_{op} is designated as the optimum frequency parameter $\delta_o(\omega_o)_{op}/V$ and is plotted versus the stiffness ratio N in Figure 13. The optimum dimensionless acceleration $\ddot{x}_o/g$, where g is the acceleration of gravity, is plotted versus the

dimensionless displacement parameter $\delta_o g/V^2$ for various values of the stiffness ratio N in Figure 14. These curves are called trade-off limit curves since they determine the minimum value of peak acceleration that can be achieved given the maximum relative displacement δ_o and the level of the velocity shock V.

Also plotted in Figure 14 is a curve labeled "BEST POSSIBLE." This result was obtained by considering the response of an isolation system using a constant force device as the isolator. From energy considerations

$$1/2\ mV^2 = F\ \delta_o \tag{24}$$

where F is the magnitude of the constant force. The maximum acceleration $\ddot{x}_o$ is F/m so that from Equation (24)

$$\frac{\delta_o \ddot{x}_o}{V^2} = 0.5 \tag{25}$$

A similar result was obtained in Reference 7.

The value of $\delta_o \ddot{x}_o/V^2$ is equal to 0.52 for the system shown in Figure 1(a) with $N = \infty$ and $\zeta = 0.4$ and, therefore, is only 4 percent worse than the best possible solution. However, the system with the spring and viscous damper will return to its initial position which could be an advantage. This is illustrated in Figure 15 where the constant force F was chosen so that the maximum isolator deflection would be the same for both systems.

Design Example

The following design example illustrates the use of the optimum design graphs. It is required that the parameters N, ζ, and ω_o which will minimize the maximum relative displacement be determined, given that the maximum allowable acceleration is 10 g's (3860 in/sec^2) and the input is a 100 in/sec velocity shock. Since no restrictions are placed on the stiffness ratio N, take

$N_{op} = \infty$. From Figure 12, $\zeta_{op} = 0.4$ and from Figure 13, $\delta_o(\omega_o)_{op}/V = 0.6$. From Figure 14, with $N = \infty$ and $\ddot{x}_o/g = 10$, the dimensionless displacement parameter is

$$\frac{\delta_o g}{V^2} = 0.052$$

so that substituting the values of V and g results in $\delta_o = 1.35$ in. Using this value of δ_o

$$(\omega_o)_{op} = 44.4 \text{ rad/sec}; \quad (f_o)_{op} = 7.07 \text{ Hz}$$

In some instances, system design or performance requirements may dictate selection of finite values of N (e.g., high frequency vibration isolation). In that case, parameters can be selected to provide the best response to impulse (from Figures 11 through 14) compatible with the desired vibration isolation performance (from Reference 1). Of necessity, this selection would involve a trial and error procedure.

RANDOM VIBRATION RESPONSE

The random excitation to be considered is white noise acceleration of the base. This type of excitation has a uniform spectral density W_o which can be expressed as mean square acceleration per cycle per second, over all frequencies from $f = 0$ to $f = \infty$ [Ref. 8, p.28]. The responses of interest are the acceleration of the mass $\ddot{x}$ and the relative deflection across the isolator δ. The transfer functions for these quantities are given by Equations (5) and (6), respectively. It is well known that for a linear system, the spectral density of the response is equal to the spectral density of the input times the square of the magnitude of the appropriate transfer function [Ref. 8, pp.69-71]. Many of the transfer functions for this system have been obtained in graphical form for a wide variation of the parameters N and ζ, and will appear in a forthcoming monograph.†

One measure of the effectiveness of the vibration isolator is the RMS values of the responses. The RMS value of the acceleration $\ddot{x}$ and the relative displacement δ are determined using the transfer functions given by Equations (5) and (6), respectively [Ref. 8, p.71]. Written in nondimensional terms, these are:

$$\frac{\ddot{x}_{RMS}}{\sqrt{W_o f_o}} = \sqrt{2\pi \frac{N^2 + 4\,(N+1)^2\,\zeta^2}{8\,N^2\zeta}} \tag{26}$$

$$\frac{\delta_{RMS}}{\sqrt{W_o/f_o^{\,3}}} = \sqrt{\frac{1}{(2\pi)^3} \quad \frac{N^2 + 4\zeta^2}{8\,N^2\zeta}} \tag{27}$$

---

† This monograph, which is being prepared under Contract No. N00173-68-C-0072 for the Shock and Vibration Information Center of the Naval Research Laboratory will be entitled "The Influence of Damping in Vibration Isolation" by Jerome E. Ruzicka and Thomas F. Derby.

Since the excitation spectral density W_o is in terms of cycles per second, the undamped natural frequency ω_o was converted to $2\pi f_o$, where f_o is in units of cycles per second. Equations (26) and (27) are displayed graphically in Figures 16 and 17, respectively.

For a random process which is stationary and normally distributed with zero mean, the expected frequency f_e (i.e., the average number of zero crossings with positive slope per second) is given as the RMS value of the derivative of the random variable divided by the RMS value of the random variable [Ref. 8, p.44]. The expected frequency f_e of the relative deflection δ has been so calculated and is given in nondimensional form as:

$$\frac{f_e}{f_o} = \sqrt{1 + \frac{4N\zeta^2}{N^2+4\zeta^2}} \tag{28}$$

This equation is displayed graphically in Figure 18. If the response of the relative deflection δ to the white noise acceleration input is a narrow-band process (i.e., the response has the appearance of a sinusoid of frequency f_e but with slowly varying random amplitude and random phase), then the expected frequency is useful in predicting the fatigue life of the isolator [Ref. 8, pp.115-125]. Therefore, care must be taken in using values of f_e from Figure 18 to insure that the response would be a narrow-band process (e.g., a system with $N = \infty$ and a high value of ζ would have a rather broad-band response).

The curves in Figures 16 and 17, representing the dimensionless acceleration $\ddot{x}_{RMS}/\sqrt{W_o f_o}$ and the dimensionless displacement $\delta_{RMS}/\sqrt{W_o/f_o^{\,3}}$, respectively, all have a minimum at some value of ζ. These values of ζ will be designated as ζ_m and are plotted versus the stiffness ratio N in Figure 19. The significance of these values of ζ_m is similar to the viscous damping ratio ζ_m defined for impulse response, namely, for given values of the mass m, the stiffness k and the stiffness ratio N, the damping c

can be determined from ζ_m such that either the RMS acceleration $\ddot{x}_{RMS}$ or the RMS relative displacement δ_{RMS} are minimized. The expressions for these values of ζ_m are found by minimizing the right side of Equations (26) and (27) with respect to ζ and are given by

$$\zeta_m = \frac{N}{2(N+1)} \qquad \text{(acceleration)} \tag{29}$$

$$\zeta_m = \frac{N}{2} \qquad \text{(displacement)} \tag{30}$$

Substituting these values of ζ_m into Equations (26) and (27) results in the following:

$$\left[\frac{\ddot{x}_{RMS}}{\sqrt{W_o f_o}}\right]_{MIN} = \sqrt{\pi\ (1+\frac{1}{N})} \tag{31}$$

$$\left[\frac{\delta_{RMS}}{\sqrt{W_o/f_o^{\,3}}}\right]_{MIN} = \frac{1}{\sqrt{16\pi^3\ N}} \tag{32}$$

Equations (31) and (32) are plotted in Figures 20 and 21, respectively.

Optimization of Parameters

Similar to the analysis of impulse response, the parameters for this system have been optimized according to the criteria: "For a given input and RMS deflection of the isolator, find the isolator parameters that will minimize the RMS acceleration of the isolated mass". To accomplish this, the cube of Equation (26)

was multiplied by Equation (27) to obtain

$$\frac{\delta_{RMS}\ \ddot{x}^3_{RMS}}{W_o^{\ 2}} = \frac{(N^2+4\zeta^2)^{1/2}\ \left[N^2+4(N+1)^2\zeta^2\right]^{3/2}}{64N^4\zeta^2} \tag{33}$$

thus eliminating the parameter f_o. Equation (33) is presented graphically in Figure 22. Minimizing Equation (33) with respect to N and ζ results in $N_{op} = \infty$ and $\zeta_{op} = 0.707$. Again, however, we will retain N as a parameter and optimize ζ as a function of N. This is done by minimizing Equation (33) with respect to ζ, which results in

$$\zeta_{op} = \sqrt{\frac{N^3(N+2)}{12(N+1)^2}\left[\sqrt{1 + \frac{12(N+1)^2}{N^2(N+2)^2}} - 1\right]} \tag{34}$$

Equation (34) is displayed graphically in Figure 23. The optimum natural frequency $(f_o)_{op}$ can be obtained as a function of the stiffness ratio N by substituting the value of ζ_{op} given in Equation (34) into either Equation (26) or Equation (27). In order to plot $(f_o)_{op}$ in the most convenient form, the reciprocal of Equation (26) squared with $\zeta = \zeta_{op}$ is designated as the optimum frequency parameter $(W_o/\ddot{x}^2_{RMS})(f_o)_{op}$ and is plotted versus the stiffness ratio N in Figure 24. A plot of an optimum dimensionless acceleration $\ddot{x}_{RMS}/g$, where g is the acceleration of gravity, versus a dimensionless displacement $\sqrt[3]{g^3\delta_{RMS}/W_o^{\ 2}}$ was obtained for various values of N by using Equation (33) with $\zeta = \zeta_{op}$. These curves, called trade-off limit curves, are shown in Figure 25. The curve labeled $N = \infty$ is also designated as "BEST POSSIBLE". This result was obtained in Reference 9.

Design Example

The following design example illustrates the use of the optimum design graphs. It is required that, the parameters N,

ζ, and f_o be determined, which will minimize the RMS acceleration, given that the allowable RMS relative displacement is 0.1 inches and the input is a random acceleration of the base with a uniform spectral density equal to 0.1 g^2/cps. The input spectral density $W_o = g^2$ (0.1) so that

$$\sqrt[3]{g^3 \delta_{RMS}/W_o{}^2} = 0.296$$

Since no restriction is placed on the stiffness ratio N, let $N = \infty$. From Figure 25 the optimum dimensionless acceleration $\ddot{x}_{RMS}/g$ is 1.83 g's. The value of ζ_{op} corresponding to $N = \infty$ is $\zeta_{op} = 0.707$. Also with $N = \infty$ the value of the optimum frequency parameter $(W_o/\ddot{x}^2_{RMS})\ (f_o)_{op}$ is 0.3 as can be seen from Figure 24. Therefore, $(f_o)_{op} = 5.5$ cps.

Similar to the discussion of the design example for the impulse response, a finite value of N may have to be chosen. For this reason the optimizations have been presented in Figures 22 through 25 retaining N as a parameter.

RESPONSE TO VARIOUS PULSE SHAPES

The pulses to be considered in this section are shown in Table II. All the pulses are acceleration time histories of the base. The peak value is defined as $\ddot{a}_o$, and the time duration as t_1. The area under the pulse is the velocity change associated with that pulse, and is designated by V. In equation form

$$V = \int_0^{t_1} \ddot{a}\, dt \tag{35}$$

Equations of the time histories of base accelerations, as well as the associated velocity changes are also given in Table II.

The velocity time histories of the base start at zero and reach a value of V at time $t = t_1$, remaining at this constant value for $t > t_1$. The only distinction in the velocity time histories is the manner in which the final value V is reached, during the time $t = 0$ to $t = t_1$. If the natural period of the responding system T is much larger than t_1, it makes very little difference how the final velocity value was reached. All the pulses can then be considered as impulses of area V. This is a fortunate result since in most cases the input can be considered as an impulse in the region of shock isolation (i.e., when the peak response of the system $\ddot{x}_o$ is less than the peak input $\ddot{a}_o$). This point will be discussed in more detail in the evaluation of the shock spectra graphs.

The responses to be considered are the acceleration of the mass $\ddot{x}$, and the relative deflection across the isolator δ. The main concern is the maximum value of these quantities, designated as $\ddot{x}_o$ and δ_o, respectively. In order to nondimensionalize these response quantities we will consider $\ddot{x}_o/\ddot{a}_o$ and $\delta_o\omega_o^2/\ddot{a}_o$ as the response parameters, where $\omega_o = \sqrt{k/m}$ is the undamped natural frequency of the system shown in Figure 1(a).

TABLE II

INPUT PULSE	TIME-HISTORY EXPRESSION FOR $\ddot{a}$	VELOCITY CHANGE V
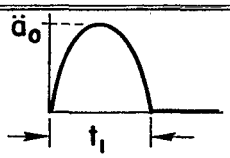 Half-Cycle Sine	$\ddot{a}_o\{\sin(\pi t/t_1)$ $+ \sin[\pi(t-t_1)/t_1]U(t-t_1)\}$	$\frac{2}{\pi}\ddot{a}_o t_1$
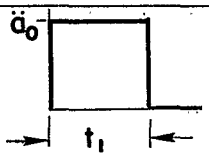 Rectangular	$\ddot{a}_o\{1-U(t-t_1)\}$	$\ddot{a}_o t_1$
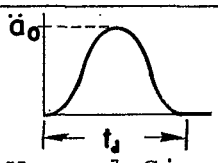 Versed-Sine	$\frac{\ddot{a}_o}{2}\{1 - \cos(2\pi t/t_1)$ $-(1-\cos[2\pi(t-t_1)/t_1])U(t-t_1)\}$	$\frac{1}{2}\ddot{a}_o t_1$
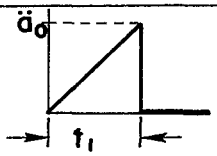 Terminal-Peak Saw-Tooth	$\ddot{a}_o\{t/t_1-[1+(t-t_1)/t_1]U(t-t_1)\}$	$\frac{1}{2}\ddot{a}_o t_1$
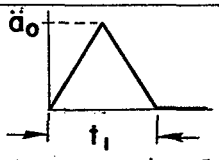 Symmetrical Triangle	$2\ddot{a}_o\{t/t_1-2(t-\frac{1}{2}t_1)/t_1U(t-\frac{1}{2}t_1)$ $+\frac{t-t_1}{t_1}U(t-t_1)\}$	$\frac{1}{2}\ddot{a}_o t_1$
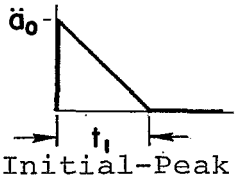 Initial-Peak Saw-Tooth	$\ddot{a}_o\{1-t/t_1 + \frac{t-t_1}{t_1}U(t-t_1)\}$	$\frac{1}{2}\ddot{a}_o t_1$

Knowing the Laplace transform of the input $\ddot{a}(s)$, we can obtain the Laplace transform of the outputs $\ddot{x}(s)$ and $\delta(s)$ from Equations (5) and (6), respectively. In the presentation of the transforms it is convenient to define

$$\tau_1 = \omega_o t_1 \tag{36}$$

as a nondimensional pulse duration similar to the definition of τ in Equation (14). Let

$$y = s/\omega_o \tag{37}$$

The transforms $\mathcal{L}[\ddot{x}/\ddot{a}_o]$ and $\mathcal{L}[\delta\omega_o^2/\ddot{a}_o]$ can then be obtained in the form

$$\mathcal{L}[Q(t)] = \frac{1}{\omega_o} g(y, \tau_1, N, \zeta) \tag{38}$$

where $Q(t)$ stands for either $\ddot{x}/\ddot{a}_o$ or $\delta\omega_o^2/\ddot{a}_o$ as a function of time t. From the change of scale theorem [Ref. 10]

$$\mathcal{L}[f(at)] = \frac{1}{a} F(\frac{s}{a}) \tag{39}$$

where $F(s) \equiv \mathcal{L}[f(t)]$. $Q(t)$ can be obtained by taking the inverse transform of $g(s, \tau_1, N, \zeta)$ and replacing t by $\omega_o t$ (i.e., using $\tau = \omega_o t$, $Q(\tau) = \mathcal{L}^{-1}[g(s, \tau_1, N, \zeta)]$. Therefore, the maximum value of $Q(\tau)$ will be a function of τ_1, N, and ζ.

The following subsections will give the equations for $\mathcal{L}[\ddot{a}]$, $\mathcal{L}[\ddot{x}/\ddot{a}_o]$, $\mathcal{L}[\delta\omega_o^2/\ddot{a}_o]$, $\ddot{x}/\ddot{a}_o$, and $\delta\omega_o^2/\ddot{a}_o$ for the six pulses: half-cycle sine, rectangular, versed-sine, terminal-peak saw-tooth, symmetrical triangle, and initial-peak saw-tooth.

Half-Cycle Sine Pulse

Using the definitions given for τ_1 and y in Equations (36) and (37), respectively, the Laplace transform of the equation for $\ddot{a}$ given in Table II is

$$\ddot{a}(s) \equiv \mathcal{L}[a] = \ddot{a}_o \frac{1}{\omega_o} \frac{\lambda}{y^2 + \lambda^2} \left(1 + e^{-\tau_1 y}\right) \tag{40}$$

where

$$\lambda \equiv \pi/\tau_1 \tag{41}$$

Since the form of Equations (5) and (6) is the same, the transforms and time histories of $\ddot{x}/\ddot{a}_o$ and $\delta\omega_o^2/\ddot{a}_o$ will have the same form. The following table defines a quantity Q and associated multiplier M and coefficient ρ to be used in the transform and time history expressions.

Q	M	ρ
$\ddot{x}/\ddot{a}_o$	$\lambda(N+1)$	$\frac{N}{2\zeta(N+1)}$
$-\delta\omega_o^2/\ddot{a}_o$	λ	$\frac{N}{2\zeta}$

Combining Equation (40) with Equations (5) and (6) results in

$$Q(s) = \frac{1}{\omega_o} M \frac{y + \rho}{(y^2 + \lambda^2)\left[y^3 + \frac{N}{2\zeta} y^2 + (N + 1)y + \frac{N}{2\zeta}\right]} \left(1 + e^{-\tau_1 y}\right) \tag{42}$$

The form of the time histories $Q(\tau)$ depends on the nature of the roots of the cubic expression in Equation (42). The case where there are either two or three equal real roots will not be considered since for the particular values of N and ζ that are to be used, the situation does not arise. The roots of the cubic will be designated as y_1, y_2, and y_3.

<u>Case 1: $y_1 = -\alpha + j\beta$, $y_2 = -\alpha - j\beta$, and $y_3 = -\gamma$.</u> The inverse transform of Equation (42) was obtained using transform pair 106 [Ref. 11], and is given by

$$Q(\tau) = M[f(\tau) + f(\tau - \tau_1)U(\tau - \tau_1)] \tag{43}$$

where

$$f(\tau) = C_1 e^{-\gamma\tau} - C_2 \sin(\lambda\tau + \phi) + C_3 e^{-\alpha\tau} \sin(\beta\tau + \theta)$$

$$C_1 = \frac{\rho-\gamma}{XY}, \quad C_2 = \left[\frac{\rho^2+\lambda^2}{\lambda^2 XY}\right]^{\frac{1}{2}}, \quad C_3 = \left[\frac{(\rho-\alpha)^2 + \beta^2}{\beta^2 YZ}\right]^{\frac{1}{2}}$$

$$X = \gamma^2 + \lambda^2, \quad Y = (\gamma-\alpha)^2 + \beta^2, \quad Z = (\alpha^2+\beta^2-\lambda^2)^2+(2\alpha\lambda)^2$$

$$\phi = \tan^{-1}\frac{\lambda}{\rho} + \tan^{-1}\frac{\gamma}{\lambda} + \tan^{-1}\frac{\alpha^2 + \beta^2 - \lambda^2}{2\alpha\lambda}$$

$$\theta = \tan^{-1}\frac{\beta}{\rho-\alpha} + \tan^{-1}\frac{\gamma-\alpha}{\beta} - \tan^{-1}\frac{\alpha^2 - \beta^2 + \lambda^2}{2\alpha\beta}$$

<u>Case 2: $y_1 = -\alpha$, $y_2 = -\beta$, and $y_3 = -\gamma$.</u> The inverse transform of Equation (42) was obtained using transform pair 244 [Ref. 11] and is given by

$$Q(\tau) = M[f(\tau) + f(\tau - \tau_1)U(\tau - \tau_1)] \tag{44}$$

where

$$f(\tau) = C_1 e^{-\alpha\tau} + C_2 e^{-\beta\tau} + C_3 e^{-\gamma\tau} + C_4 \sin(\lambda\tau - \psi)$$

$$C_1 = \frac{\rho-\alpha}{(\beta-\alpha)(\gamma-\alpha)(\alpha^2+\lambda^2)}, \quad C_2 = \frac{\rho-\beta}{(\alpha-\beta)(\gamma-\beta)(\beta^2+\lambda^2)}$$

$$C_3 = \frac{\rho-\gamma}{(\alpha-\gamma)(\beta-\gamma)(\gamma^2+\lambda^2)}, \quad C_4 = \frac{1}{\lambda}\left[\frac{\rho^2+\lambda^2}{(\alpha^2+\lambda^2)(\beta^2+\lambda^2)(\gamma^2+\lambda^2)}\right]^{\frac{1}{2}}$$

$$\psi = \tan^{-1}\frac{\lambda}{\alpha} + \tan^{-1}\frac{\lambda}{\beta} + \tan^{-1}\frac{\lambda}{\gamma} - \tan^{-1}\frac{\lambda}{\rho}$$

Rectangular Pulse

The Laplace transform of the equation for $\ddot{a}$ given in Table II is

$$\ddot{a}(s) \equiv \mathcal{L}[\ddot{a}] = \ddot{a}_o \frac{1}{\omega_o}\frac{1}{Y}\left(1-e^{-\tau_1 Y}\right) \tag{45}$$

The following table defines a quantity Q and associated multiplier M and coefficient ρ to be used in the transform and time history expressions.

Q	M	ρ
$\ddot{x}/\ddot{a}_o$	N + 1	$\frac{N}{2\zeta(N+1)}$
$-\delta\omega_o^2/\ddot{a}_o$	1	$\frac{N}{2\zeta}$

Combining Equation (45) with Equations (5) and (6) results in

$$Q(s) = \frac{1}{\omega_o} M \frac{y + \rho}{y\left[y^3 + \frac{N}{2\zeta} y^2 + (N+1)\ y + \frac{N}{2\zeta}\right]} \left(1-e^{-\tau_1 y}\right) \tag{46}$$

The roots of the cubic expression in Equation (46) will be designated as y_1, y_2, and y_3.

<u>Case 1: $y_1 = -\alpha + j\beta$, $y_2 = -\alpha - j\beta$, and $y_3 = -\gamma$.</u> The inverse transform of Equation (46) was obtained using transform pair 86 [Ref. 11] and is given by:

$$Q(\tau) = M[f(\tau) - f(\tau - \tau_1)U(\tau - \tau_1)] \tag{47}$$

where

$$f(\tau) = C_1 + C_2 e^{-\gamma\tau} + C_3 e^{-\alpha\tau} \sin(\beta\tau + \psi)$$

$$C_1 = \frac{\rho}{\gamma X}\ ,\ C_2 = \frac{\gamma-\rho}{\gamma Y}\ ,\ C_3 = \frac{1}{\beta}\left[\frac{Z}{XY}\right]^{\frac{1}{2}}$$

$$X = \alpha^2 + \beta^2\ ,\ Y = (\alpha-\gamma)^2 + \beta^2\ ,\ Z = (\rho-\alpha)^2 + \beta^2$$

$$\psi = \tan^{-1}\frac{\beta}{\alpha-\gamma} + \tan^{-1}\frac{\beta}{\alpha} + \tan^{-1}\frac{\beta}{\rho-\alpha}$$

<u>Case 2: $y_1 = -\alpha$, $y_2 = -\beta$, and $y_3 = -\gamma$.</u> The inverse transform of Equation (46) was obtained using transform pair 27 [Ref. 11] and is given by

$$Q(\tau) = M[f(\tau) - f(\tau - \tau_1)U(\tau - \tau_1)] \tag{48}$$

where

$$f(\tau) = C_1 - C_2 e^{-\alpha\tau} - C_3 e^{-\beta\tau} - C_4 e^{-\gamma\tau}$$

$$C_1 = \frac{\rho}{\alpha\beta\gamma}, \quad C_2 = \frac{\rho-\alpha}{\alpha(\beta-\alpha)(\gamma-\alpha)}$$

$$C_3 = \frac{\rho\ \beta}{\beta(\alpha-\beta)(\gamma-\beta)}, \quad C_4 = \frac{\rho-\gamma}{\gamma(\alpha-\gamma)(\beta-\gamma)}$$

Versed-Sine Pulse

The Laplace transform of the equation for $\ddot{a}$ given in Table II is

$$\ddot{a}(s) \equiv \mathcal{L}[\ddot{a}] = \ddot{a}_o \frac{1}{\omega_o} \frac{\lambda^2/2}{y(y^2+\lambda^2)} \left(1-e^{-\tau_1 y}\right) \tag{49}$$

where

$$\lambda \equiv 2\pi/\tau_1 \tag{50}$$

The following table defines a quantity Q and associated multiplier M and coefficient ρ to be used in the transform and time history expressions.

Q	M	ρ
$\ddot{x}/\ddot{a}_o$	$\frac{(N+1)\lambda^2}{2}$	$\frac{N}{2\zeta(N+1)}$
$-\delta\omega_o^2/a_o$	$\lambda^2/2$	$\frac{N}{2\zeta}$

Combining Equation (49) with Equations (5) and (6) results in

$$Q(s) = \frac{1}{\omega_o} M \frac{y + \rho}{y(y^2+\lambda^2)\left[y^3 + \frac{N}{2\zeta} y^2 + (N+1)\ y + \frac{N}{2\zeta}\right]} \left(1-e^{-\tau_1 y}\right) \quad (51)$$

The roots of the cubic expression in Equation (51) will be designated as y_1, y_2, and y_3.

<u>Case 1: $y_1 = -\alpha + j\beta$, $y_2 = -\alpha - j\beta$, and $y_3 = -\gamma$.</u> The inverse transform of Equation (51) was obtained using transform pair 251 [Ref. 11] and is given by

$$Q(\tau) = M[f(\tau) - f(\tau - \tau_1)U(\tau - \tau_1)] \quad (52)$$

where

$$f(\tau) = C_1 - C_2 e^{-\gamma\tau} - C_3 e^{-\alpha\tau} \sin(\beta\tau+\phi) - C_4 \sin(\lambda\tau+\theta)$$

$$C_1 = \frac{\rho}{\gamma(\alpha^2+\beta^2)\lambda^2}, \quad C_2 = \frac{\rho - \gamma}{\gamma[(\alpha-\gamma)^2 + \beta^2][\gamma^2+\lambda^2]}$$

$$C_3 = \frac{1}{\beta}\left[\frac{(\rho-\alpha)^2 + \beta^2}{(\alpha^2+\beta^2)[(2\alpha\beta)^2 + (\alpha^2-\beta^2+\lambda^2)^2][(\gamma-\alpha)^2 + \beta^2]}\right]^{\frac{1}{2}}$$

$$C_4 = \frac{1}{\lambda}\left[\frac{\rho^2 + \lambda^2}{(\gamma^2+\lambda^2)[(2\alpha\lambda)^2 + (\alpha^2+\beta^2-\lambda^2)^2]}\right]^{\frac{1}{2}}$$

$$\phi = \tan^{-1}\frac{\beta}{\rho-\alpha} + \tan^{-1}\frac{\gamma-\alpha}{\beta} - \tan^{-1}\frac{\alpha}{\beta} - \tan^{-1}\frac{-2\alpha\beta}{\alpha^2-\beta^2+\lambda^2}$$

$$\theta = \tan^{-1}\frac{\lambda}{\rho} + \tan^{-1}\frac{\gamma}{\lambda} - \tan^{-1}\frac{2\alpha\lambda}{\alpha^2+\beta^2-\lambda^2}$$

<u>Case 2: $y_1 = -\alpha$, $y_2 = -\beta$, and $y_3 = -\gamma$.</u> The inverse transform of Equation (51) was obtained using transform pair 245 [Ref. 11] and is given by

$$Q(\tau) = M[f(\tau) - f(\tau - \tau_1)U(\tau - \tau_1)] \tag{53}$$

where

$$f(\tau) = C_1 - C_2e^{-\alpha\tau} - C_3e^{-\beta\tau} - C_4e^{-\gamma\tau} + C_5\cos(\lambda\tau+\psi)$$

$$C_1 = \frac{\rho}{\alpha\beta\gamma\lambda^2}, \quad C_2 = \frac{\rho - \alpha}{\alpha(\beta-\alpha)(\gamma-\alpha)(\alpha^2+\lambda^2)}$$

$$C_3 = \frac{\rho - \beta}{\beta(\alpha-\beta)(\gamma-\beta)(\beta^2+\lambda^2)}, \quad C_4 = \frac{\rho - \gamma}{\gamma(\alpha-\gamma)(\beta-\gamma)(\gamma^2+\lambda^2)}$$

$$C_5 = \frac{1}{\lambda^2}\left[\frac{\rho^2 + \lambda^2}{(\alpha^2+\lambda^2)(\beta^2+\lambda^2)(\gamma^2+\lambda^2)}\right]^{\frac{1}{2}}$$

$$\psi = \tan^{-1}\frac{\lambda}{\rho} + \tan^{-1}\frac{\beta}{\lambda} + \tan^{-1}\frac{\alpha}{\lambda} - \tan^{-1}\frac{\lambda}{\gamma}$$

Terminal-Peak Saw-Tooth Pulse

The Laplace transform of the equation for $\ddot{a}$ given in Table II is

$$\ddot{a}(s) \equiv \mathcal{L}[\ddot{a}] = \ddot{a}_o \frac{1}{\omega_o} \left[\frac{1/\tau_1}{y^2} \left(1-e^{-\tau_1 y}\right) - \frac{1}{y} e^{-\tau_1 y} \right] \tag{54}$$

The following table defines a quantity Q and associated multiplier M and coefficient ρ to be used in the transform and time history expressions.

Q	M	ρ
$\ddot{x}/\ddot{a}_o$	$\frac{N+1}{\tau_1}$	$\frac{N}{2\zeta(N+1)}$
$-\delta\omega_o^2/\ddot{a}_o$	$1/\tau_1$	$\frac{N}{2\zeta}$

Combining Equation (54) with Equations (5) and (6) results in

$$Q(s) = \frac{1}{\omega_o} M \left\{ \frac{y + \rho}{y^2 \left[y^3 + \frac{N}{2\zeta} y^2 + (N+1)\, y + \frac{N}{2\zeta} \right]} \left(1-e^{-\tau_1 y}\right) - \tau_1 \frac{y + \rho}{y \left[y^3 + \frac{N}{2\zeta} y^2 + (N+1)\, y + \frac{N}{2\zeta} \right]} e^{-\tau_1 y} \right\} . \tag{55}$$

The roots of the cubic expression in Equation (55) will be designated as y_1, y_2, and y_3.

Case 1: $y_1 = -\alpha + j\beta$, $y_2 = -\alpha - j\beta$, and $y_3 = -\gamma$. The inverse transform of Equation (55) was obtained using transform pairs 90 and 86 [Ref. 11] and is given by

$$Q(\tau) = M\{f_1(\tau) - [f_1(\tau - \tau_1) + f_2(\tau - \tau_1)]U(\tau - \tau_1)\} \qquad (56)$$

where

$$f_1(\tau) = C_1(\tau+C_2) + C_3e^{-\gamma\tau} + C_4e^{-\alpha\tau}\sin(\beta\tau+\phi)$$

$$f_2(\tau) = \tau_1[C_1-\gamma C_3e^{-\gamma\tau} + \sqrt{\alpha^2+\beta^2}\, C_4e^{-\alpha\tau}\sin(\beta\tau+\theta)]$$

$$C_1 = \frac{\rho}{\gamma(\alpha^2+\beta^2)}, \quad C_2 = \frac{1}{\rho} - \frac{1}{\gamma} - \frac{2\alpha}{\alpha^2+\beta^2}$$

$$C_3 = \frac{\rho - \gamma}{\gamma^2[(\gamma-\alpha)^2 + \beta^2]}, \quad C_4 = \frac{1}{\beta(\alpha^2+\beta^2)}\sqrt{\frac{(\rho-\alpha)^2 + \beta^2}{(\gamma-\alpha)^2 + \beta^2}}$$

$$\phi = 2\tan^{-1}\frac{\beta}{\alpha} - \tan^{-1}\frac{\beta}{\gamma-\alpha} + \tan^{-1}\frac{\beta}{\rho-\alpha}$$

$$\theta = \tan^{-1}\frac{\beta}{\alpha-\gamma} + \tan^{-1}\frac{\beta}{\alpha} + \tan^{-1}\frac{\beta}{\rho-\alpha}$$

Case 2: $y_1 = -\alpha$, $y_2 = -\beta$, and $y_3 = -\gamma$. The inverse transform Equation (55) was obtained using transform pairs 31 and 27 [Ref. 11] and is given by

$$Q(\tau) = M\{f_1(\tau) - [f_1(\tau - \tau_1) + f_2(\tau - \tau_1)]U(\tau - \tau_1)\} \qquad (57)$$

where

$$f_1(\tau) = C_1(1+\rho\tau) - C_2 + C_3 e^{-\alpha\tau} + C_4 e^{-\beta\tau} + C_5 e^{-\gamma\tau}$$

$$f_2(\tau) = \tau_1\left[C_1\rho - \alpha C_3 e^{-\alpha\tau} - \beta C_4 e^{-\beta\tau} - \gamma C_5 e^{-\gamma\tau}\right]$$

$$C_1 = \frac{1}{\alpha\beta\gamma}, \quad C_2 = \frac{\rho(\alpha\beta+\alpha\gamma+\beta\gamma)}{(\alpha\beta\gamma)^2}, \quad C_3 = \frac{\rho - \alpha}{\alpha^2(\beta-\alpha)(\gamma-\alpha)}$$

$$C_4 = \frac{\rho - \beta}{\beta^2(\alpha-\beta)(\gamma-\beta)}, \quad C_5 = \frac{\rho - \gamma}{\gamma^2(\alpha-\gamma)(\beta-\gamma)}$$

Symmetrical Triangle Pulse

The Laplace transform of the Equation for $\ddot{a}$ given in Table II is

$$\ddot{a}(s) \equiv \mathcal{L}[\ddot{a}] = \ddot{a}_o \frac{1}{\omega_o} \frac{2/\tau_1}{y^2}\left(1 - 2e^{-\frac{\tau_1}{2}y} + e^{-\tau_1 y}\right) \tag{58}$$

The following table defines a quantity Q and associated multiplier M and coefficient ρ to be used in the transform and time history expressions.

Q	M	ρ
$\ddot{x}/\ddot{a}_o$	$\frac{2(N+1)}{\tau_1}$	$\frac{N}{2\zeta(N+1)}$
$-\delta\omega_o^2/\ddot{a}_o$	$2/\tau_1$	$\frac{N}{2\zeta}$

Combining Equation (58) with Equations (5) and (6) results in

$$Q(s) = \frac{1}{\omega_o} M \frac{y + \rho}{y^2\left[y^3 + \frac{N}{2\zeta} y^2 + (N+1)\ y + \frac{N}{2\zeta}\right]}\left(1-2e^{-\frac{\tau_1}{2}} y + e^{-\tau_1 y}\right) \quad (59)$$

The roots of the cubic expression in Equation (59) will be designated as y_1, y_2, and y_3.

<u>Case 1: $y_1 = -\alpha + j\beta$, $y_2 = -\alpha - j\beta$, and $y_3 = -\gamma$.</u> The inverse transform of Equation (59) was obtained using transform pair 90 [Ref. 11] and is given by

$$Q(\tau) = M[f(\tau) - 2f(\tau-\tau_1/2)U(\tau-\tau_1/2) + f(\tau-\tau_1)U(\tau-\tau_1)] \quad (60)$$

where

$$f(\tau) = C_1(\tau + C_2) + C_3e^{-\gamma\tau} + C_4e^{-\alpha\tau} \sin(\beta\tau + \psi)$$

$$C_1 = \frac{\rho}{\gamma(\alpha^2 + \beta^2)}, \quad C_2 = \frac{1}{\rho} - \frac{1}{\gamma} - \frac{2\alpha}{\alpha^2 + \beta^2}$$

$$C_3 = \frac{\rho - \gamma}{\gamma^2[(\gamma-\alpha)^2 + \beta^2]}, \quad C_4 = \frac{1}{\beta(\alpha^2+\beta^2)} \sqrt{\frac{(\rho-\alpha)^2 + \beta^2}{(\gamma-\alpha)^2 + \beta^2}}$$

$$\psi = 2 \tan^{-1} \frac{\beta}{\alpha} - \tan^{-1} \frac{\beta}{\gamma-\alpha} + \tan^{-1} \frac{\beta}{\rho-\alpha}$$

Case 2: $y_1 = -\alpha$, $y_2 = -\beta$, and $y_3 = -\gamma$. The inverse transform of Equation (59) was obtained using transform pair 31 [Ref. 11] and is given by

$$Q(\tau) = M[f(\tau) - 2f(\tau-\tau_1/2)U(\tau-\tau_1/2) + f(\tau-\tau_1)U(\tau-\tau_1)] \qquad (61)$$

where

$$f(\tau) = C_1(1 + \rho\tau) - C_2 + C_3e^{-\alpha\tau} + C_4e^{-\beta\tau} + C_5e^{-\gamma\tau}$$

$$C_1 = \frac{1}{\alpha\beta\gamma}, \quad C_2 = \frac{\rho(\alpha\beta+\alpha\gamma+\beta\gamma)}{(\alpha\beta\gamma)^2}, \quad C_3 = \frac{\rho - \alpha}{\alpha^2(\beta-\alpha)(\gamma-\alpha)}$$

$$C_4 = \frac{\rho - \beta}{\beta^2(\alpha-\beta)(\gamma-\beta)}, \quad C_5 = \frac{\rho - \gamma}{\gamma^2(\alpha-\gamma)(\beta-\gamma)}$$

Initial-Peak Saw-Tooth Pulse

The Laplace transform of the equation for $\ddot{a}$ given in Table II is

$$\ddot{a}(s) \equiv \mathcal{L}[\ddot{a}] = \ddot{a}_o \frac{1}{\omega_o}\left[\frac{1}{y} - \frac{1/\tau_1}{y^2}\left(1-e^{-\tau_1 y}\right)\right] \tag{62}$$

The following table defines a quantity Q and associated multiplier M and coefficient ρ to be used in the transform and time history expressions.

Q	M	ρ
$\ddot{x}/\ddot{a}_o$	$\frac{N+1}{\tau_1}$	$\frac{N}{2\zeta(N+1)}$
$-\delta\omega_o^2/\ddot{a}_o$	$1/\tau_1$	$\frac{N}{2\zeta}$

Combining Equation (62) with Equations (5) and (6) results in

$$Q(s) = \frac{1}{\omega_\rho} M \left\{ \frac{\tau_1 (y + \rho)}{y\left[y^3 + \frac{N}{2\zeta} y^2 + (N+1)\, y + \frac{N}{2\zeta}\right]} - \frac{y + \rho}{y^2\left[y^3 + \frac{N}{2\zeta} y^2 + (N+1)\, y + \frac{N}{2\zeta}\right]}\left(1-e^{-\tau_1 y}\right)\right\} \tag{63}$$

The roots of the cubic expression in Equation (63) will be designated as y_1, y_2, and y_3.

<u>Case 1: $y_1 = -\alpha + j\beta$, $y_2 = -\alpha - j\beta$, and $y_3 = -\gamma$.</u> The inverse transform of Equation (63) was obtained using transform pairs 90 and 86 [Ref. 11] and is given by

$$Q(\tau) = M[f_2(\tau) - f_1(\tau) + f_1(\tau-\tau_1)U(\tau-\tau_1)] \tag{64}$$

where

$$f_1(\tau) = C_1(\tau+C_2) + C_3e^{-\gamma\tau} + C_4e^{-\alpha\tau}\sin(\beta\tau+\phi)$$

$$f_2(\tau) = \tau_1\left[C_1-\gamma C_3e^{-\gamma\tau} + \sqrt{\alpha^2+\beta^2}\,C_4e^{-\alpha\tau}\sin(\beta\tau+\theta)\right]$$

$$C_1 = \frac{\rho}{\gamma(\alpha^2+\beta^2)}, \quad C_2 = \frac{1}{\rho} - \frac{1}{\gamma} - \frac{2\alpha}{\alpha^2+\beta^2}$$

$$C_3 = \frac{\rho-\gamma}{\gamma^2[(\gamma-\alpha)^2+\beta^2]}, \quad C_4 = \frac{1}{\beta(\alpha^2+\beta^2)}\sqrt{\frac{(\rho-\alpha)^2+\beta^2}{(\gamma-\alpha)^2+\beta^2}}$$

$$\phi = 2\tan^{-1}\frac{\beta}{\alpha} - \tan^{-1}\frac{\beta}{\gamma-\alpha} + \tan^{-1}\frac{\beta}{\rho-\alpha}$$

$$\theta = \tan^{-1}\frac{\beta}{\alpha-\gamma} + \tan^{-1}\frac{\beta}{\alpha} + \tan^{-1}\frac{\beta}{\rho-\alpha}$$

Case 2: $y_1 = -\alpha$, $y_2 = -\beta$, and $y_3 = -\gamma$. The inverse transform of Equation (63) was obtained using transform pairs 31 and 27 [Ref. 11] and is given by

$$Q(\tau) = M[f_2(\tau) - f_1(\tau) + f_1(\tau-\tau_1)U(\tau-\tau_1)] \tag{65}$$

where

$$f_1(\tau) = C_1(1+\rho\tau) - C_2 + C_3e^{-\alpha\tau} + C^4e^{-\beta\tau} + C_5e^{-\gamma\tau}$$

$$f_2(\tau) = \tau_1\left[C_1\rho-\alpha C_3e^{-\alpha\tau} - \beta C_4e^{-\beta\tau} - \gamma C_5e^{-\gamma\tau}\right]$$

$$C_1 = \frac{1}{\alpha\beta\gamma}, \quad C_2 = \frac{\rho(\alpha\beta+\alpha\gamma+\beta\gamma)}{(\alpha\beta\gamma)^2}, \quad C_3 = \frac{\rho - \alpha}{\alpha^2(\beta-\alpha)(\gamma-\alpha)}$$

$$C_4 = \frac{\rho - \beta}{\beta^2(\alpha-\beta)(\gamma-\beta)}, \quad C_5 = \frac{\rho - \gamma}{\gamma^2(\alpha-\gamma)(\beta-\gamma)}$$

Graphical Presentation of Results

For each pulse, the results are presented in terms of the peak values of the quantities $\ddot{x}/\ddot{a}_o$ and $\delta\,\omega_o^2/\ddot{a}_o$. The peak values are designated as a dimensionless acceleration $\ddot{x}_o/\ddot{a}_o$ and a dimensionless displacement $\delta_o\omega_o^2/\ddot{a}_o$. Both $\ddot{x}_o/\ddot{a}_o$ and $\delta_o\omega_o^2/\ddot{a}_o$ are functions of the system parameters N and ζ, and of the nondimensional pulse duration $\tau_1 = \omega_o t_1$. In the presentation of the results, the stiffness ratio N takes on the values 1, 3, 8, 24, and ∞. The viscous damping ratio ζ takes on the values 0, 0.1, 0.2, 0.3, 0.5, 1, 2, 5, 10, and ∞ for the finite values of N and the values 0, 0.1, 0.5, and 1 for $N = \infty$. The dimensionless acceleration $\ddot{x}_o/\ddot{a}_o$ and the dimensionless

displacement $\delta_o \omega_o^2/\ddot{a}_o$ are plotted versus a time ratio t_1/T where $T = 2\pi/\omega_o$ (i.e., $t_1/T = \tau_1/2\pi$). For each graph there is a particular value of the stiffness ratio N and each curve on the graph is for a particular value of the viscous damping ratio ζ. The results are presented for the six pulses in the following order: half-cycle sine, rectangular, versed-sine, terminal-peak saw-tooth, symmetrical triangle, and initial-peak saw-tooth. Each pulse has ten graphs associated with it in the following order: the dimensionless acceleration for the five values of N, and the dimensionless displacement for the five values of N. Hence, there are a total of 60 shock spectra graphs comprising Figures 26 through 85.

Numerical Procedures.-For the finite values of N, the results were obtained using a digital computer and the graphs were plotted automatically. It was determined that at least 150 points per curve were necessary to adequately define each curve. There are two response quantities, four values of N, ten values of ζ, and 150 points per curve for each of the six pulse shapes. Therefore, 72,000 time histories were analyzed to determine their peak values. Since there are so many time histories it is important to determine a fairly simple automated procedure to find their maximum value.

The procedure of setting the derivative of the time history to zero, solving for the time, and then substituting the time into the original equation was not used for two reasons: (1) the equations to be solved are fairly complicated transcendental equations; and (2) most of the time histories have many local maxima and minima so that the transcendental equation would have to be solved many times to find the global maximum. Instead, the problem was first set up on an analog computer and estimates were made of where the maximum would occur in time, and how fast the function was varying with time. Then values of the time history were computed over a range including the estimated time of the maximum value.

For those time histories that had sharp peaks at their maximum value an approximate damped natural frequency was determined, using the undamped natural frequency expression and substituting the real part of the complex stiffness of the system for the stiffness K of the undamped system. This resulted in a damped natural frequency ω_d that was related to the undamped natural frequency ω_o as follows [Ref. 12]

$$\left(\frac{\omega_d}{\omega_o}\right)^4 + \left[\left(\frac{N}{2\zeta}\right)^2 - (N+1)\right]\left(\frac{\omega_d}{\omega_o}\right)^2 - \left(\frac{N}{2\zeta}\right)^2 = 0 \tag{66}$$

Solving this equation, and using the definitions $T_d = 2\pi/\omega_d$; $T = 2\pi/\omega_o$; $A = \left[\frac{N}{2\zeta}\right]^2$; and $B = N + 1$, the expression for the damped natural period is given by:

$$T_d = \frac{\sqrt{2}}{\sqrt{B-A + \sqrt{(B-A)^2 + 4A}}}\, T \tag{67}$$

Since the time histories are written in terms of a nondimensional time $\tau = \omega_o t$, it is desirable to define a nondimensional natural period as

$$\tau_d \equiv \omega_o T_d \tag{68}$$

To achieve the desired degree of accuracy (approximately one percent error) it was found by trial and error that 20 points per period were necessary. A nondimensional time increment $\Delta\tau$ was determined from Equations (67) and (68) as follows

$$\Delta\tau = \frac{\sqrt{2}\,(2\pi)/20}{\sqrt{B-A + \sqrt{(B-A)^2 + 4A}}} \tag{69}$$

where

$$A = (N/2\zeta)^2 \ , \ B = N + 1$$

The damped free vibration natural frequency (i.e., the imaginary part of the complex roots obtained from the characteristic equation) cannot be used to determine $\Delta\tau$. For the overdamped condition, the damped free vibration natural frequency does not exist. When the system is close to being critically damped, this frequency is very low, and is not at all indicative of how fast the system can respond to the input.

When the time history was being computed, the maximum value as well as the values on each side of maximum were determined. A parabola was then passed through these three points, and the peak value of the parabola was taken as the maximum value of the time history.

Comparison to Impulse Response

As the pulse duration t_1 becomes very small compared to the natural period T, the response cannot follow the input and the input becomes essentially an impulse. On the graphs, the straight line asymptotes that the curves follow as $t_1/T \to 0$, are the curves that would be obtained if the pulses were considered as impulses.

From Figure 6, for some particular values of N and ζ, there will be a particular value, say Q_1, for the quantity $\ddot{x}_o/\omega_o V$. In equation form

$$\frac{\ddot{x}_o}{\omega_o V} = Q_1(N, \zeta) \tag{70}$$

From Table II, $V = \frac{2}{\pi} \ddot{a}_o t_1$ for the half-cycle sine pulse. Using $\omega_o = 2\pi/T$, Equation (70) can be rewritten as

$$\frac{\ddot{x}_o}{\ddot{a}_o} = 4Q_1(N, \zeta)\ t_1/T \tag{71}$$

Equation (71) is the equation for the straight line asymptotes in Figures 26 to 29. Similarly the equation for the straight line asymptotes for the rectangular pulse is

$$\frac{\ddot{x}_o}{\ddot{a}_o} = 2\pi Q_1(N, \zeta)\ t_1/T \tag{72}$$

and the equation for the straight line asymptotes for the versed-sine, terminal-peak saw-tooth, symmetrical triangle, and initial-peak saw-tooth pulses is

$$\frac{\ddot{x}_o}{\ddot{a}_o} = \pi Q_1(N, \zeta)\ t_1/T \tag{73}$$

Since most of the shock spectra curves for $\ddot{x}_o/\ddot{a}_o$ are essentially straight lines below $\ddot{x}_o/\ddot{a}_o = 1$, which is the shock isolation region, the pulse can be considered as an impulse in this region and all of the results in the section dealing with the response of the system to an impulse are applicable. This is a fortunate result, since if the isolation system is being designed primarily to isolate one of these pulses, certainly the desired value of $\ddot{x}_o/\ddot{a}_o$ would be less than unity. Therefore, the shock spectra graphs (Figures 26 through 85) would be used primarily for analysis of shock response of a system designed to provide vibration isolation

RESULTS AND CONCLUSIONS

The results of this investigation of an isolation system using relaxation type damping are:

(1) Determination and graphical presentation of the regions where the system is underdamped and overdamped as a function of the system parameters.

(2) Expressions and graphical presentation for the acceleration of the mass and the deflection of the isolator in response to an impulse acceleration of the foundation.

(3) Optimization of the parameters for the impulse response according to the criteria: for a given input and maximum deflection of the isolator, minimize the maximum acceleration of the isolated mass.

(4) Presentation of trade-off limit curves for the optimized system.

(5) Same as (2), (3), and (4) above except that the input is white noise acceleration of the foundation and the responses are the RMS levels of the acceleration of the mass and the deflection of the isolator.

(6) Expressions and graphical presentation for the acceleration of the mass and the deflection of the isolator in response to six acceleration pulses of the foundation as follows: half-cycle sine, rectangular, versed-sine, terminal-peak saw-tooth, symmetrical triangle, and initial-peak saw-tooth.

(7) Comparison of the pulse excitation responses to the impulse responses.

Specific conclusions drawn are:

(1) For values of the stiffness ratio N less than eight, the system is underdamped regardless of the value of the viscous damping ratio ζ; for values of N greater than eight there are two values of ζ for which the system is critically damped and the system is overdamped for values of ζ between these two values.

(2) The optimum value of the viscous damping ratio ζ is different for different criteria. In this report, five different criteria were used resulting in the five different curves shown in Figures 10, 12, 19, and 23. Also, these curves differ from similar optimum viscous damping ratio curves obtained by minimizing the resonant response to sinusoidal vibration [Ref. 13].

(3) The optimum value of the stiffness ratio N was found to be infinity for both the impulse response and random vibration using the criteria: for a given impulse (white noise) input and a maximum (RMS level) deflection of the isolator, minimize the maximum (RMS level) acceleration of the mass. The optimum values of the viscous damping ratio corresponding to $N = \infty$ are $\zeta_{op} = 0.4$ for impulse response and $\zeta_{op} = 0.707$ for random vibration. However, both of these isolation systems would make very poor high frequency vibration isolators.

(4) Comparing the optimum relaxation system for impulse response in (3) above to the best possible system, showed that the optimum relaxation system was only 4 percent worse (i.e., for a given input and deflection, the acceleration was only 4 percent greater than the acceleration obtained by the best possible system). The best possible isolator for this criteria is a constant force device (e.g., Coulomb friction damper or crushing material). Unless an active

mechanism is employed, the constant force device does not return to its initial position whereas the system with a spring and viscous damper does. Another distinction is that if the input were doubled, both the acceleration and deflection of the system with the spring and damper would be doubled whereas, for the system with a constant force device, the acceleration would stay the same and the deflection would be quadrupled.

(5) The optimum relaxation system for random vibration in (3) above is identical to the best possible linear system for this criteria [Ref. 9].

(6) The optimum values of N and ζ for both impulse response and random vibration are not dependent on the desired trade-off between acceleration and deflection. The trade-off between acceleration and deflection is dependent only on the undamped natural frequency ω_o and the magnitude of the input.

(7) The optimum solutions for both impulse response and random vibration are not overly sensitive to changes in the parameters N and ζ from their optimum values. This sensitivity is depicted in Figure 11 (impulse response) and Figure 22 (random vibration).

(8) In the region of shock isolation (i.e., for the peak acceleration of the mass less than the peak input acceleration) the responses to the six pulses are essentially equal to the impulse responses. Therefore, in this region all of the results for the impulse response, including the optimizations, are applicable to the responses to the pulses.

A final comment must be made regarding the selection of values of N other than $N = \infty$. The difference between the vibration isolators shown in Figures 1(a) and (b), and the

conventional model of an isolator (i.e., a spring and damper in parallel) can be thought of in terms of the stiffness ratio N. If $N = \infty$, both systems shown in Figure 1 reduce to the conventional model. Values of N other than $N = \infty$ have to be considered since: (1) many isolation systems can be represented by models having a finite value of N; and (2) there are certain desirable features of an isolation system having a finite value of N.

An example of an isolation system having a finite value of N is one that uses an elastomer as a resilient element. Elastomers can be very effectively modeled by the systems shown in Figure 1, but not by the conventional model [Ref. 4]. Another example is the suspension system of automobiles. This system can be represented by the model shown in Figure 1(b) where k represents the stiffness of the suspension system and Nk represents the stiffness of the tires. To obtain a value of N equal to infinity, the tires would have to be infinitely stiff.

One desirable feature of an isolation system employing an elastically coupled damper resides in the fact that it acts as though it were undamped for high frequency excitation but damped at resonance, thereby giving good high frequency isolation while controlling the maximum response at resonance. Another desirable feature is that a finite value of N greatly reduces the jerk (i.e., the derivative of acceleration) of the isolated mass. If the isolated mass happens to be a human, this results in a much more comfortable ride.

Therefore, although in the examples discussed for the impulse response and random vibrations the optimum value of N is $N = \infty$, the results are shown as a function of N since they would be useful in many actual design applications.

REFERENCES

1. Ruzicka, Jerome E.: Resonance Characteristics of Unidirectional Viscous and Coulomb-Damped Vibration Isolation Systems. Trans. ASME, Vol. 89, Series B, No. 4, Nov. 1967, p. 729.

2. de Carbon, C.B.: Perfectionnement a la Suspension des vehicules routiers. Amortisseur a relaxation. Comptes-Rendus de l'Academie des Sciences de Paris, France, Vol. 225, 1947, pp. 722-724.

3. Gallagher, J.; and Volterra, E.: Mathematical Analysis of the Relaxation Type of Vehicle Suspension. J. Appl. Mech., Trans. ASME, Vol. 74, 1952, pp. 389-396.

4. Newton, R. E.; and Matthews, L. E.: Representing Frequency Response Characteristics of Elastomers for Shock Isolation. SAE Preprint No. 236B, For Presentation at the SAE National Aeronautic Meeting, The Ambassador, Los Angeles, Calif., Oct. 10-14, 1960.

5. Yamakawa, I.: On the Free Vibration and the Transient State of One-Degree-of-Freedom System with Elastically Supported Viscous Damper. Jour. Japan Soc. Mech. Engrs., Vol. 4, No. 16, 1961, pp. 641-644.

6. Snowdon, J. C.: Vibration and Shock in Damped Mechanical Systems. John Wiley & Sons, New York, 1968, pp. 33-38, 397-405.

7. Karnopp, D. C.; and Trikha, A. K.: Comparative Study of Optimization Techniques for Shock and Vibration Isolation. Air Force Office of Scientific Research, AFOSR 68-0242, Jan. 1968.

8. Crandall, S. H.; and Mark, W. D.: Random Vibration in Mechanical Systems. Academic Press, New York, 1963, p. 28.

9. Trikha, A. K.; and Karnopp, D. C.: A New Criterion for Optimizing Linear Vibration Isolator Systems Subject to Random Input. ASME Paper No. 69-Vibr-45, Presented at the Vibration Conference, Philadelphia, Pa., March 30-April 2, 1969.

10. Aseltine, John A.: Transform Method in Linear System Analysis. McGraw-Hill Book Co., Inc., 1958, p. 108.

11. Langill, A. W., Jr.: Automatic Control Systems Engineering. Vol. 1. Prentice Hall, Inc., 1965, pp. 306-363.

12. Derby, Thomas F.; Ruzicka, Jerome E.: Loss Factor and Resonant Frequency of Viscoelastic Shear-Damped Structural Composites. NASA CR-1269, 1969.

13. Ruzicka, Jerome E.; Cavanaugh, Richard D.: New Method for Vibration Isolation. Machine Design, October 16, 1958, pp. 114-121.

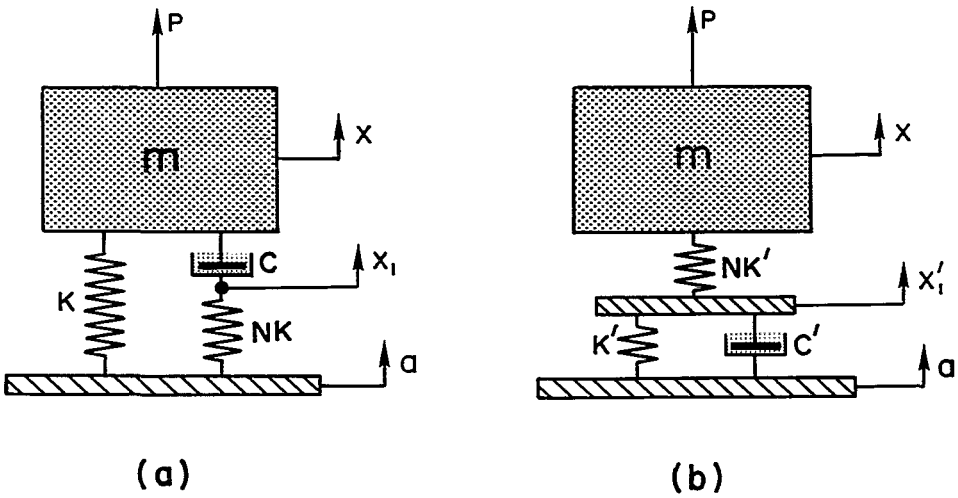

Figure 1.-Schematic diagrams of isolation systems with elastically coupled viscous damping

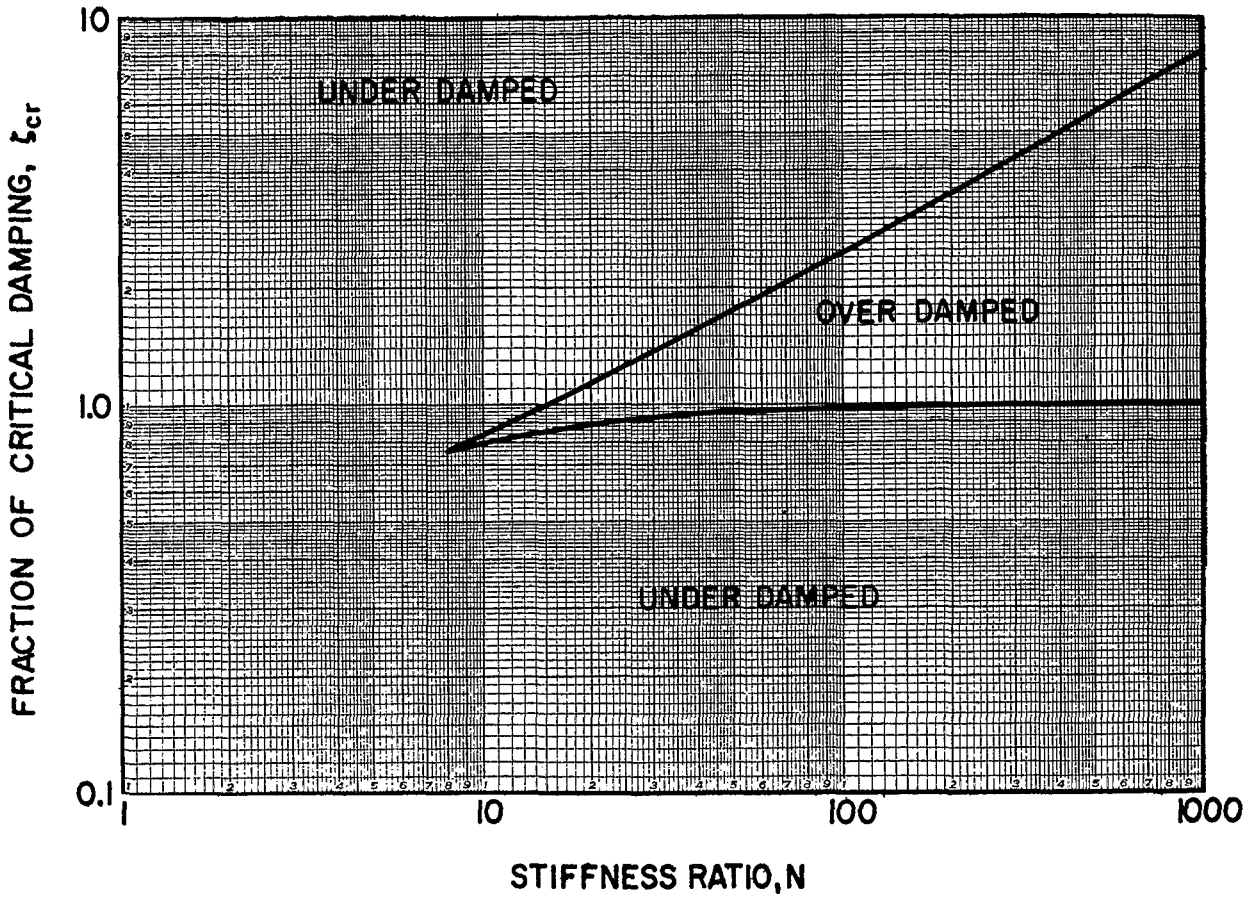

Figure 2.-Fraction of critical damping for the isolation system shown in Figure 1(a)

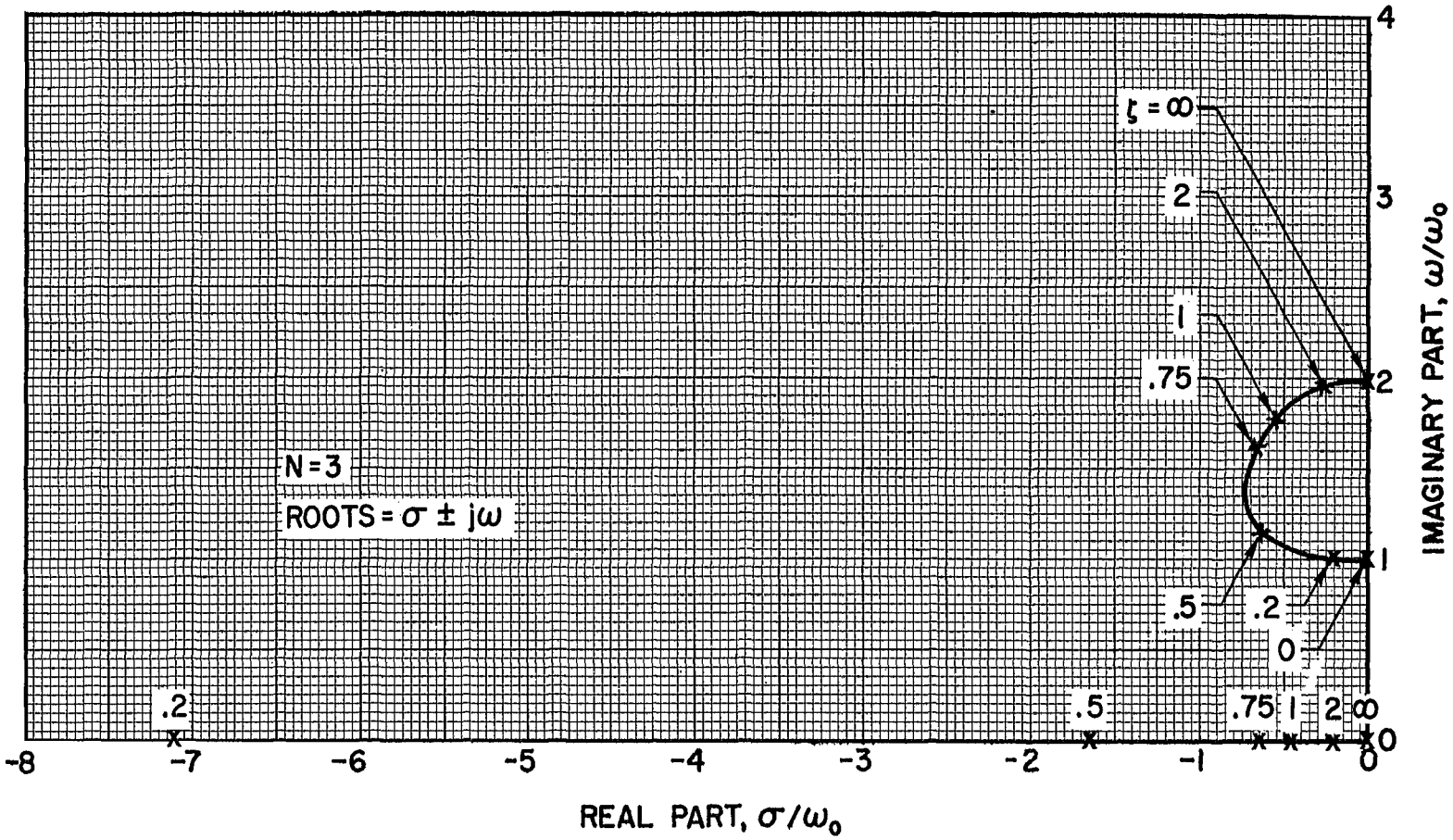

Figure 3.-Root locus plot of the denominator of Equations (5) and (6) with N = 3

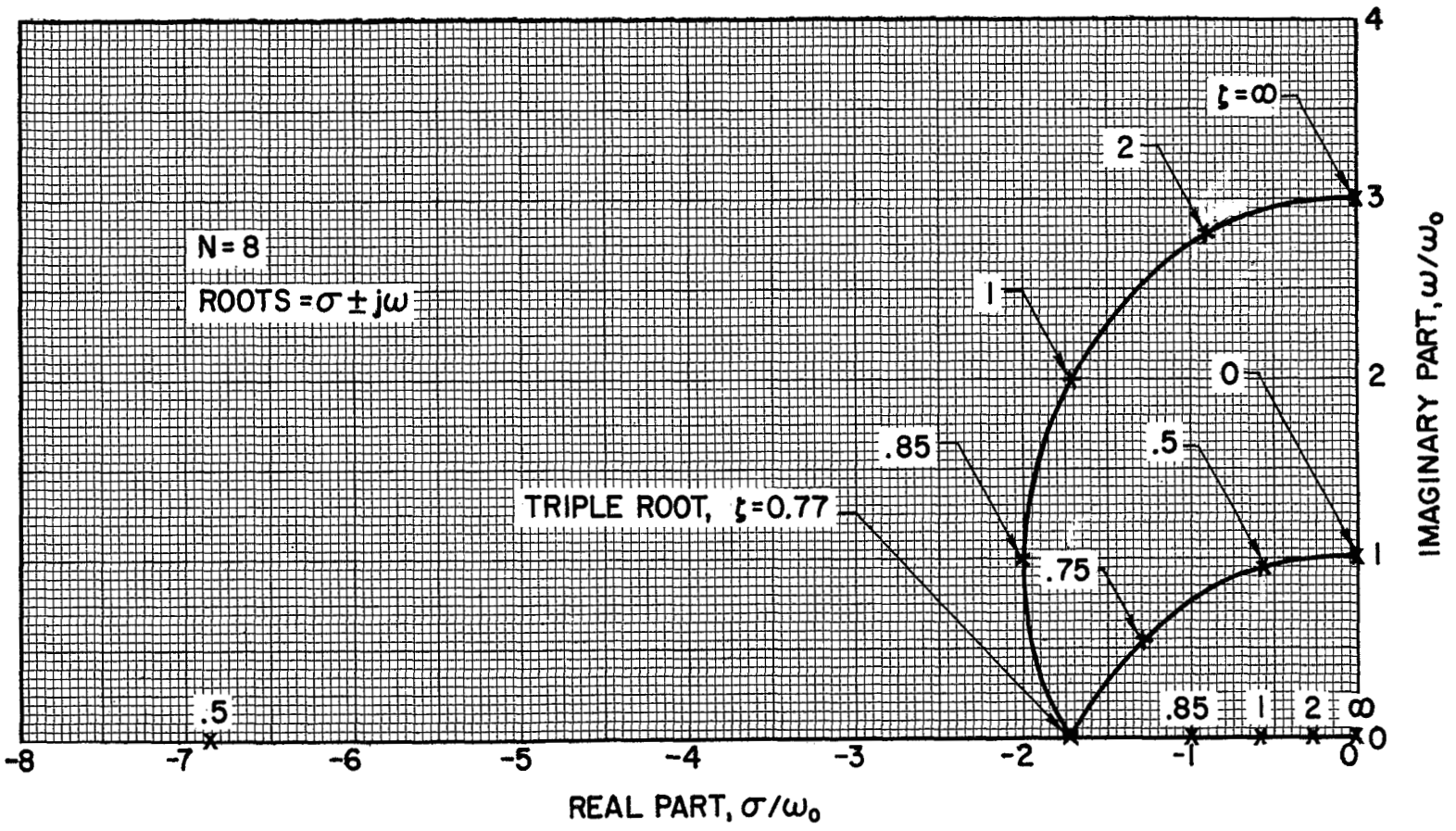

Figure 4.-Root locus plot of the denominator of Equations (5) and (6) with N = 8

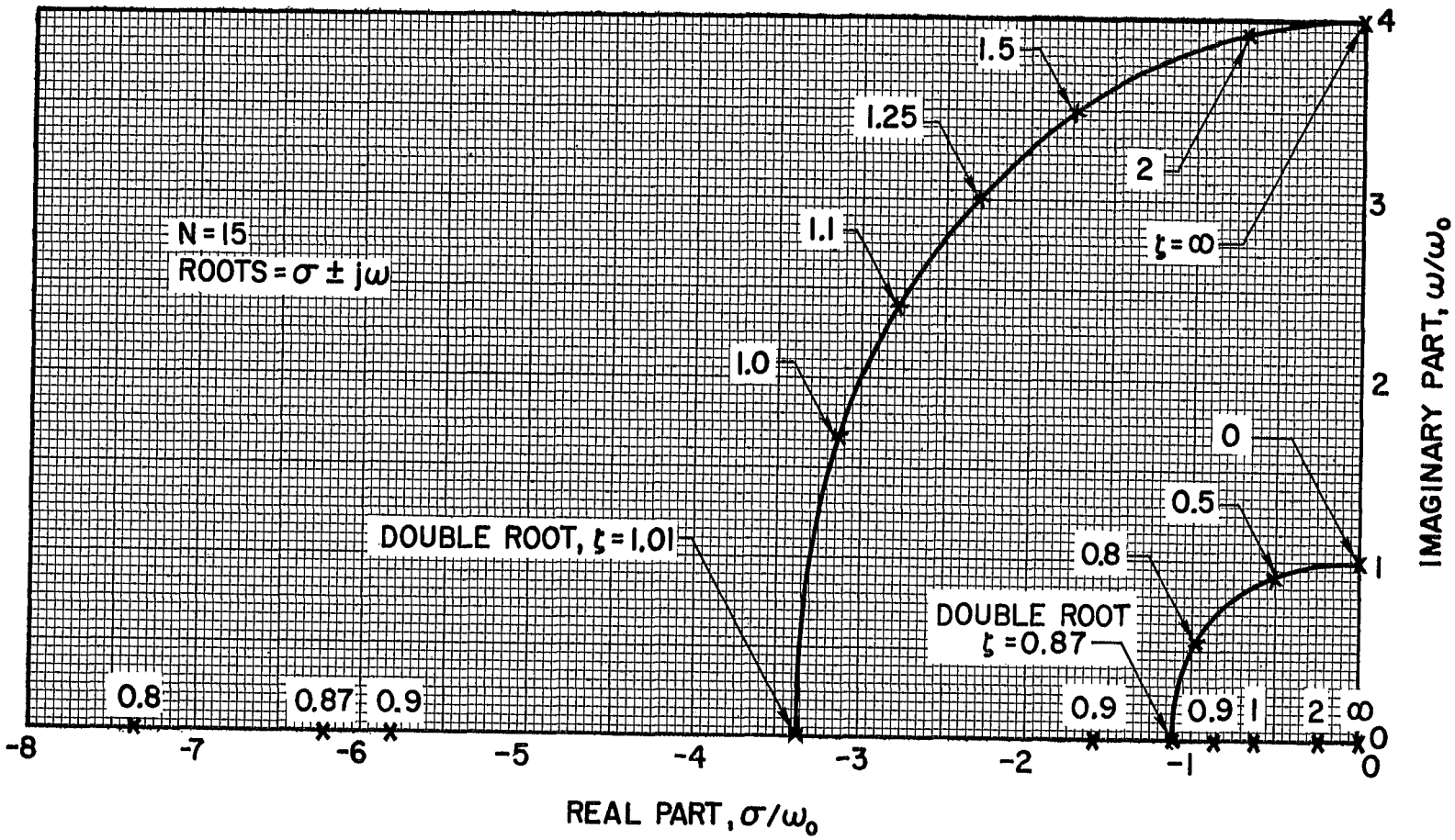

Figure 5.-Root locus plot of the denominator of Equations (5) and (6) with N = 15

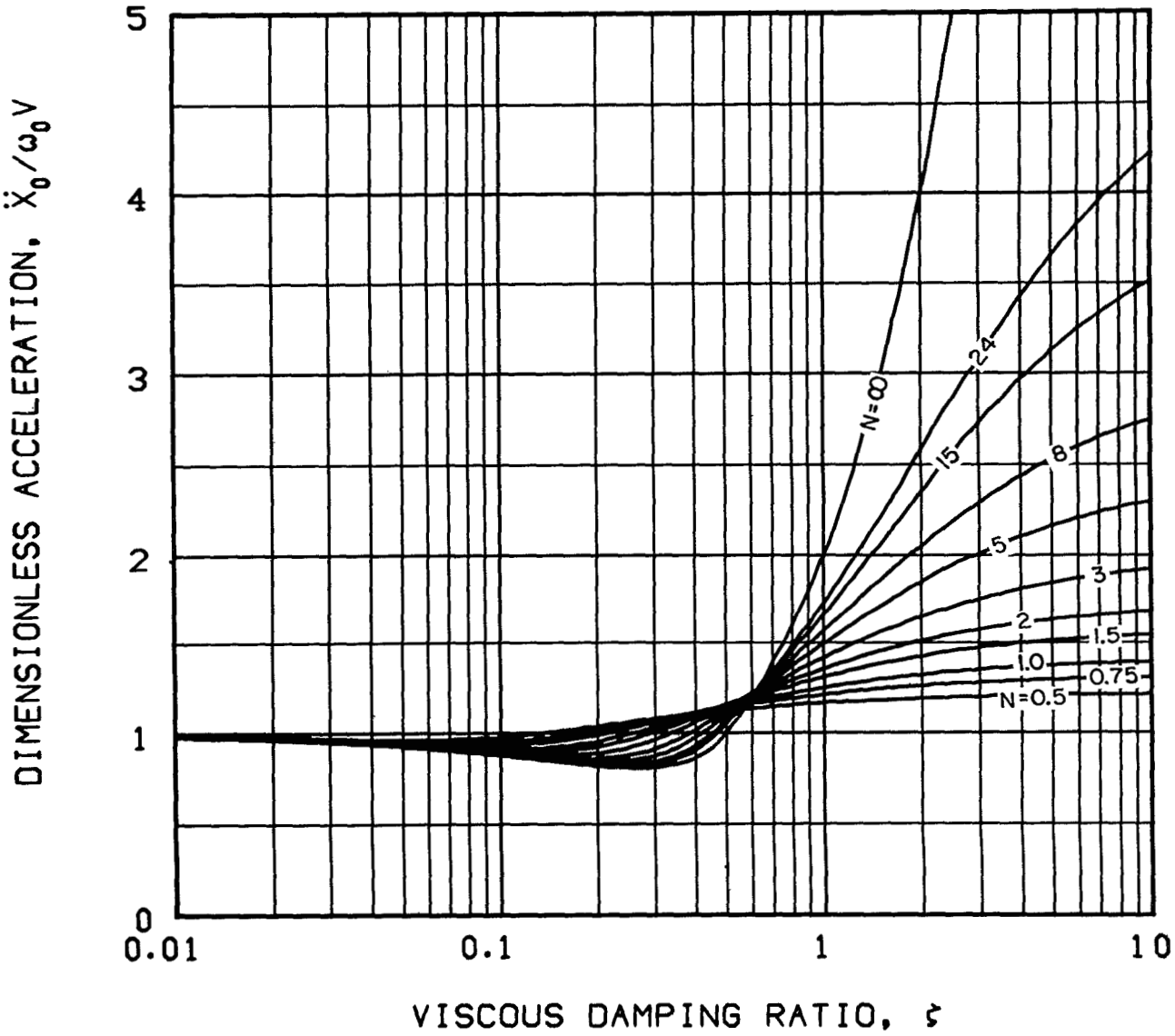

Figure 6.-Acceleration response to a velocity step for the isolation system shown in Figure 1(a)

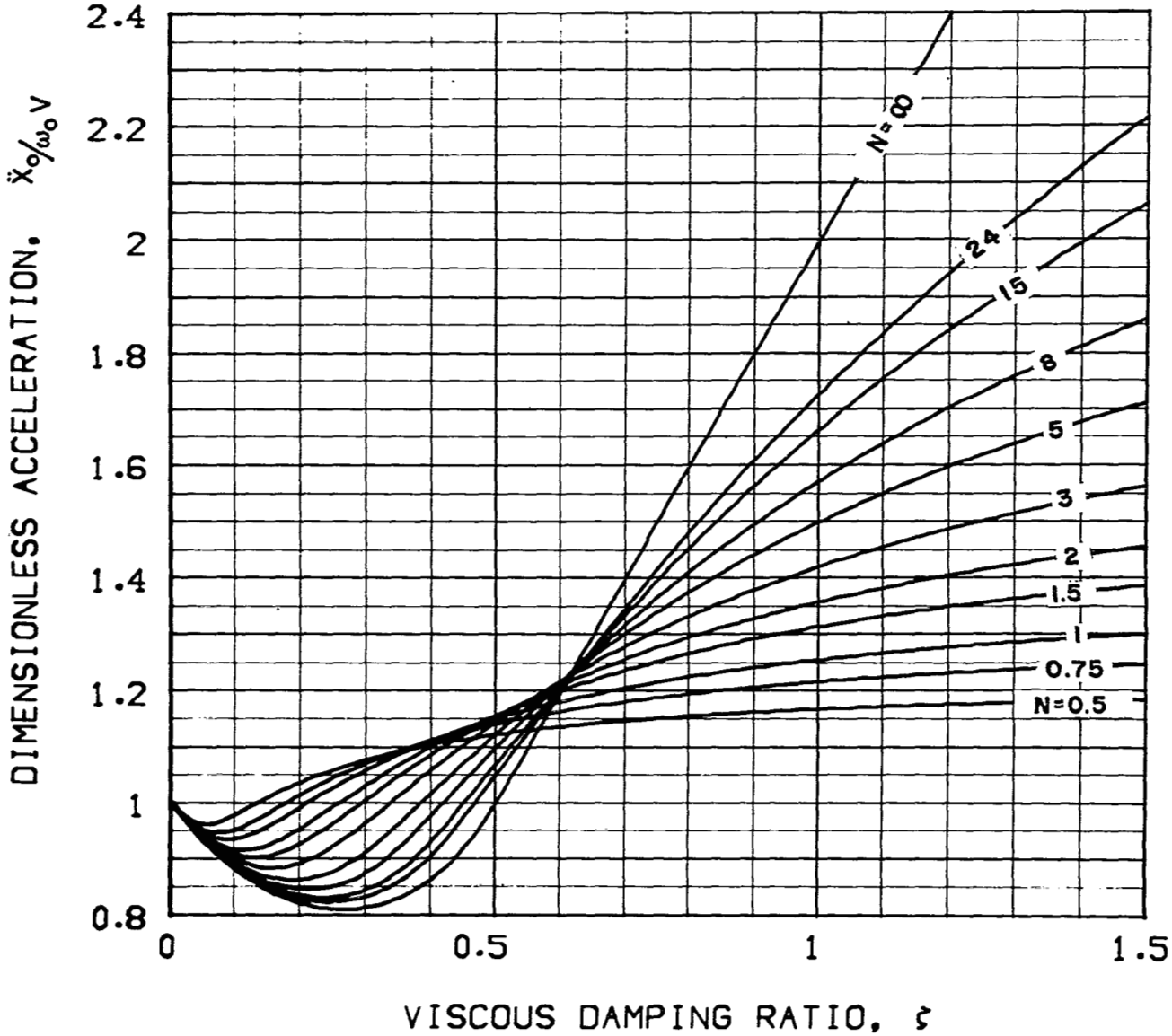

Figure 7.-Acceleration response to a velocity step for the isolation system shown in Figure 1(a) (Figure 6 expanded)

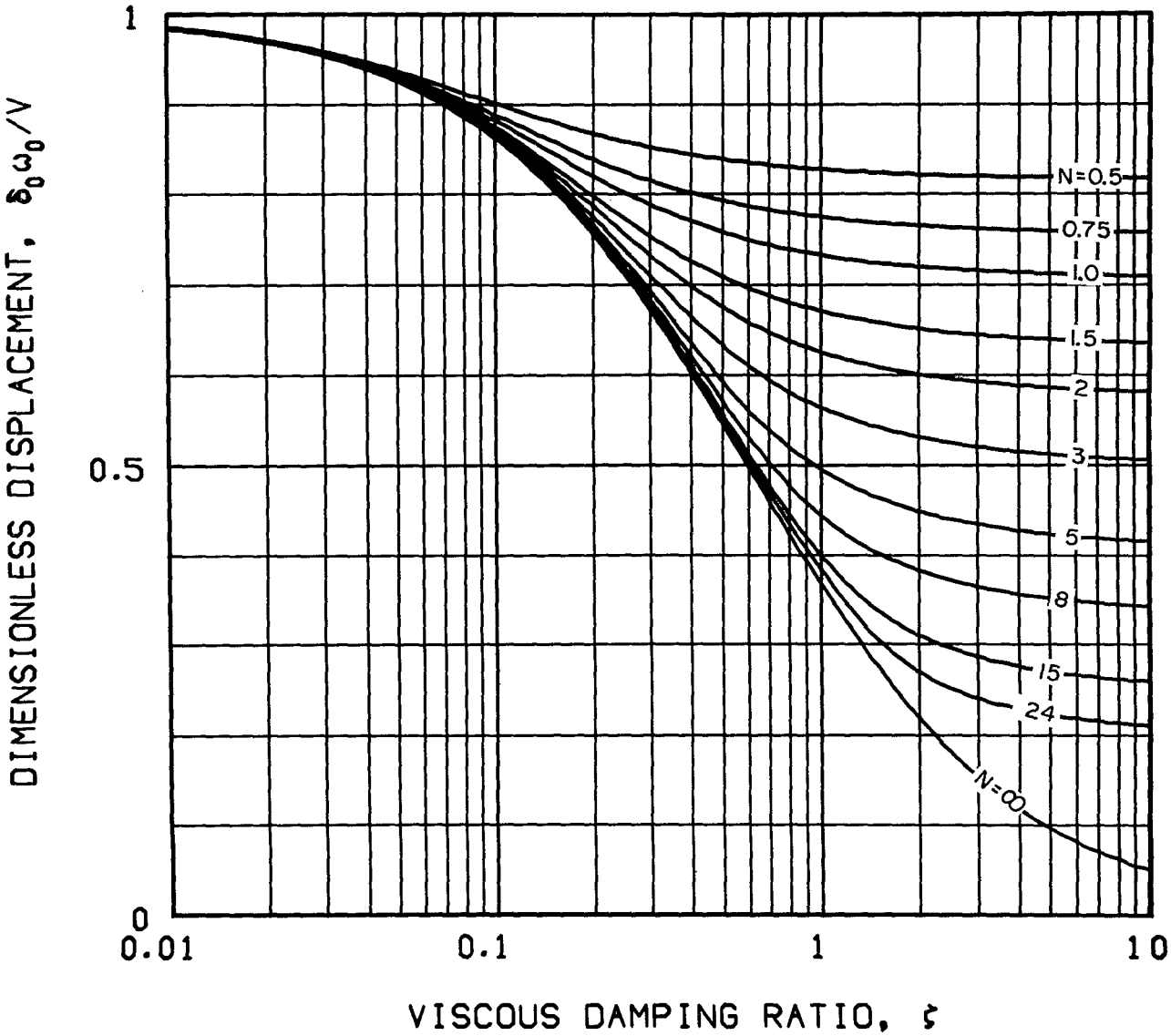

Figure 8.-Displacement response to a velocity step for the isolation system shown in Figure 1(a)

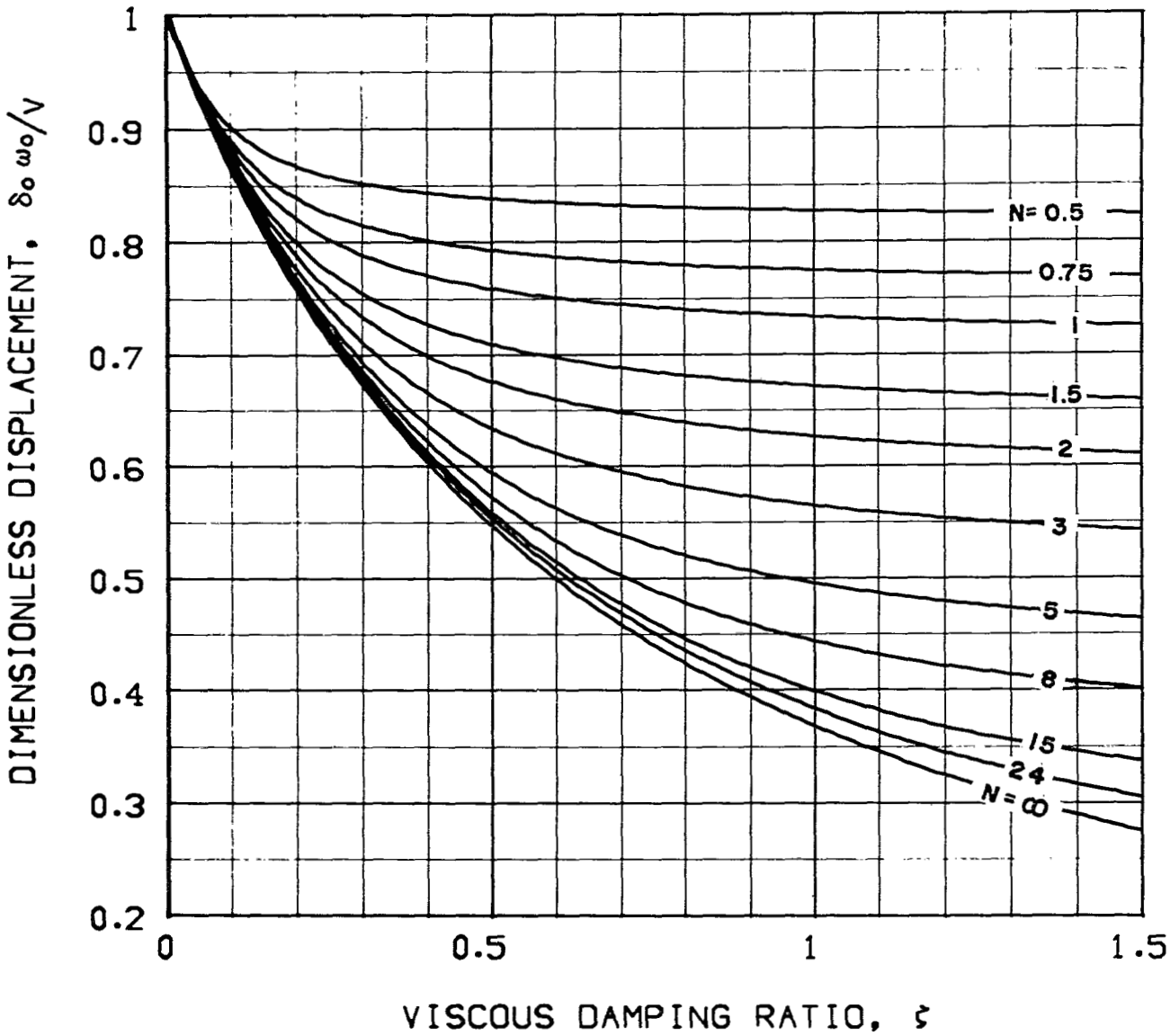

Figure 9.-Displacement response to a velocity step for the isolation system shown in Figure 1(a) (Figure 8 expanded)

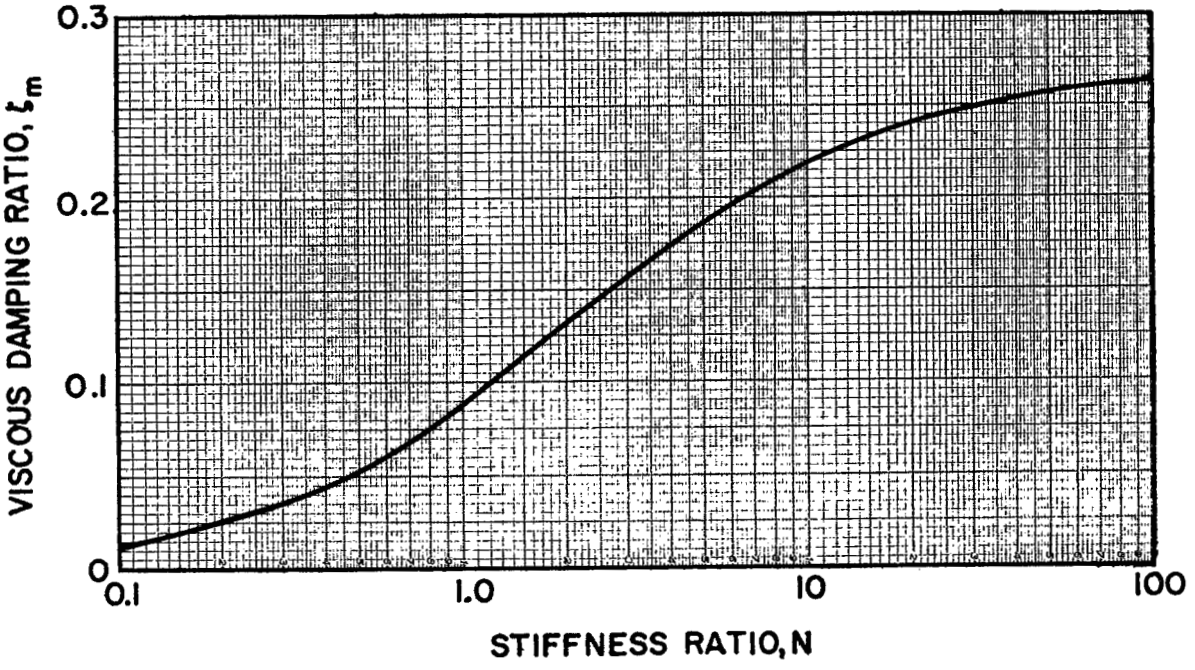

Figure 10.-Viscous damping ratio that minimizes the values of the dimensionless acceleration (Figure 7)

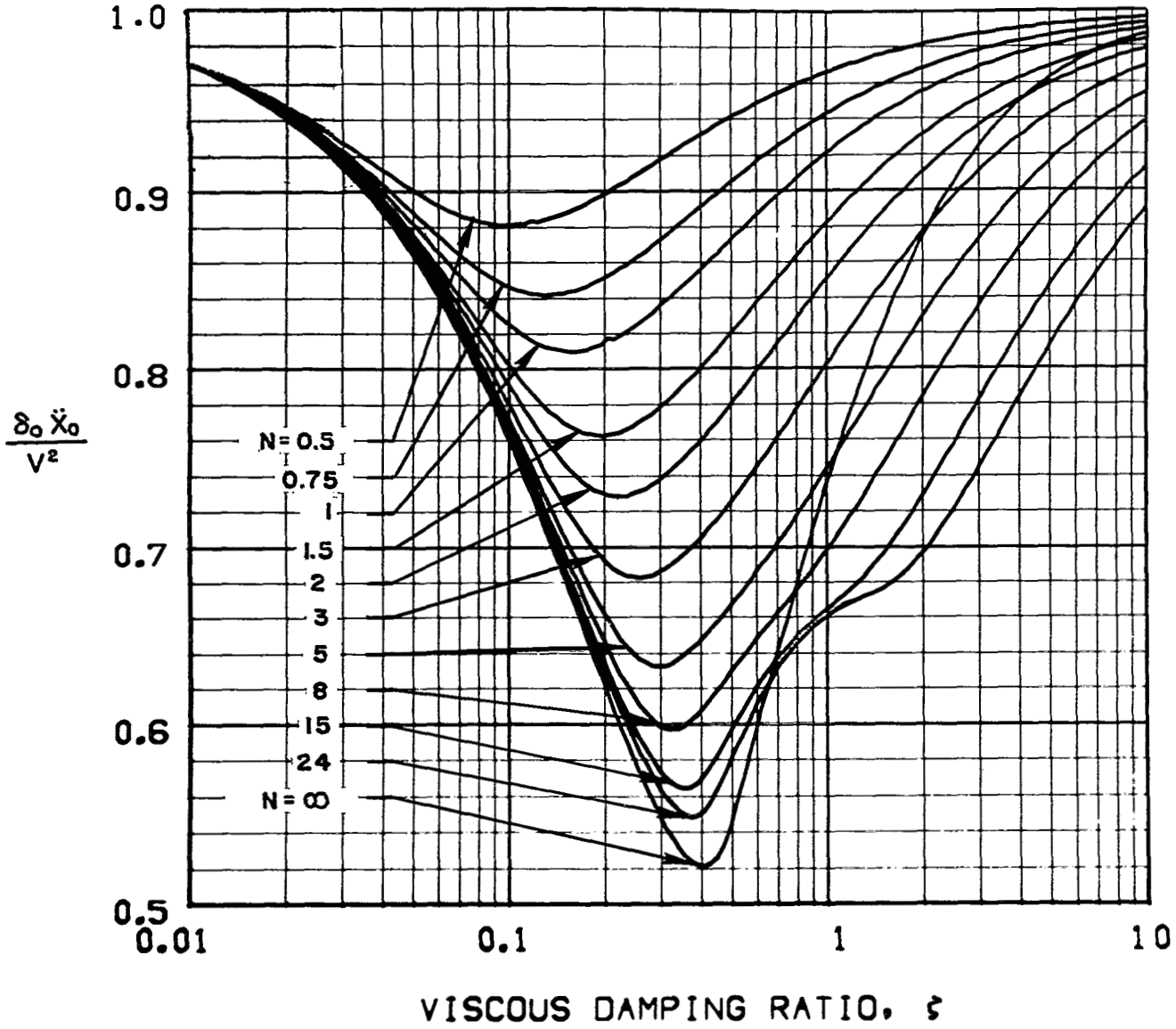

Figure 11.-The displacement times the acceleration divided by the velocity step squared for the isolation system shown in Figure 1(a)

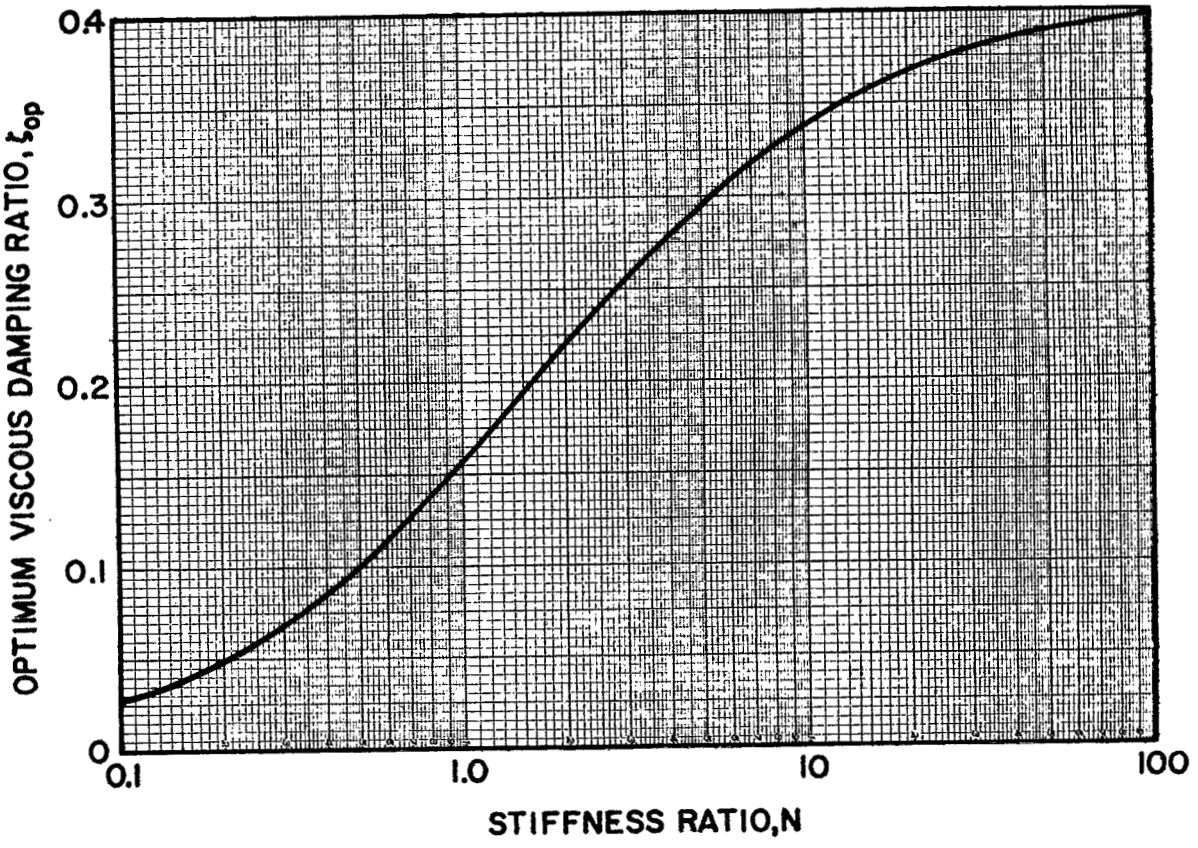

Figure 12.-Optimum viscous damping ratio obtained by minimizing the parameter $\delta_o \ddot{x}_o/V^2$ (Figure 11)

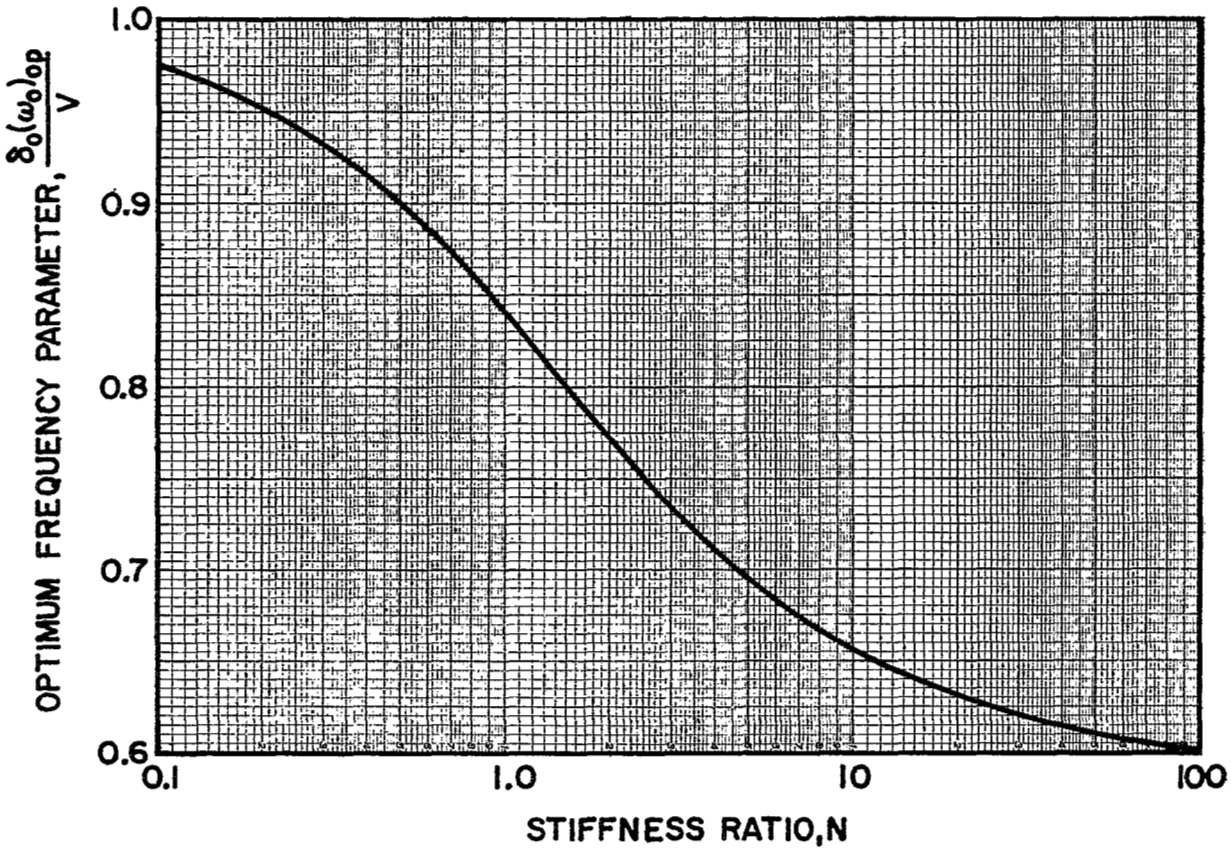

Figure 13.-Optimum frequency parameter obtained by using the optimum viscous damping ratio (Figure 12) with the dimensionless displacement (Figure 9)

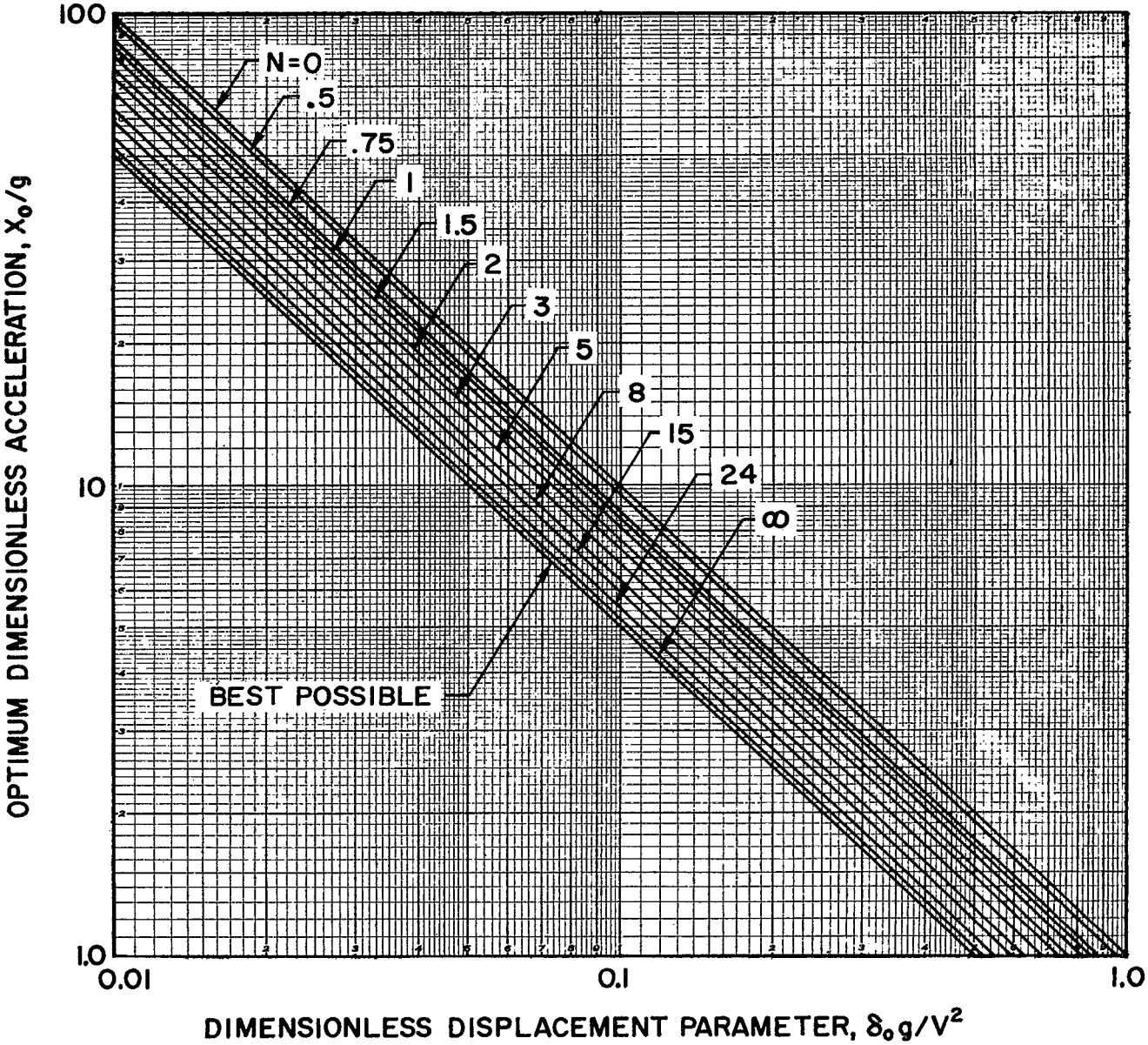

Figure 14.-Trade-off limit curves for the response to a velocity step of the isolation system shown in Figure 1(a)

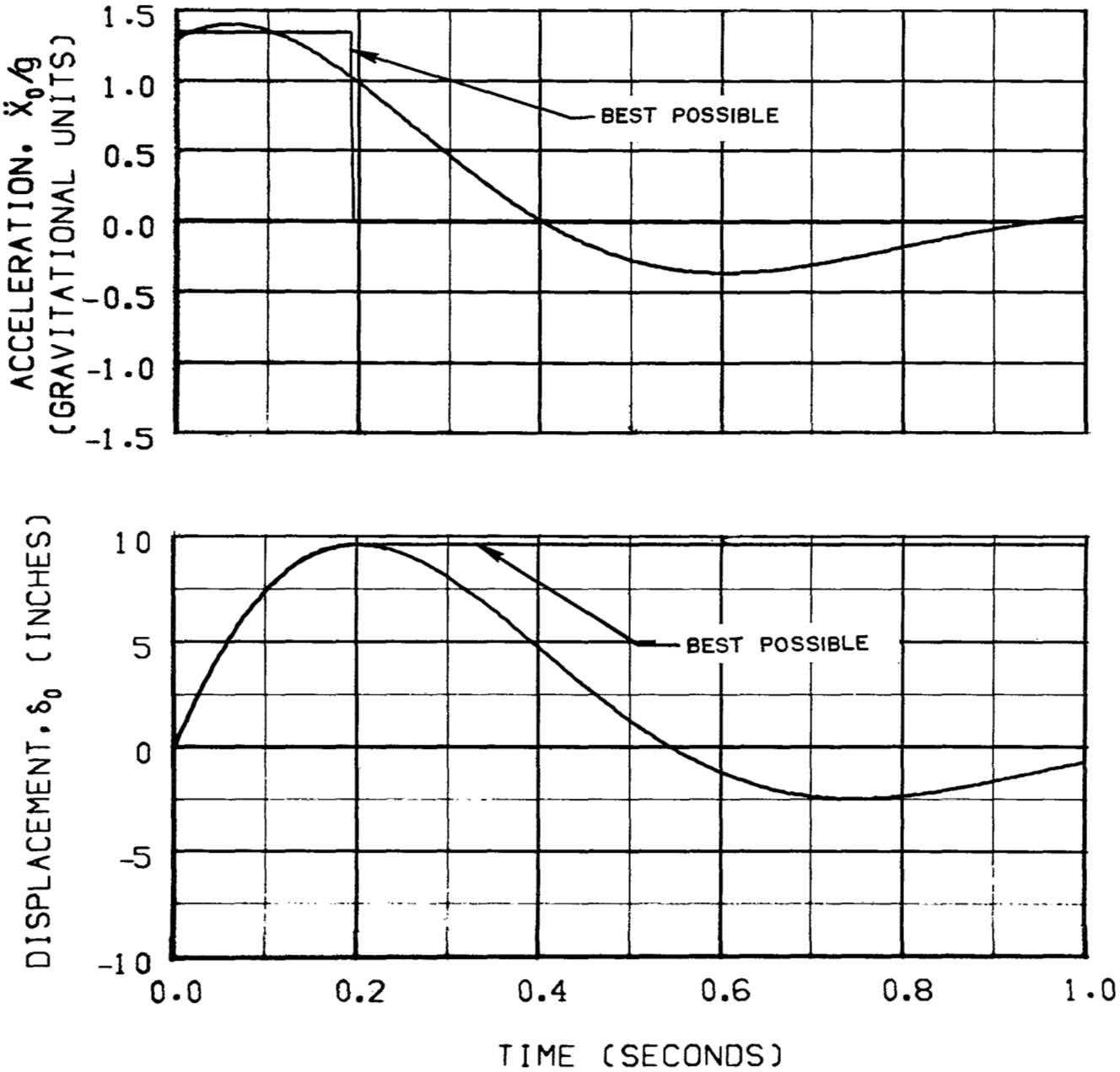

Figure 15.-Time histories of acceleration and displacement in response to a velocity step of 100 in/sec where $N = \infty$, $\zeta = 0.4$, and $\omega_o = 2\pi$ rad/sec compared to the best possible solution

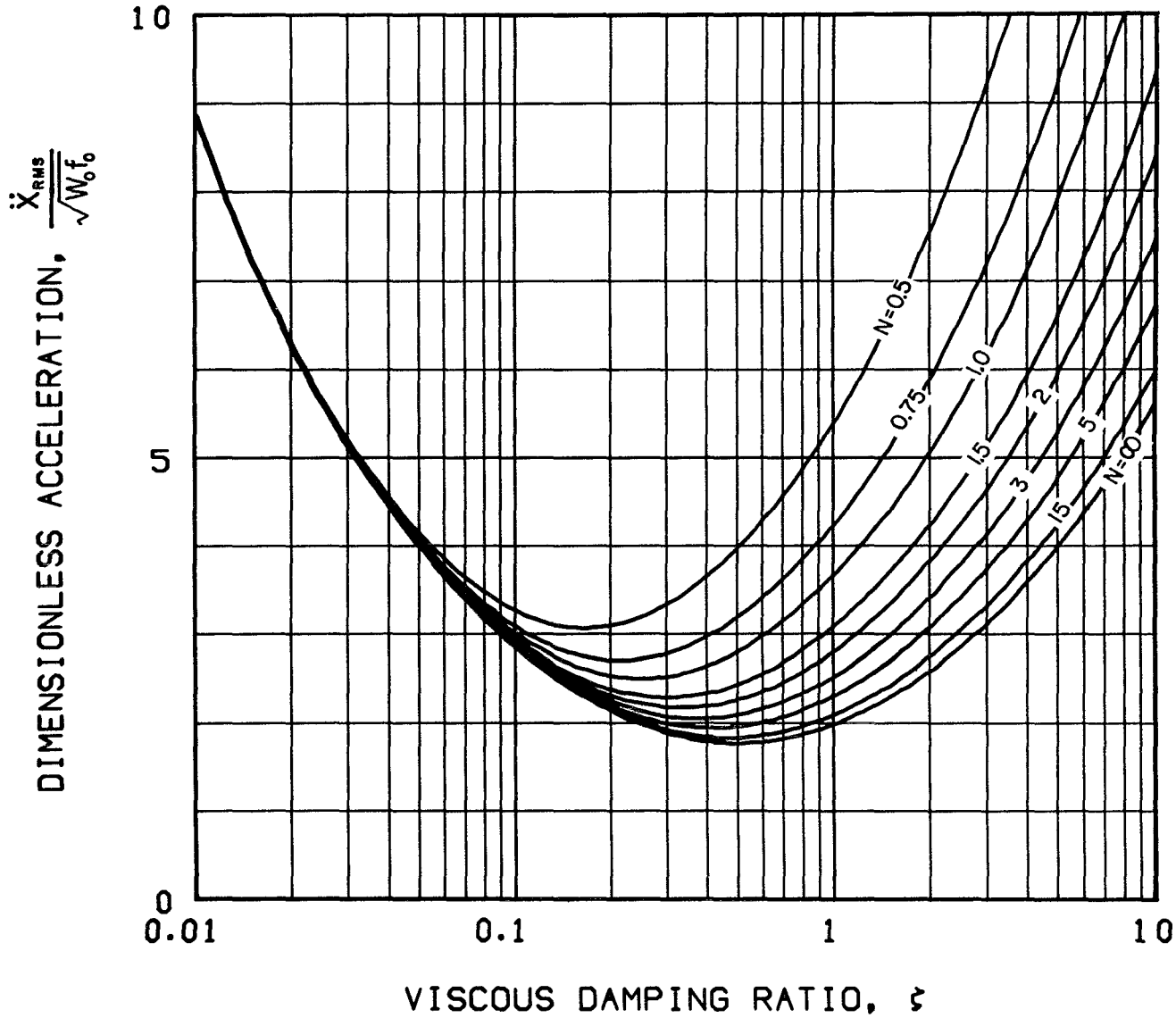

Figure 16.-RMS acceleration response to white noise acceleration input for the isolation system shown in Figure 1(a)

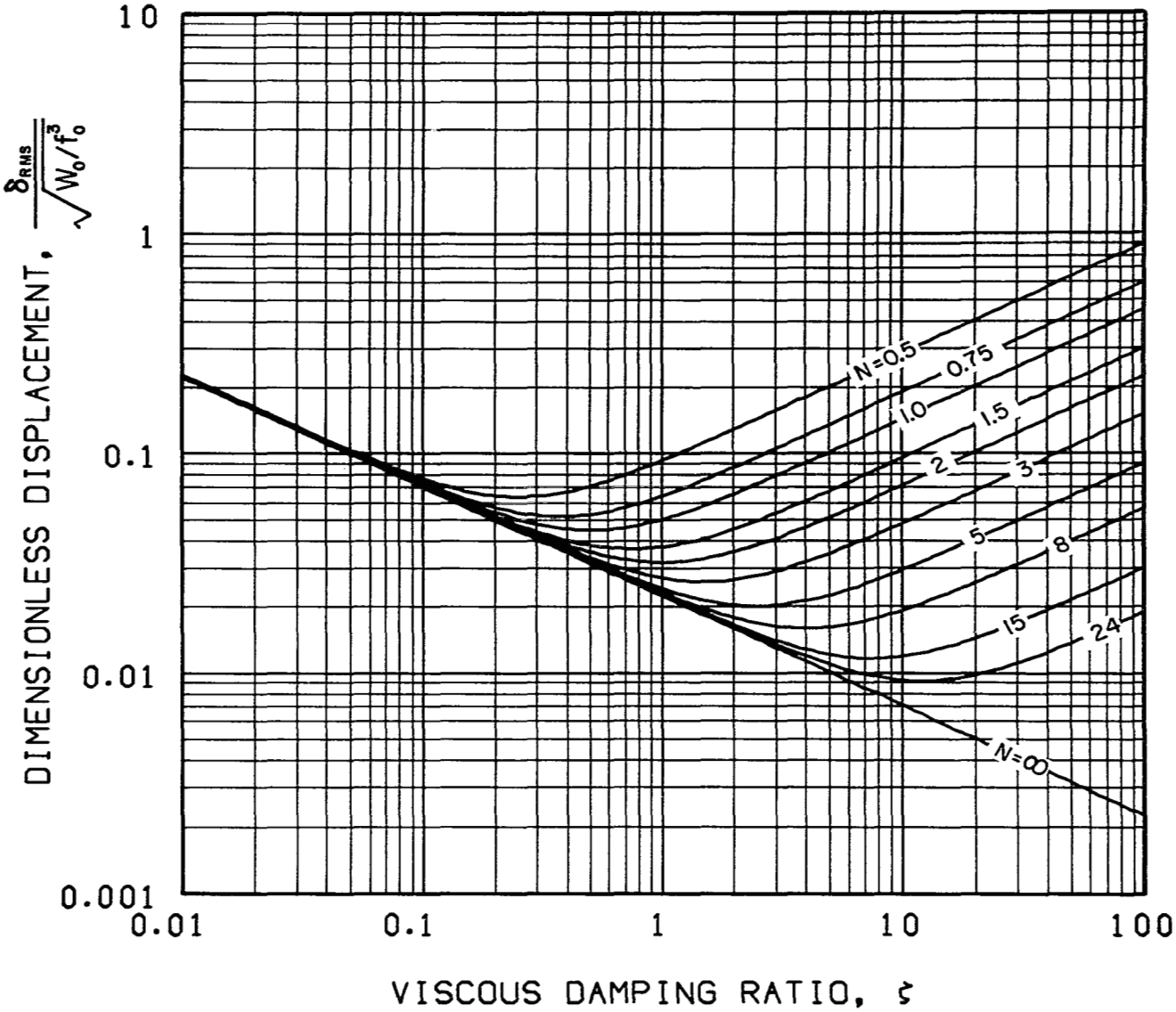

Figure 17.-RMS displacement response to white noise acceleration input for the isolation system shown in Figure 1(a)

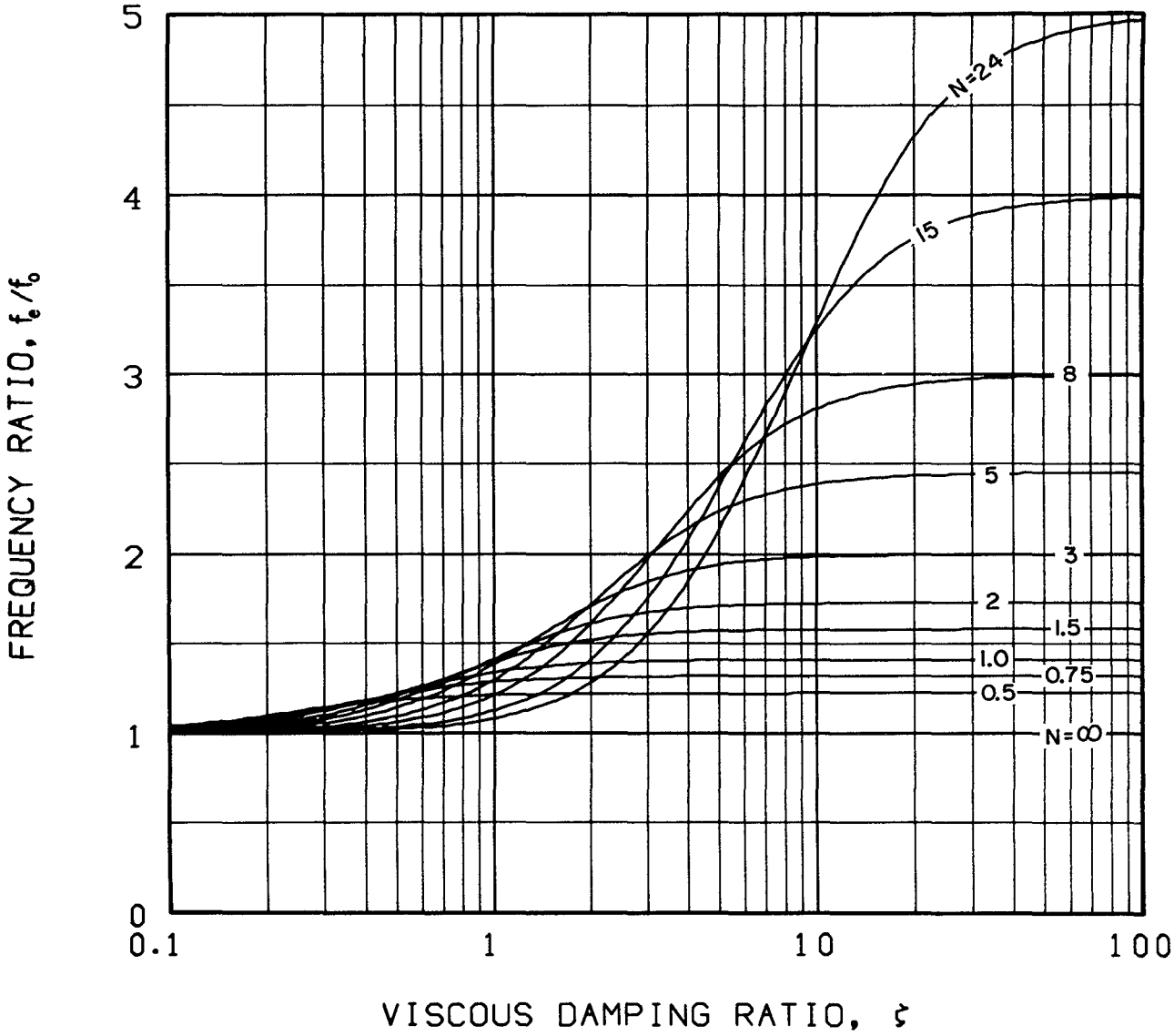

Figure 18.-Ratio of the expected frequency of the displacement response to white noise acceleration input to the undamped natural frequency for the isolation system shown in Figure 1(a)

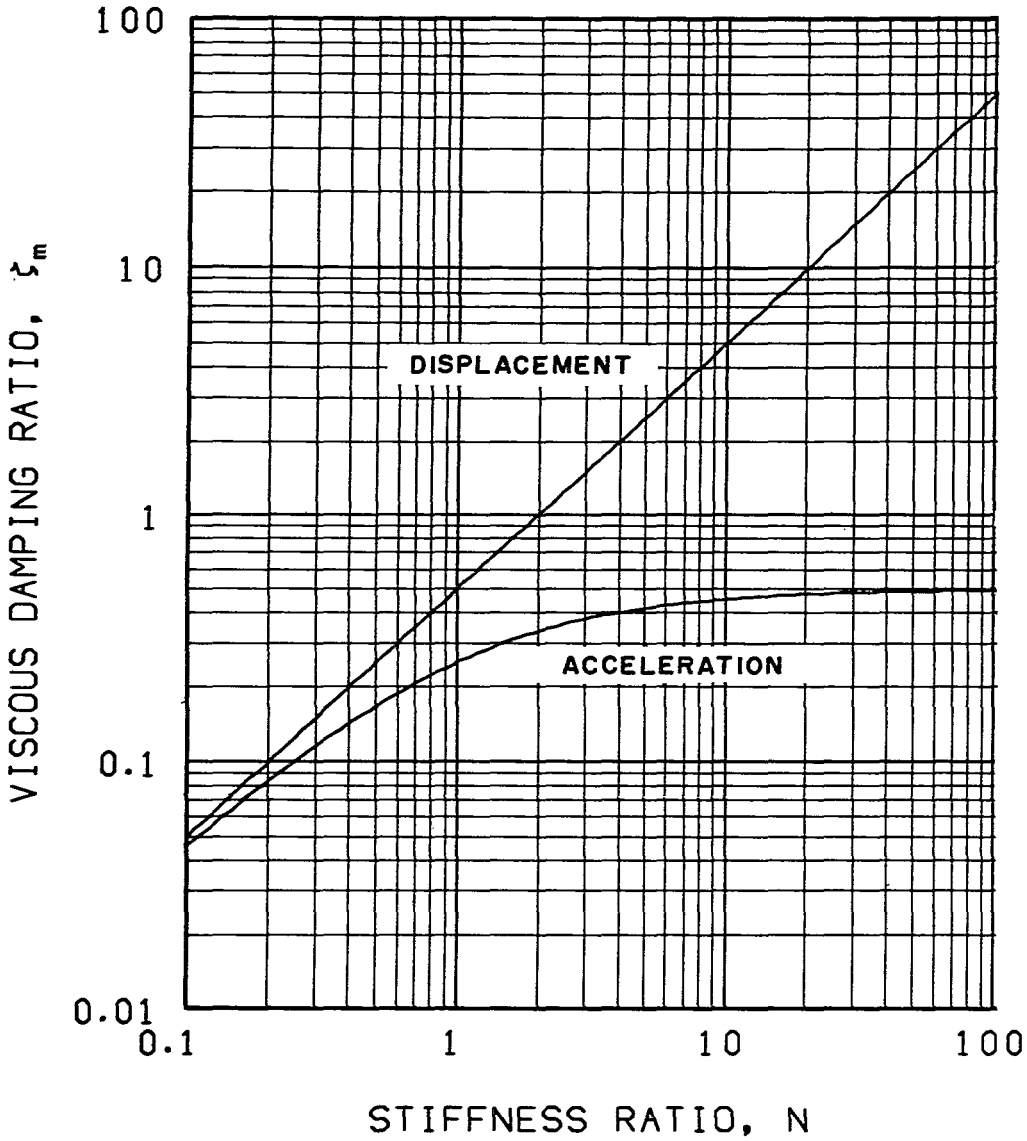

Figure 19.-Viscous damping ratios that minimize the values of the dimensionless acceleration (Figure 16) and the dimensionless displacement (Figure 17)

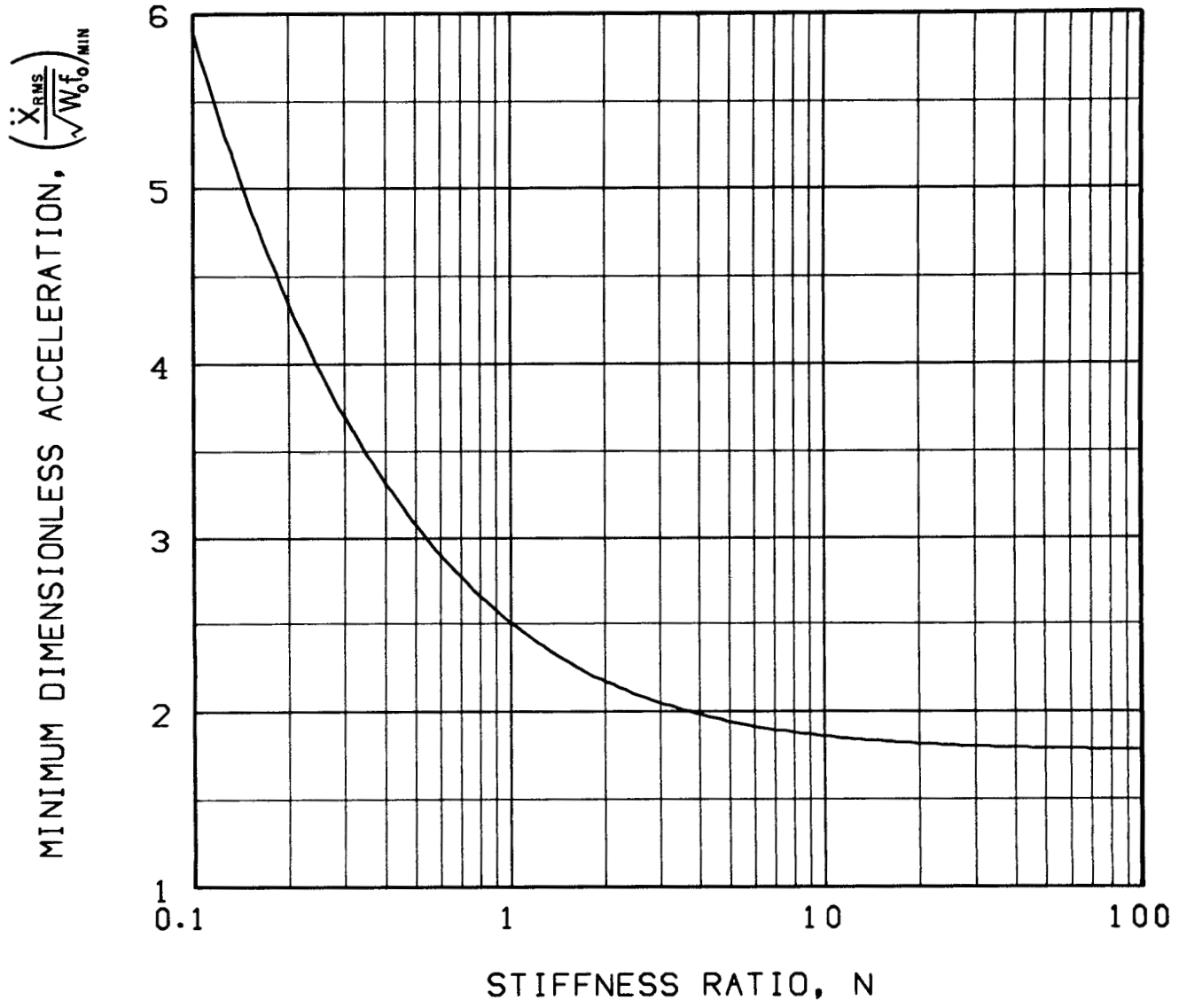

Figure 20.-Minimum values of the dimensionless acceleration (Figure 16)

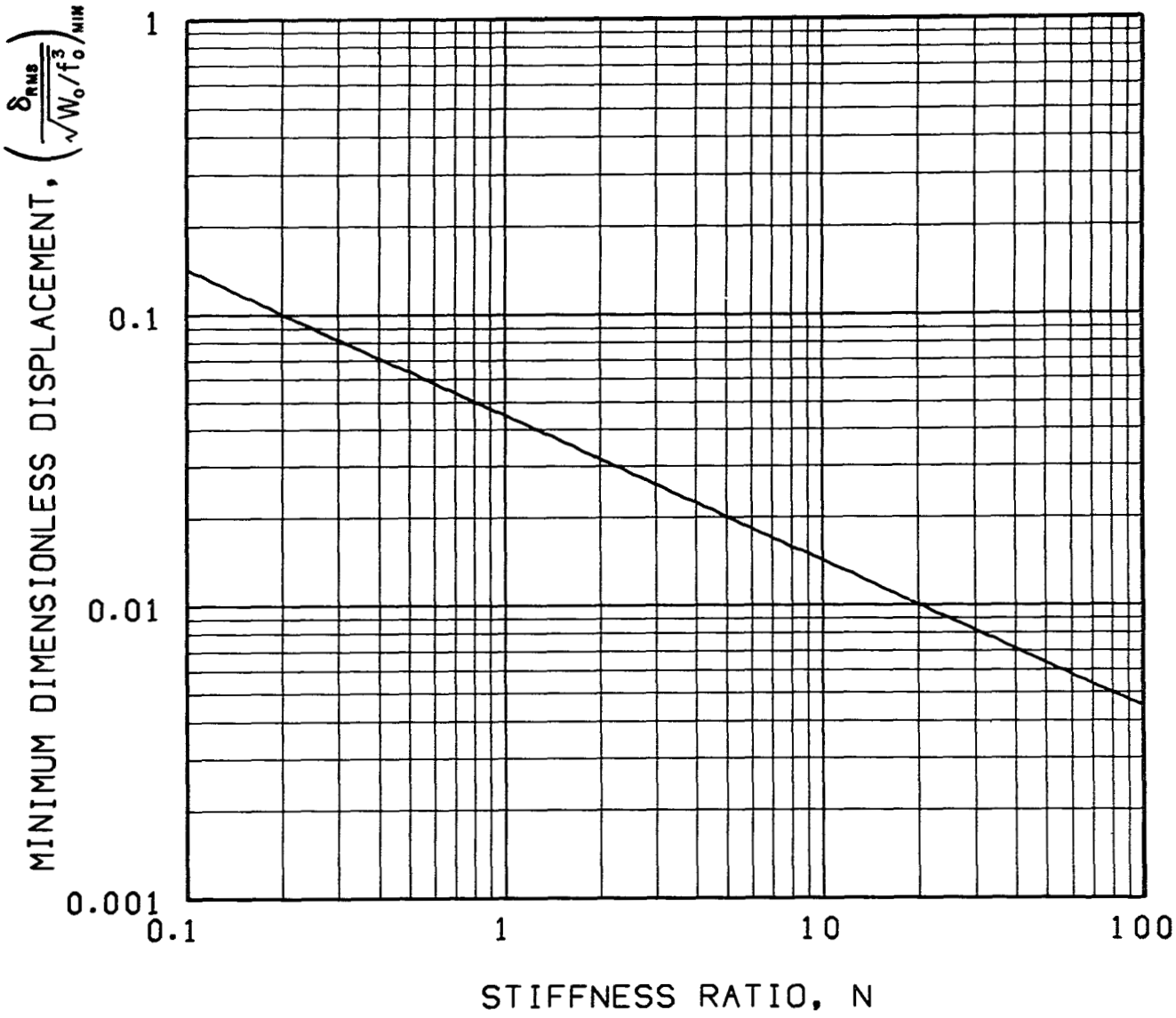

Figure 21.-Minimum values of the dimensionless displacement (Figure 17)

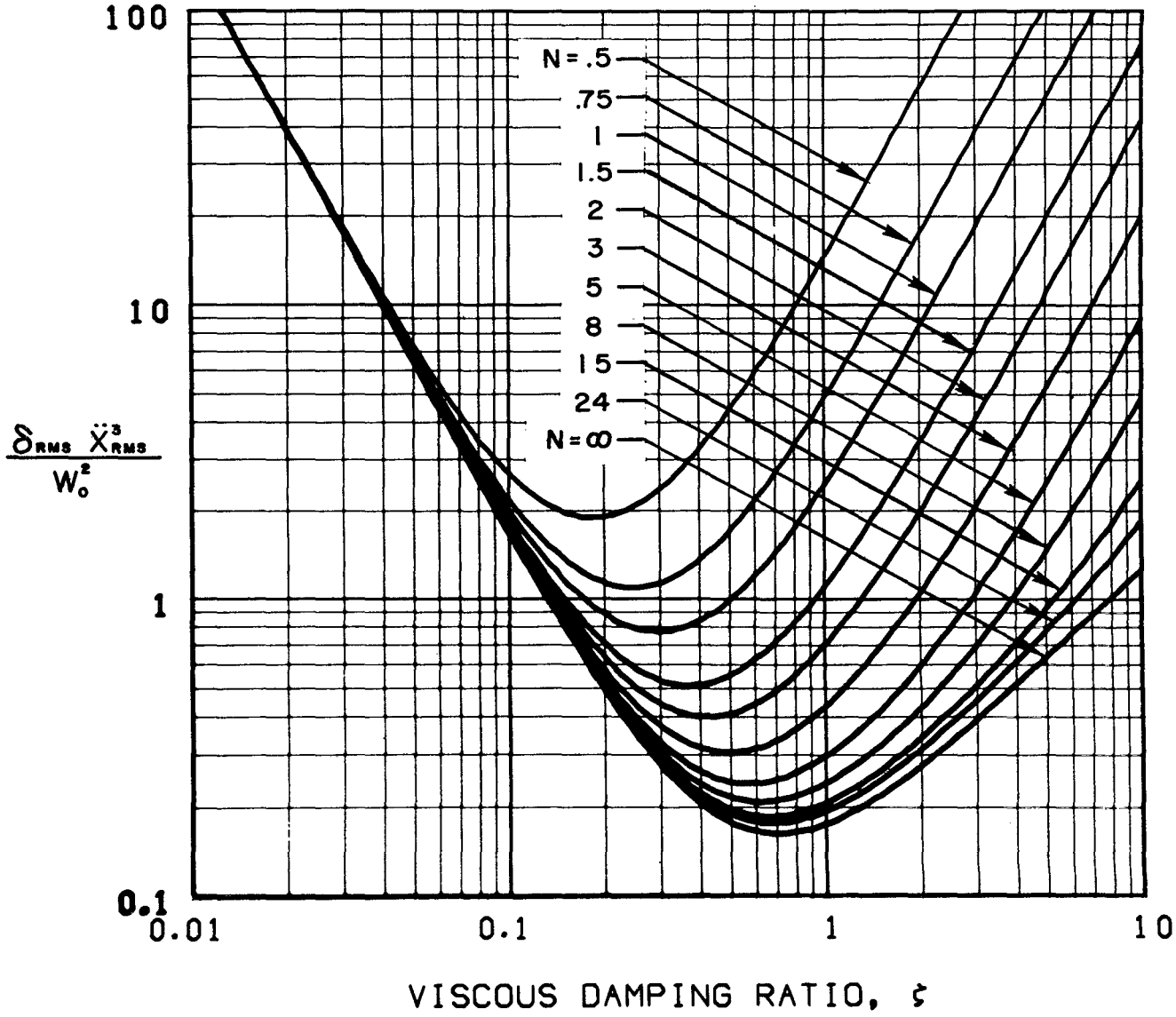

Figure 22.-The RMS displacement times the RMS acceleration cubed divided by the input acceleration spectral density squared for the isolation system shown in Figure 1(a)

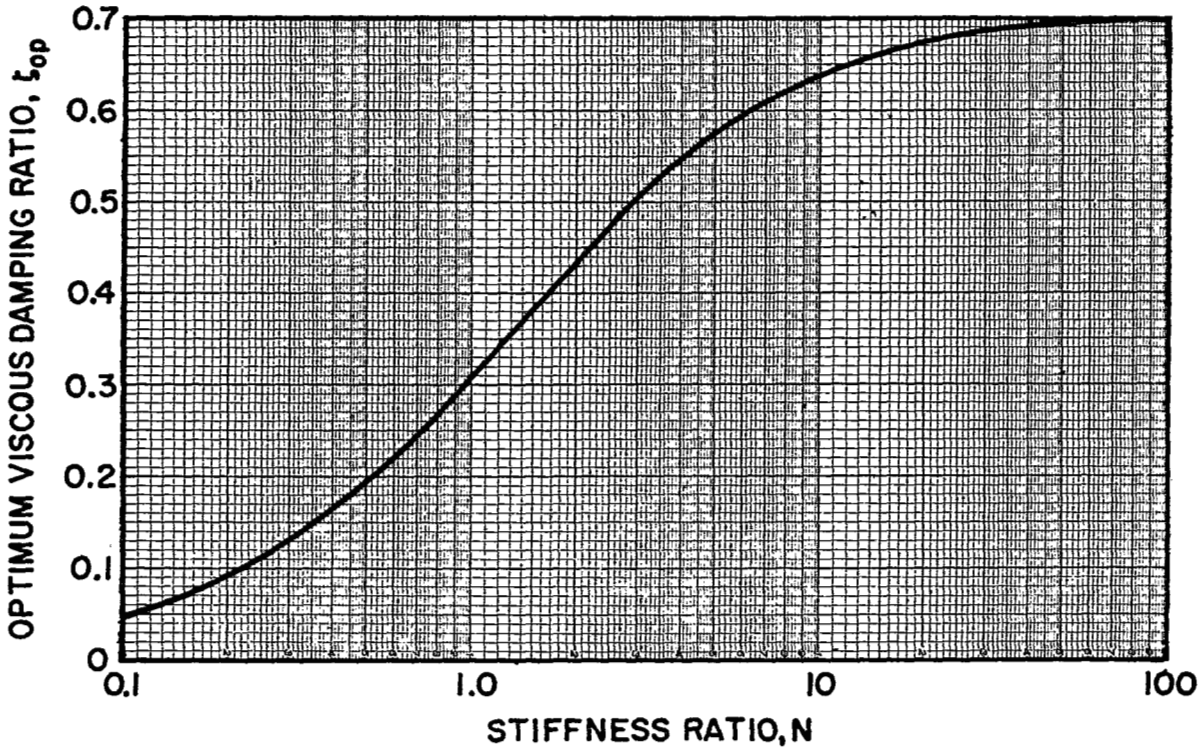

Figure 23.-Optimum viscous damping ratio obtained by minimizing the parameter $\delta_{RMS}\ \ddot{x}^3_{RMS}/W_o^2$ (Figure 22)

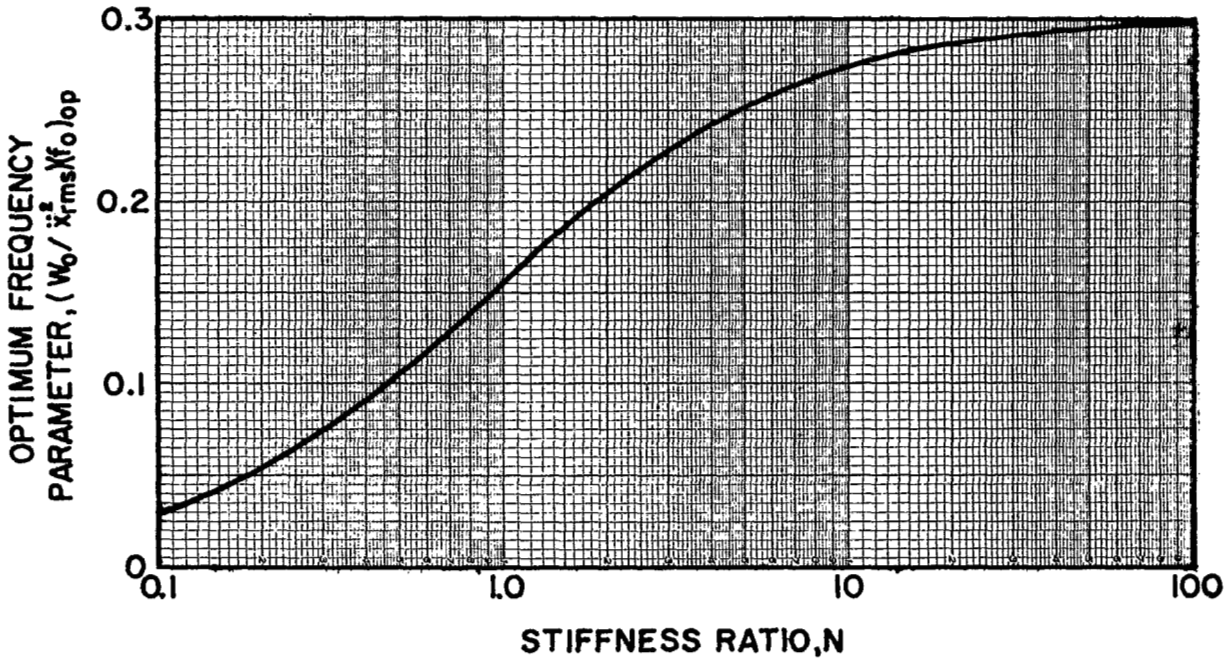

Figure 24.-Optimum frequency parameter obtained by using the optimum viscous damping ratio (Figure 23) with the dimensionless acceleration (Figure 16)

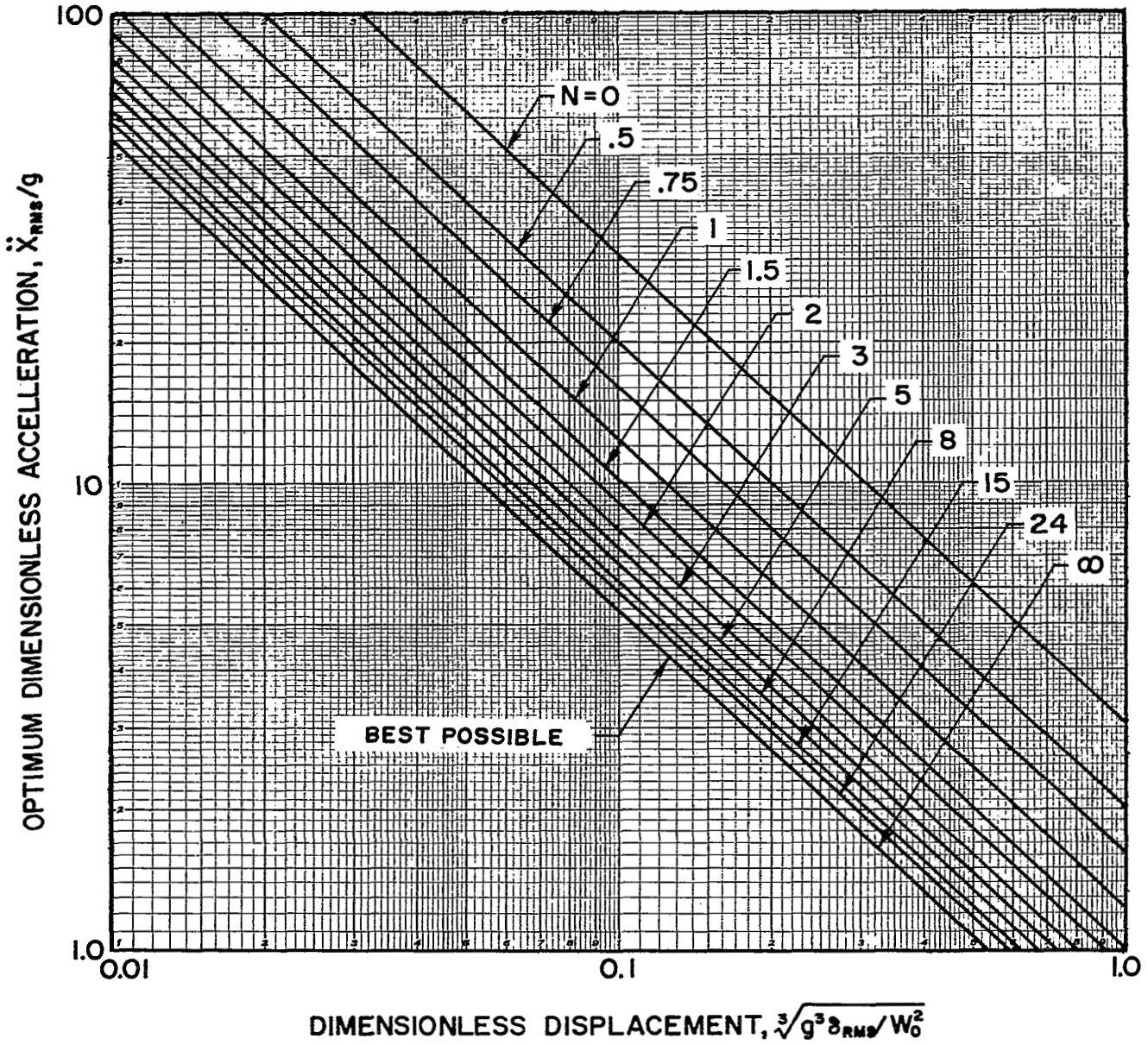

Figure 25.-Trade-off limit curves for the response to white noise acceleration input for the isolation system shown in Figure 1(a)

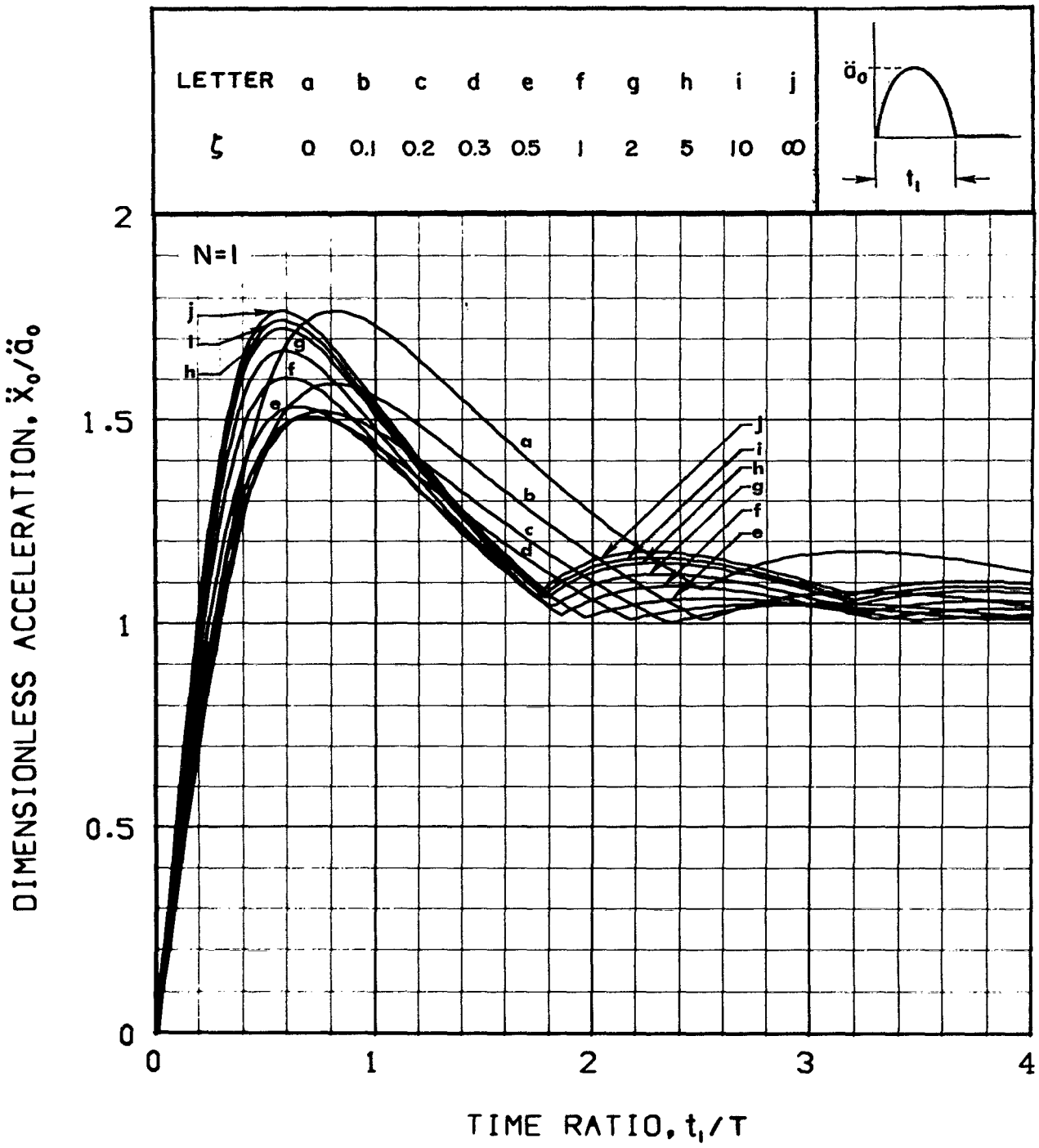

Figure 26.-Peak acceleration response to an acceleration half-cycle sine pulse input for the isolation system shown in Figure 1(a) with N = 1

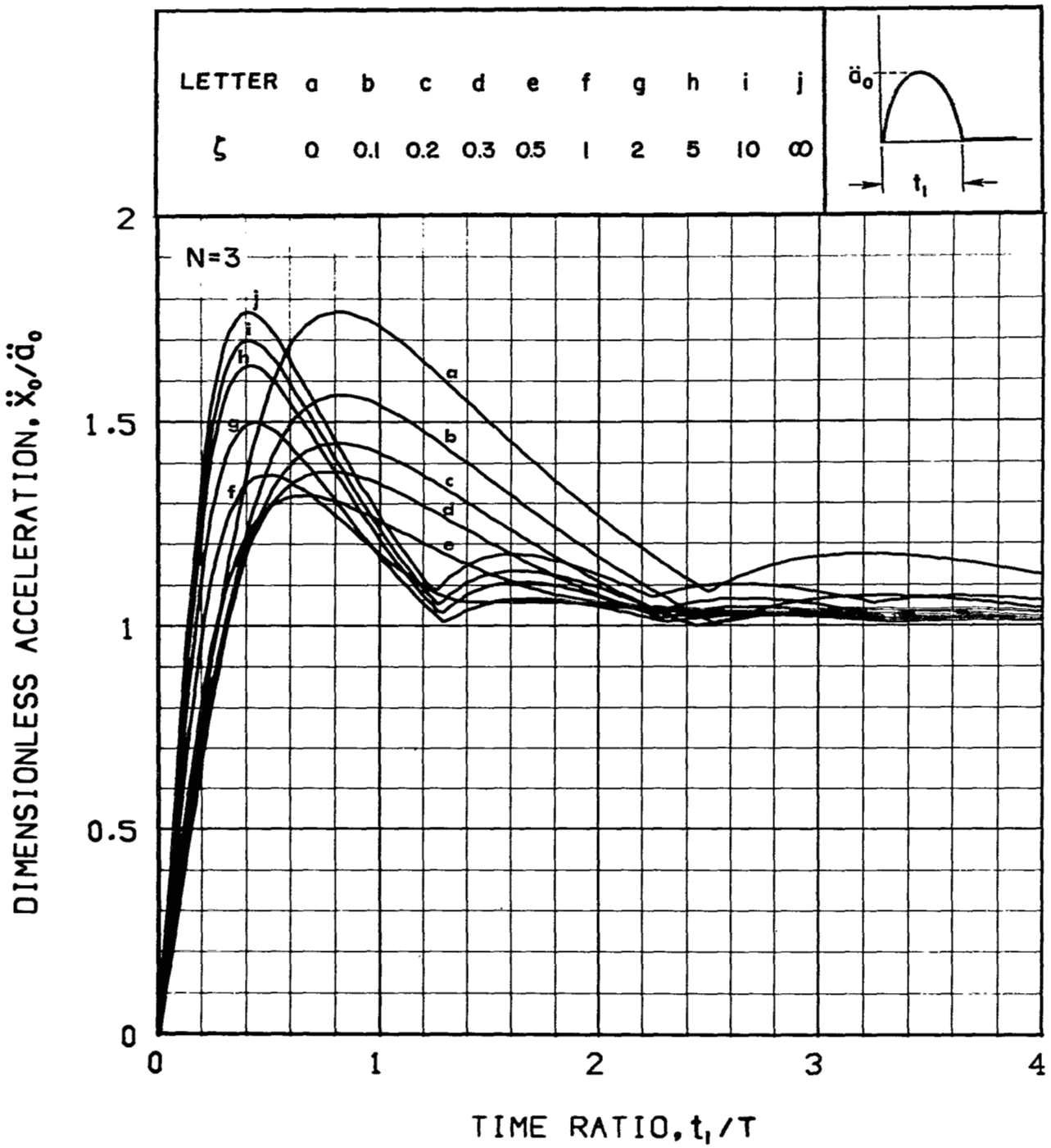

Figure 27.-Peak acceleration response to an acceleration half-cycle sine pulse input for the isolation system shown in Figure 1(a) with N = 3

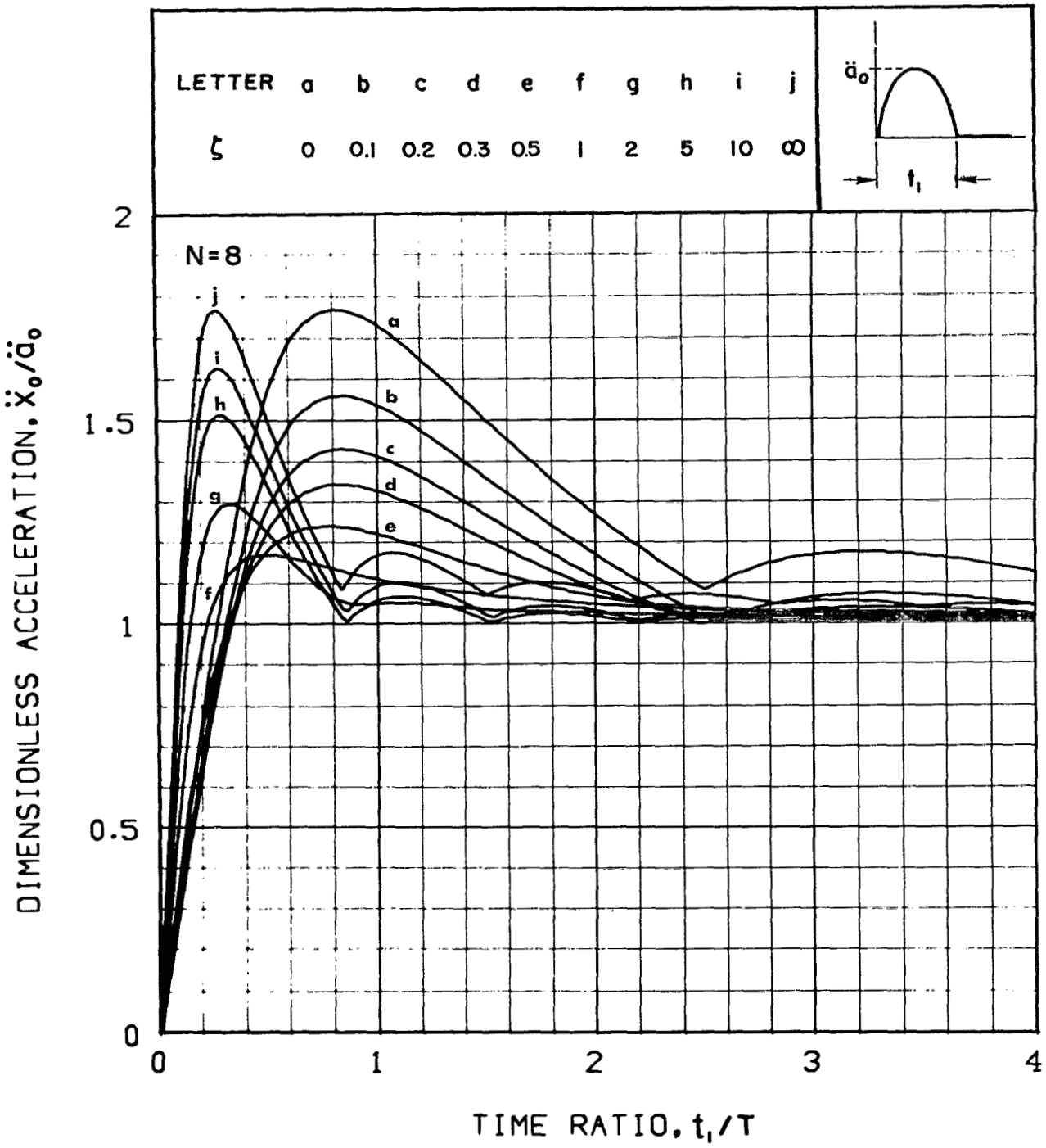

Figure 28.-Peak acceleration response to an acceleration half-cycle sine pulse input for the isolation system shown in Figure 1(a) with N = 8

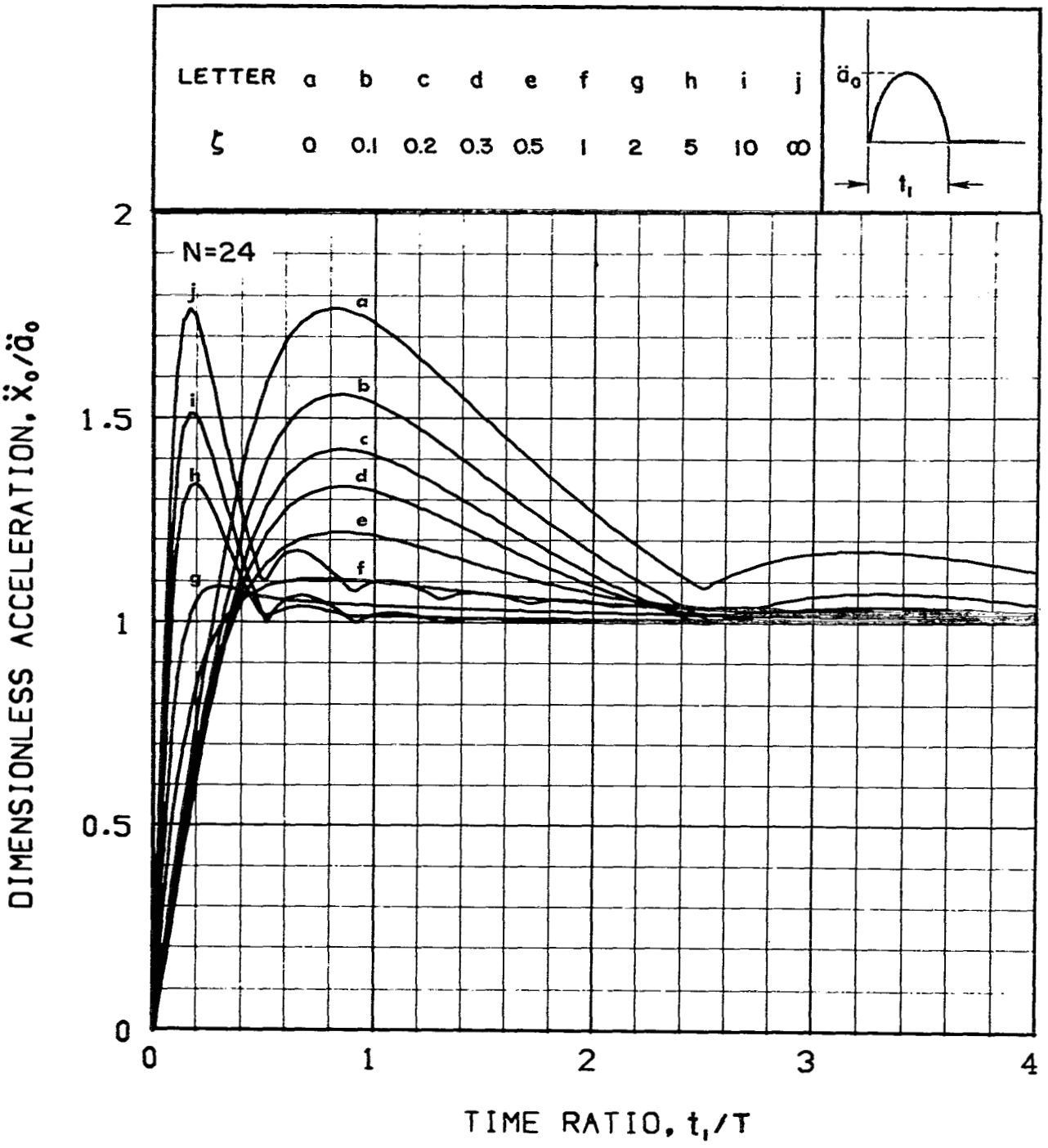

Figure 29.-Peak acceleration response to an acceleration half-cycle sine pulse input for the isolation system shown in Figure 1(a) with N = 24

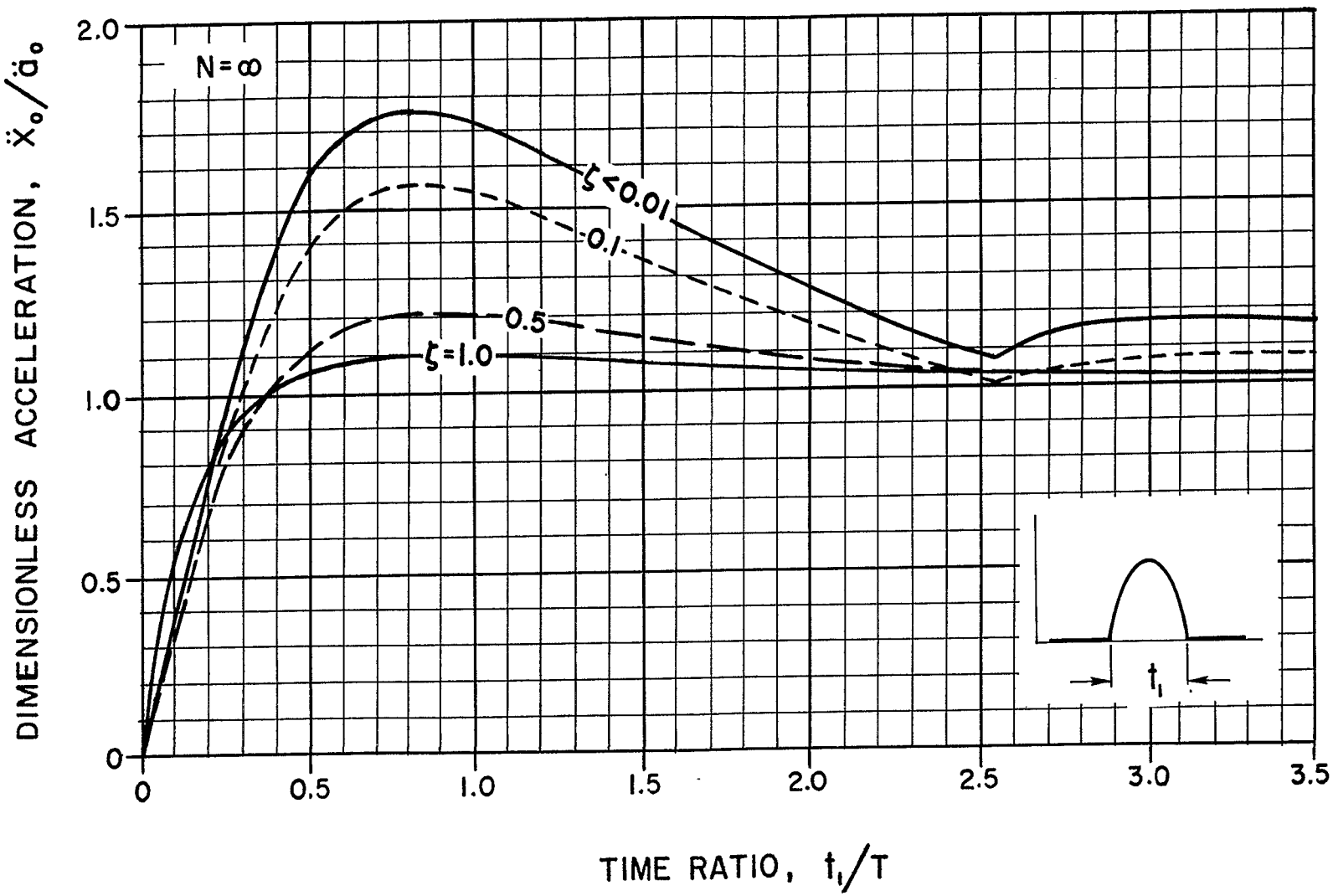

Figure 30.-Peak acceleration response to an acceleration half-cycle sine pulse input for the isolation system shown in Figure 1(a) with N = ∞

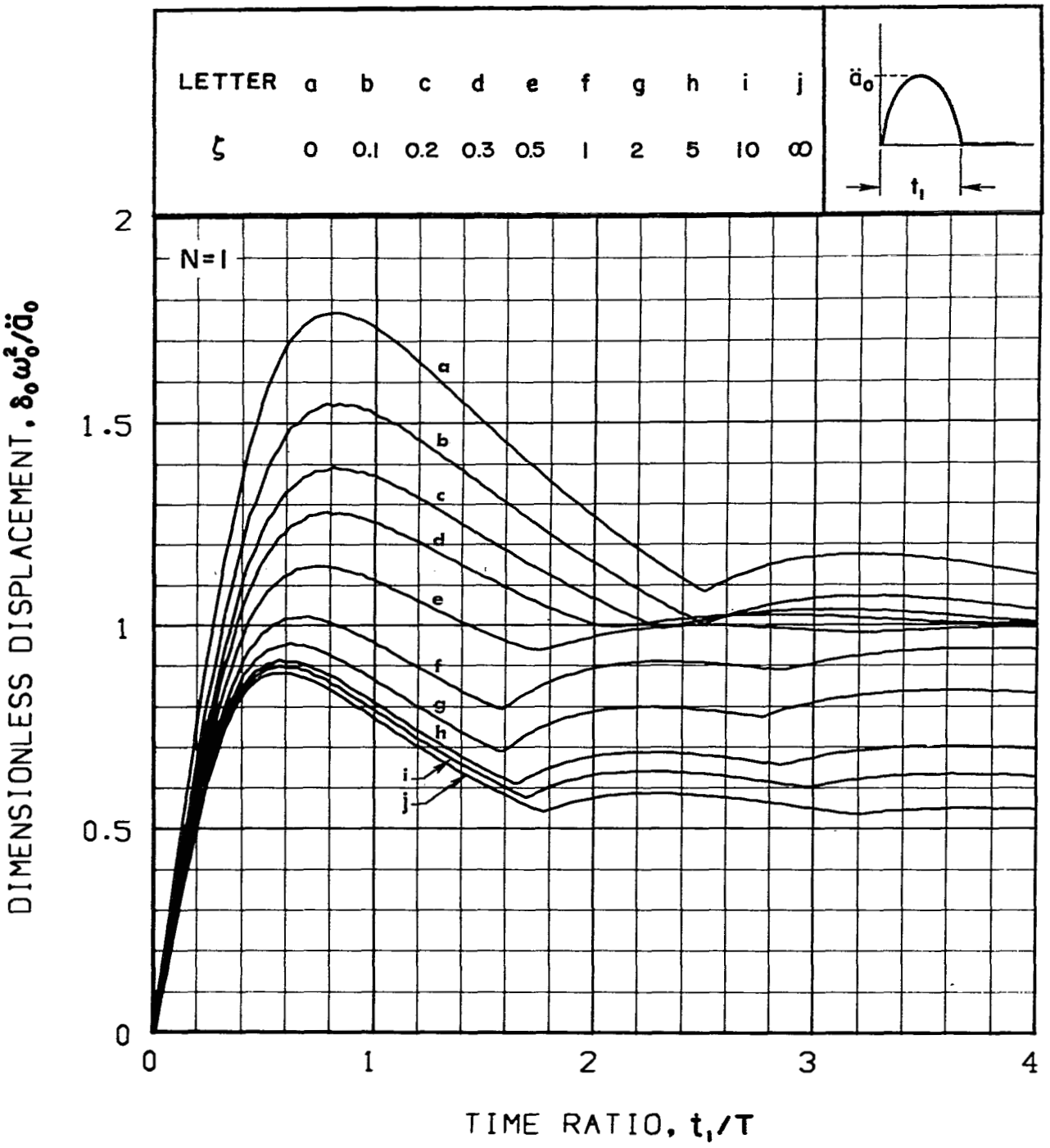

Figure 31.-Peak displacement response to an acceleration half-cycle sine pulse input for the isolation system shown in Figure 1(a) with N = 1

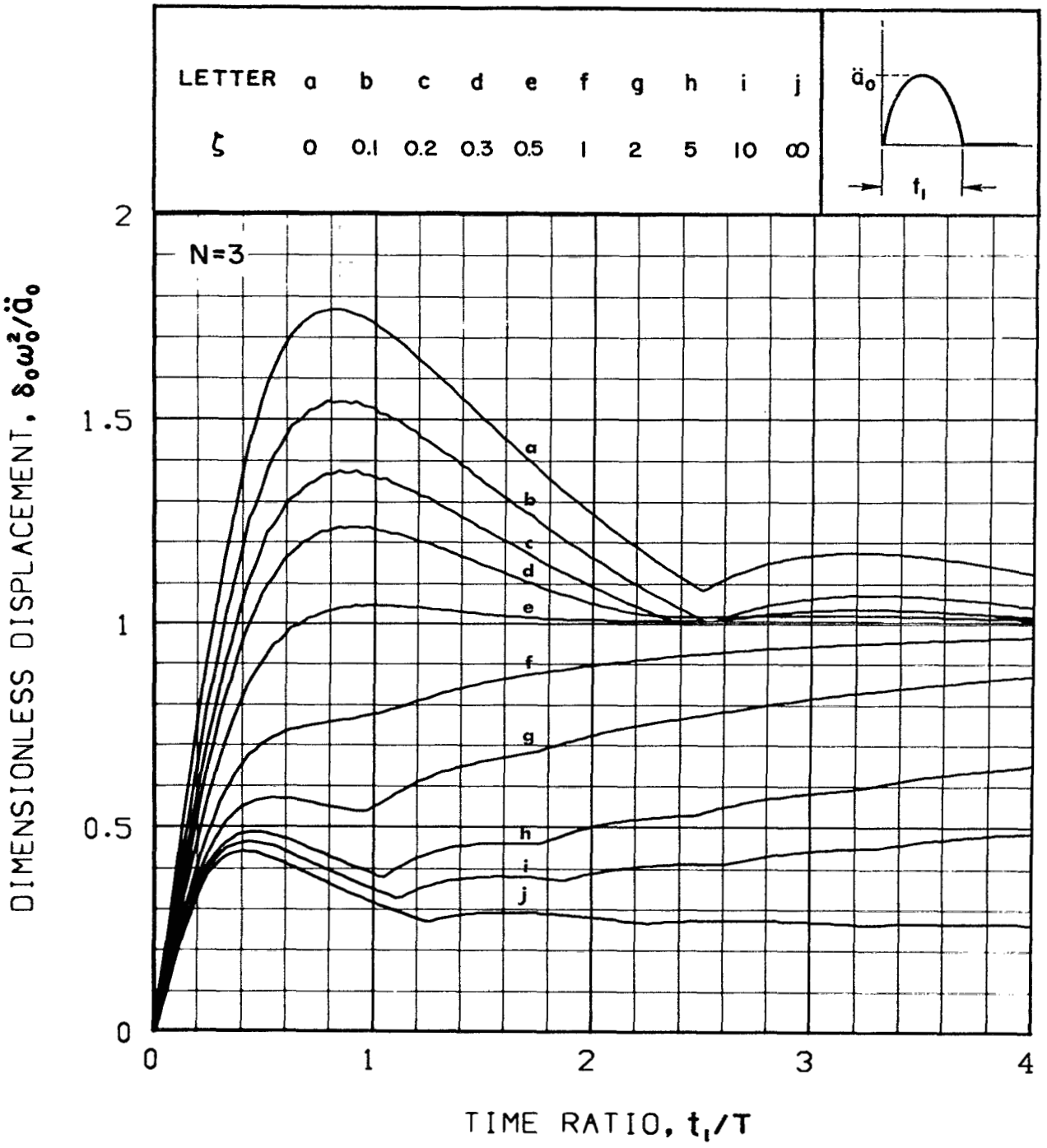

Figure 32.-Peak displacement response to an acceleration half-cycle sine pulse input for the isolation system shown in Figure 1(a) with N = 3

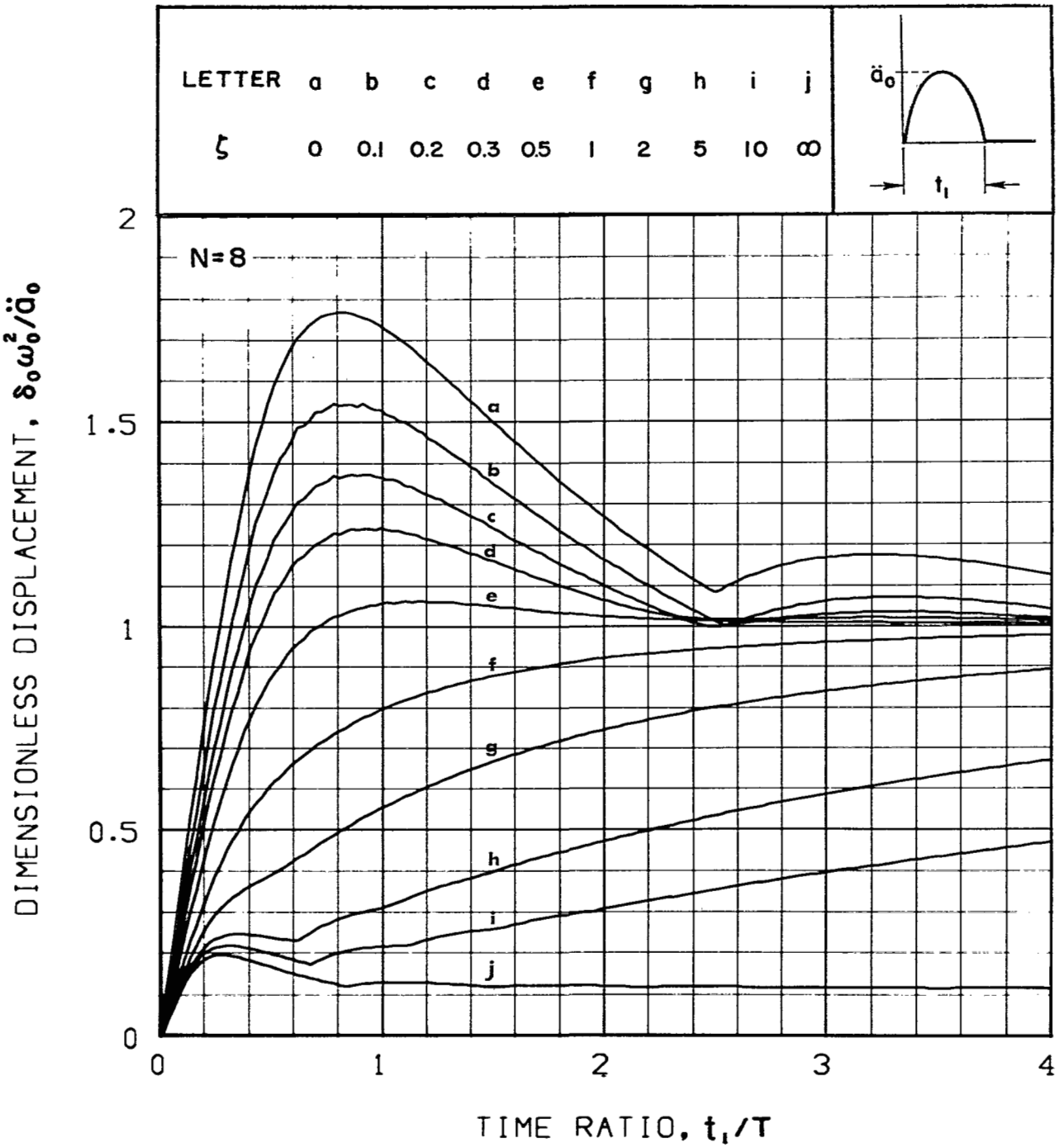

Figure 33.-Peak displacement response to an acceleration half-cycle sine pulse input for the isolation system shown in Figure 1(a) with N = 8

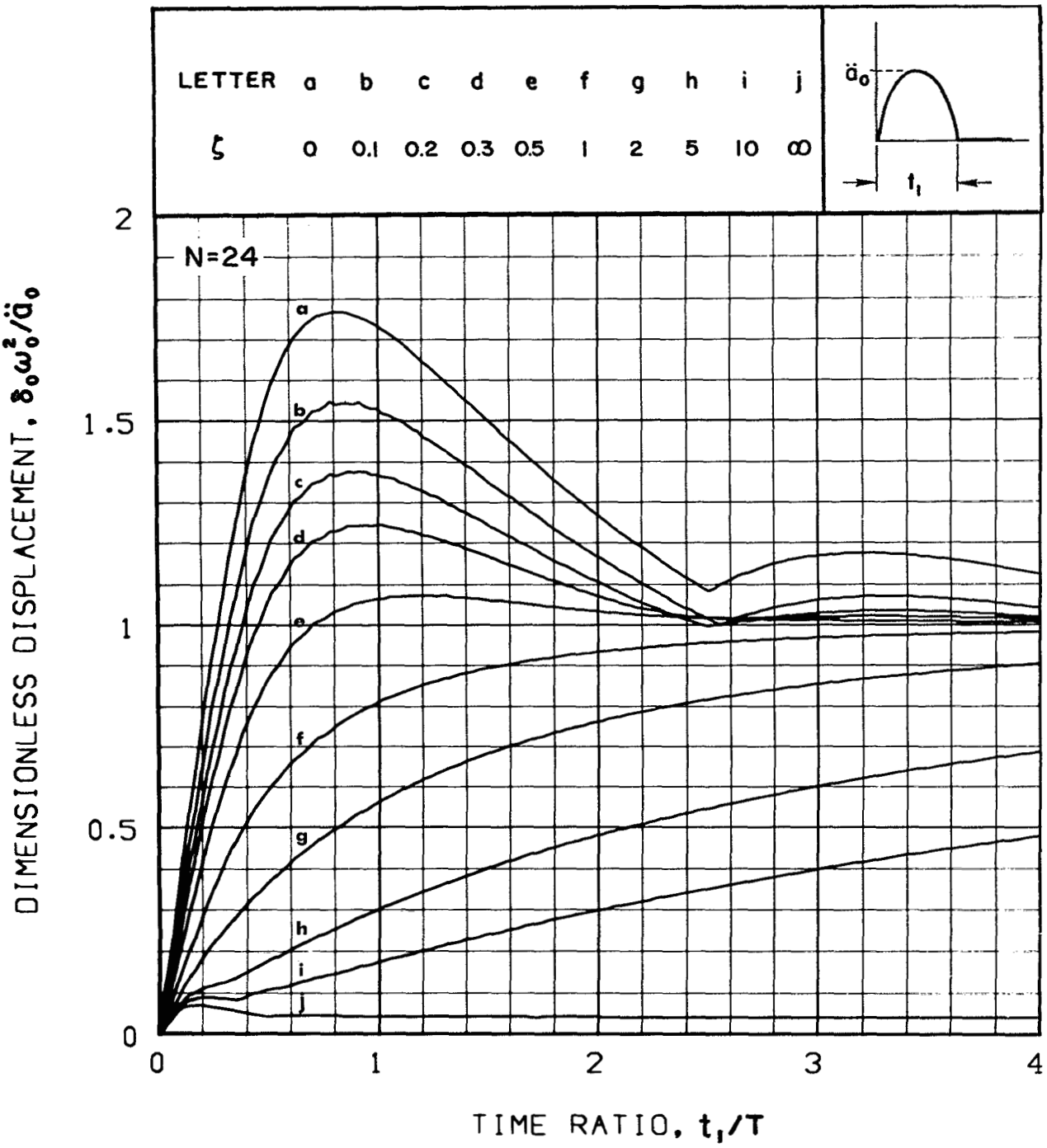

Figure 34.-Peak displacement response to an acceleration half-cycle sine pulse input for the isolation system shown in Figure 1(a) with N = 24

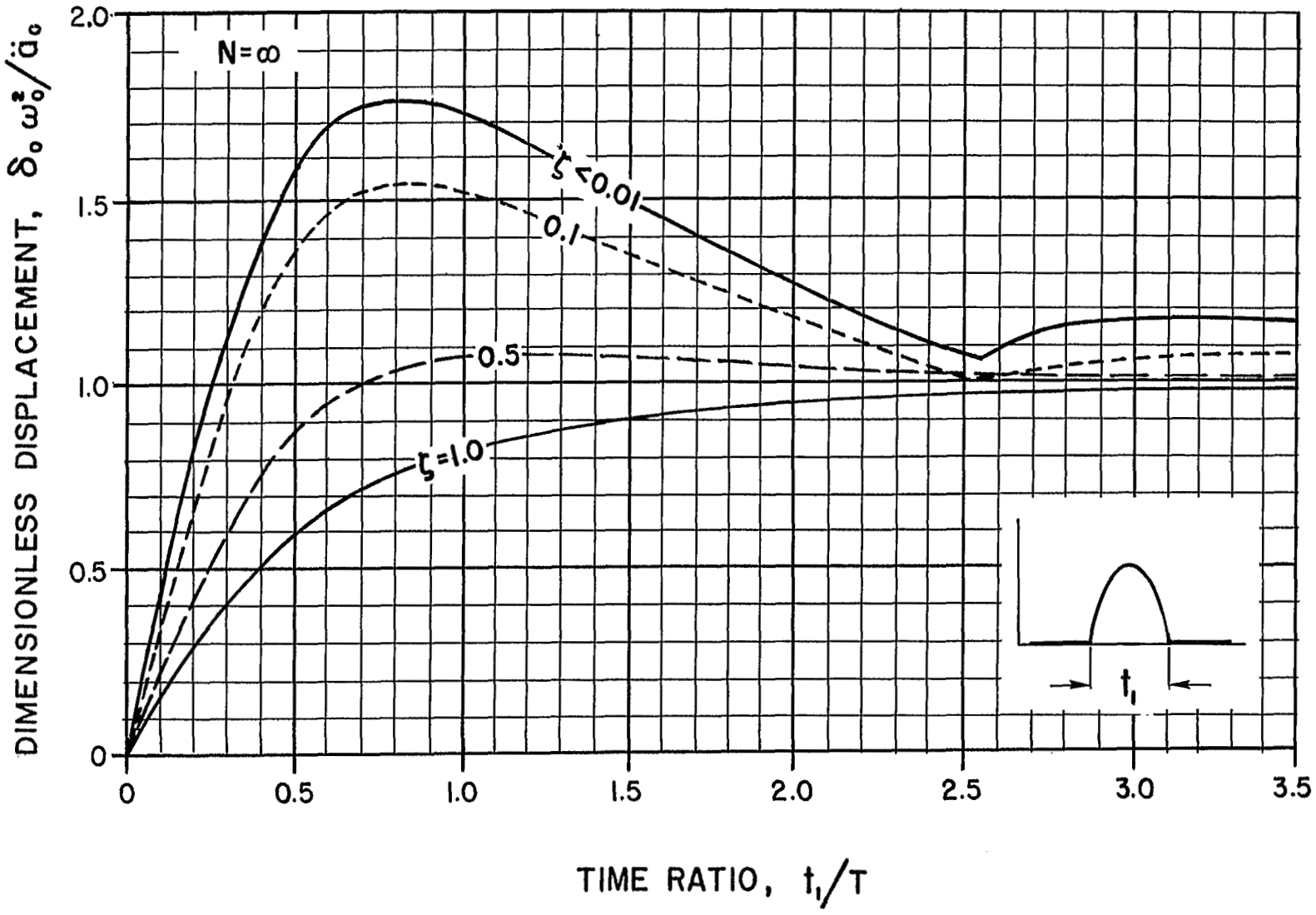

Figure 35.-Peak displacement response to an acceleration half-cycle sine pulse input for the isolation system shown in Figure 1(a) with N = ∞

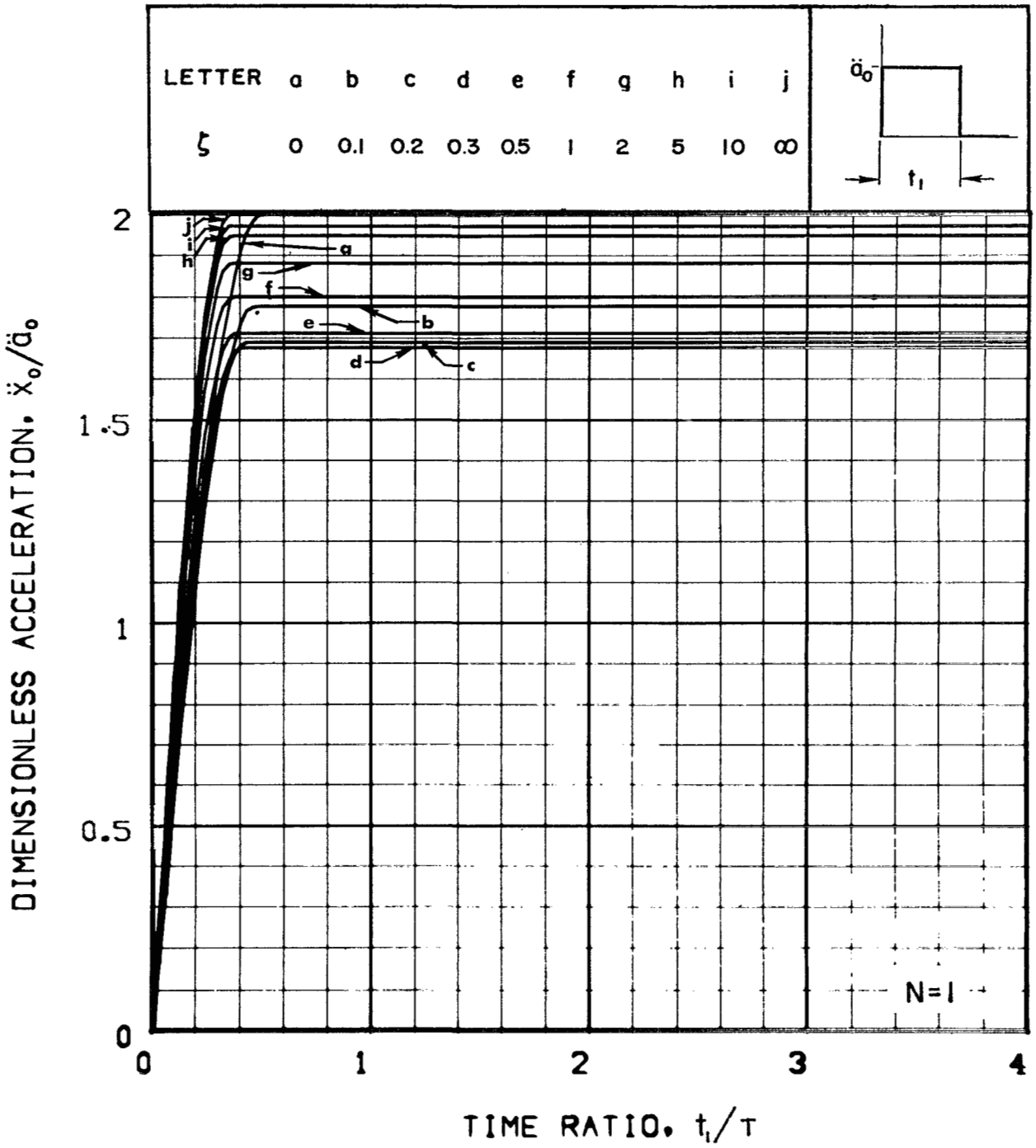

Figure 36.-Peak acceleration response to an acceleration rectangular pulse input for the isolation system shown in Figure 1(a) with N = 1

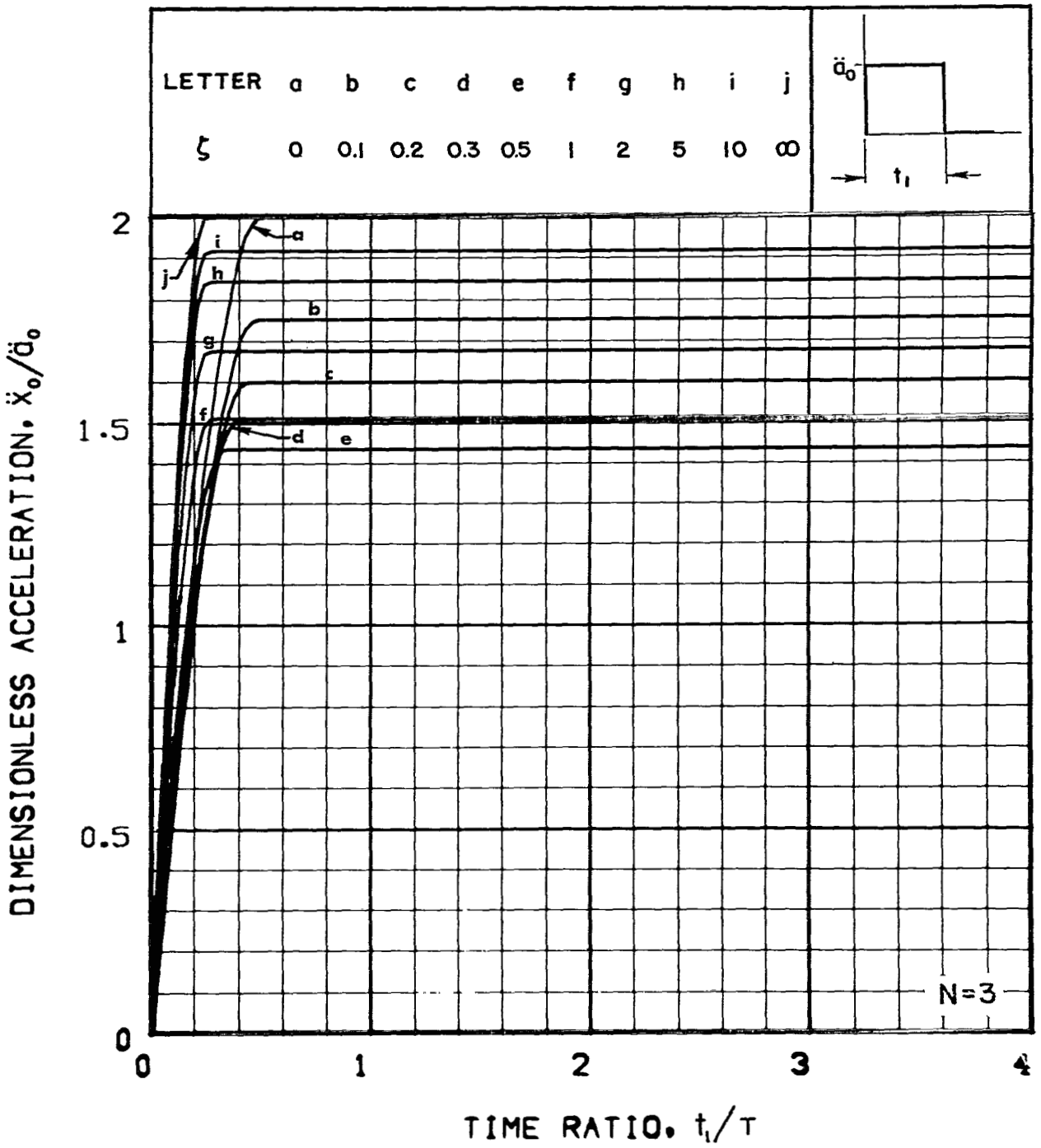

Figure 37.-Peak acceleration response to an acceleration rectangular pulse input for the isolation system shown in Figure 1(a) with N = 3

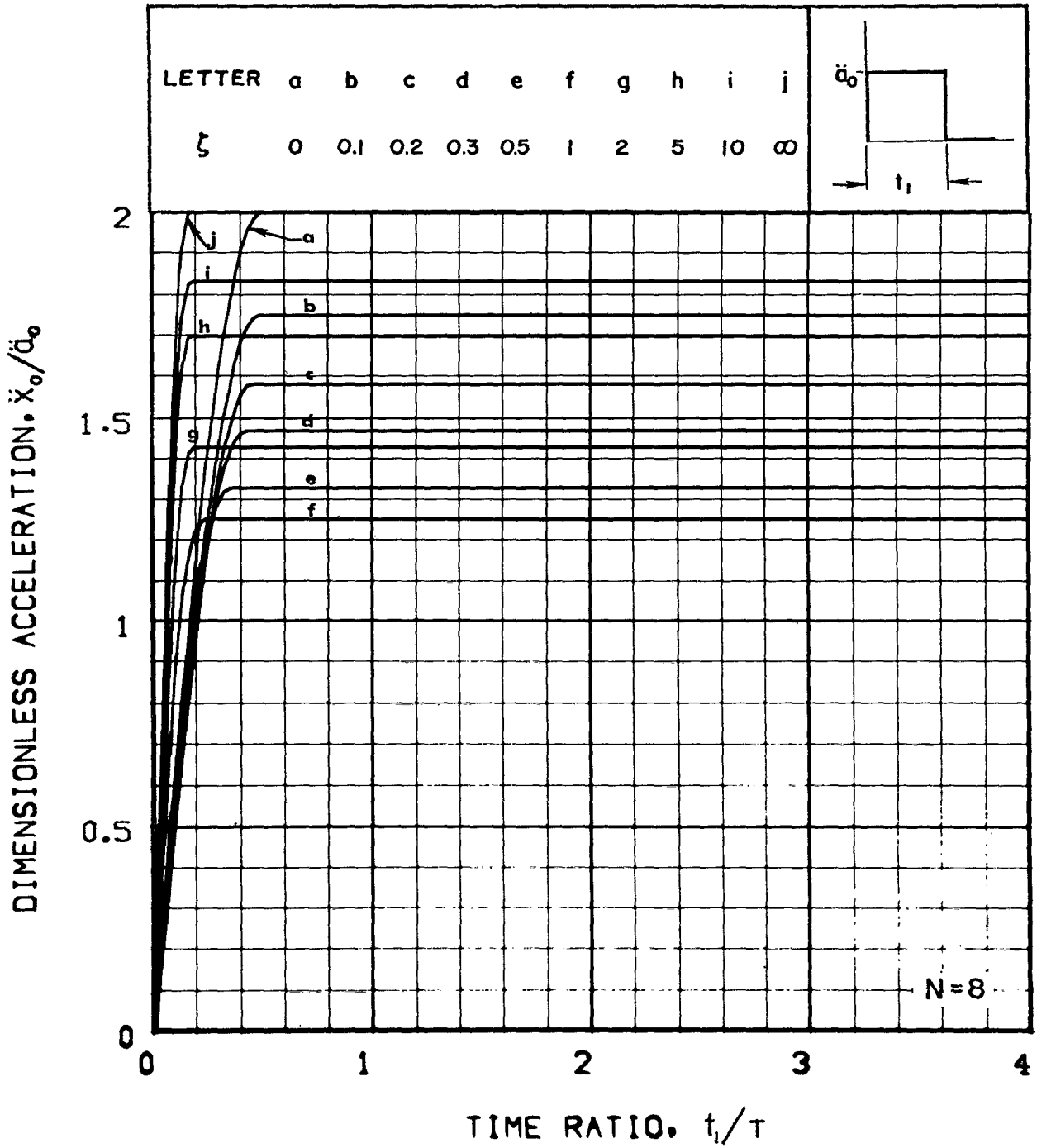

Figure 38.-Peak acceleration response to an acceleration rectangular pulse input for the isolation system shown in Figure 1(a) with N = 8

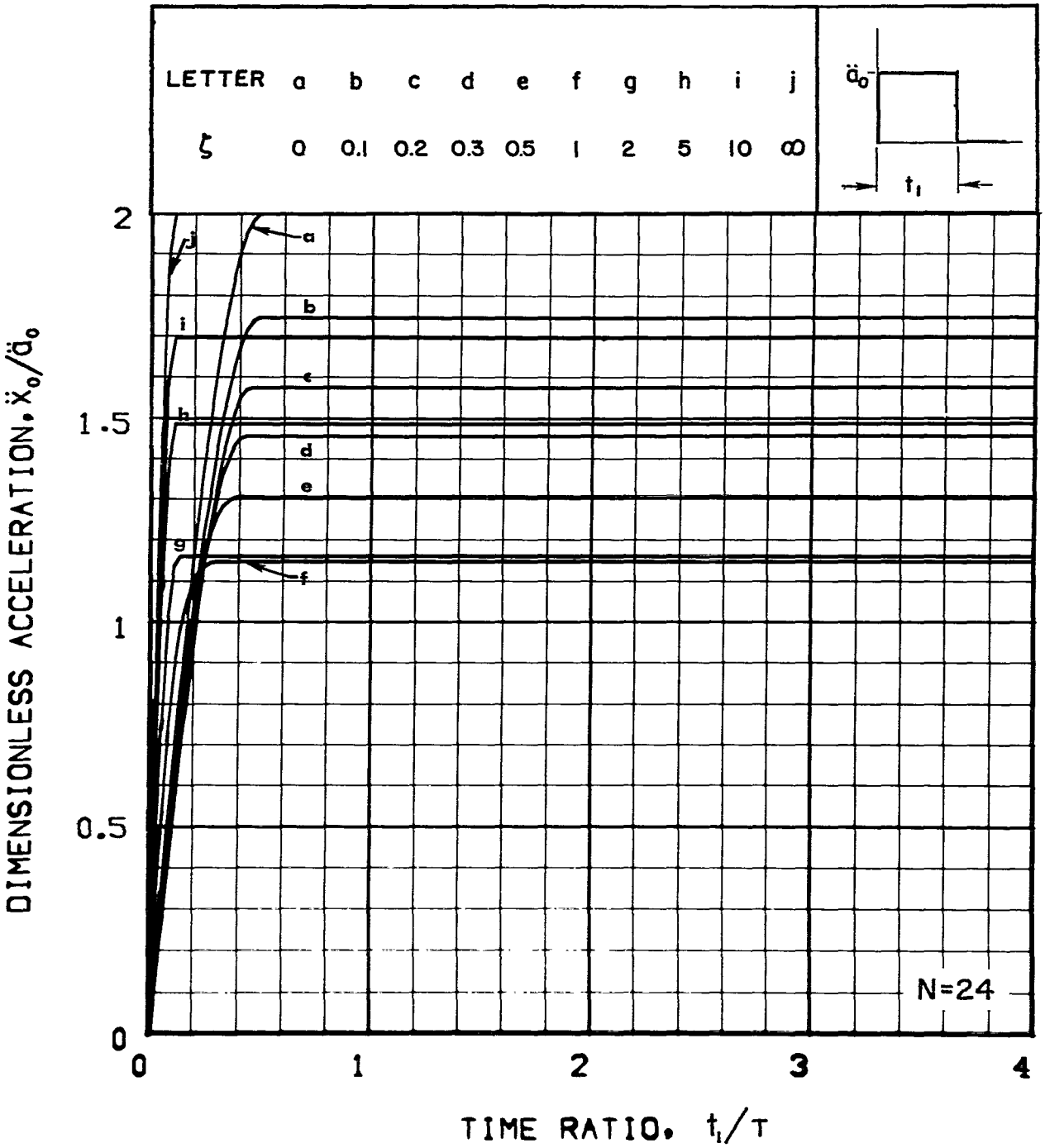

Figure 39.-Peak acceleration response to an acceleration rectangular pulse input for the isolation system shown in Figure 1(a) with N = 24

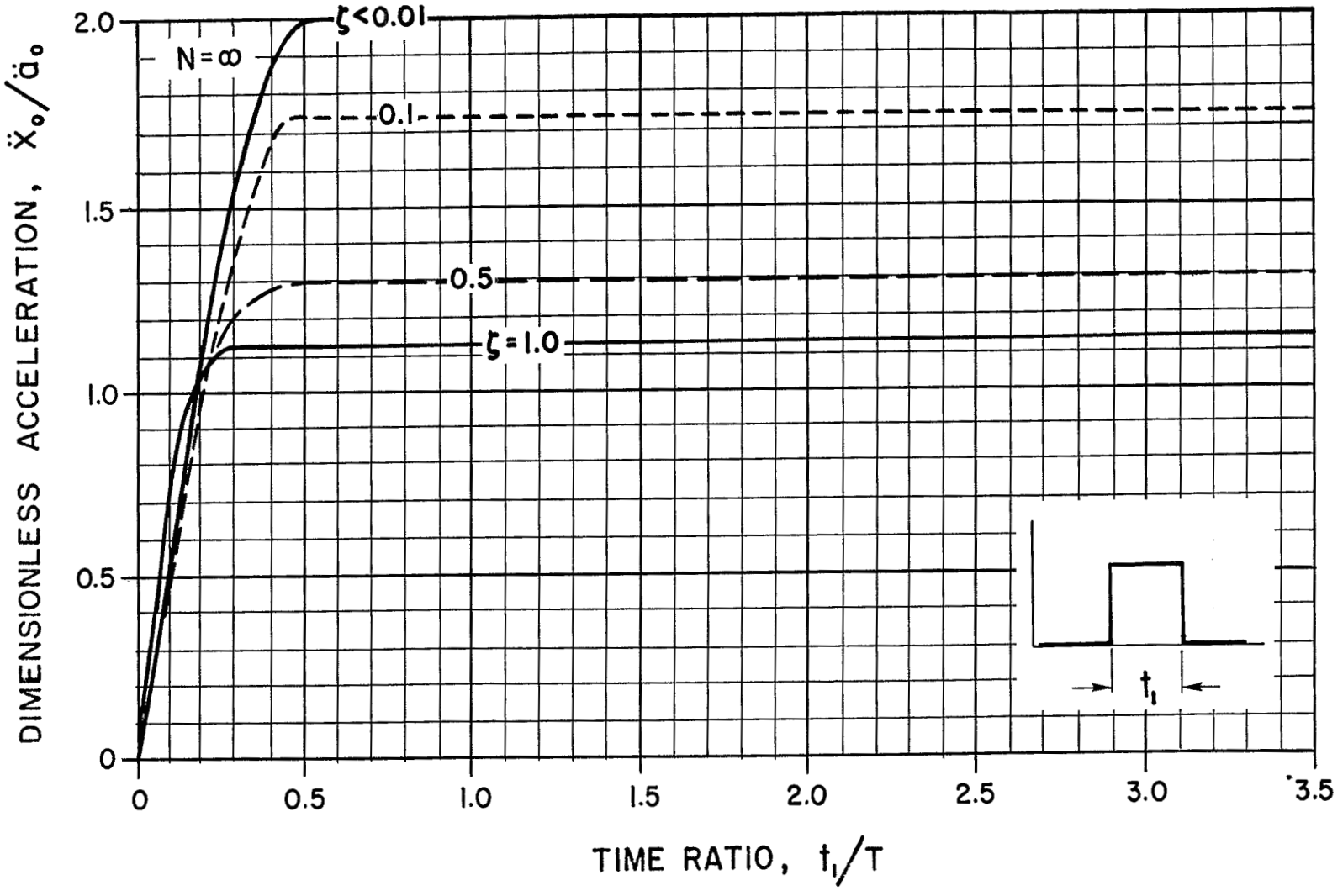

Figure 40.-Peak acceleration response to an acceleration rectangular pulse input for the isolation system shown in Figure 1(a) with N = ∞

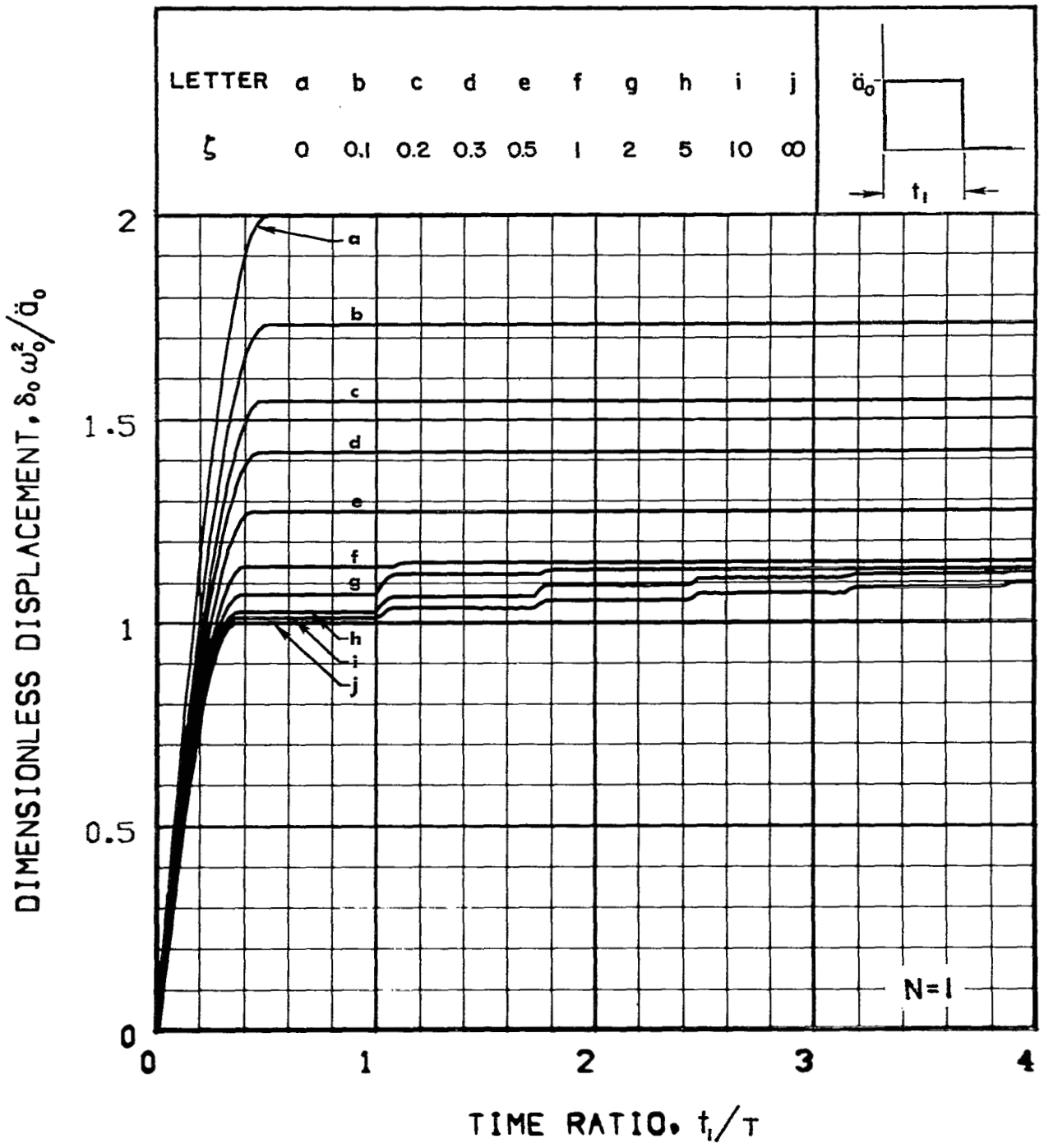

Figure 41.-Peak displacement response to an acceleration rectangular pulse input for the isolation system shown in Figure 1(a) with N = 1

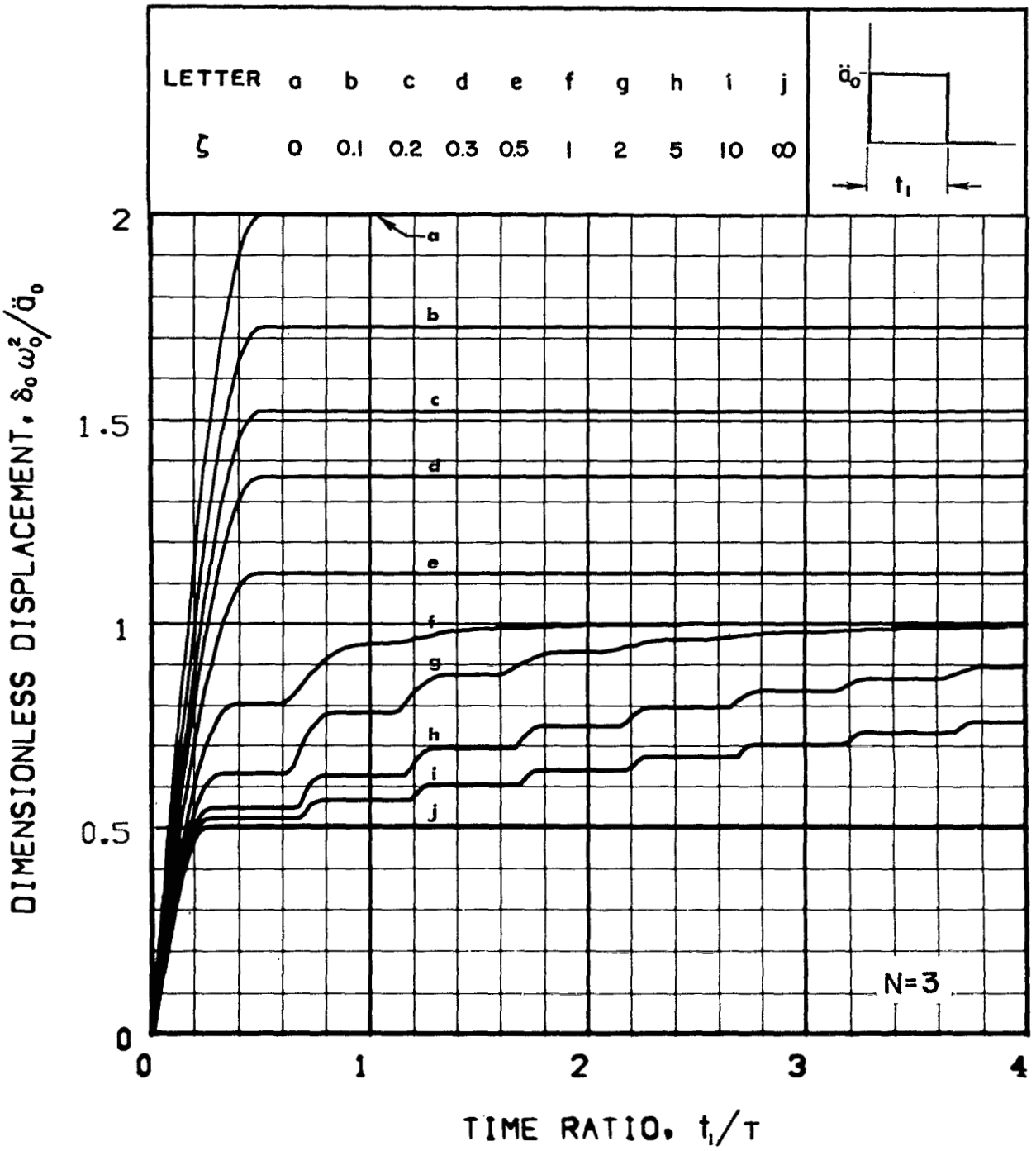

Figure 42.-Peak displacement response to an acceleration rectangular pulse input for the isolation system shown in Figure 1(a) with N = 3

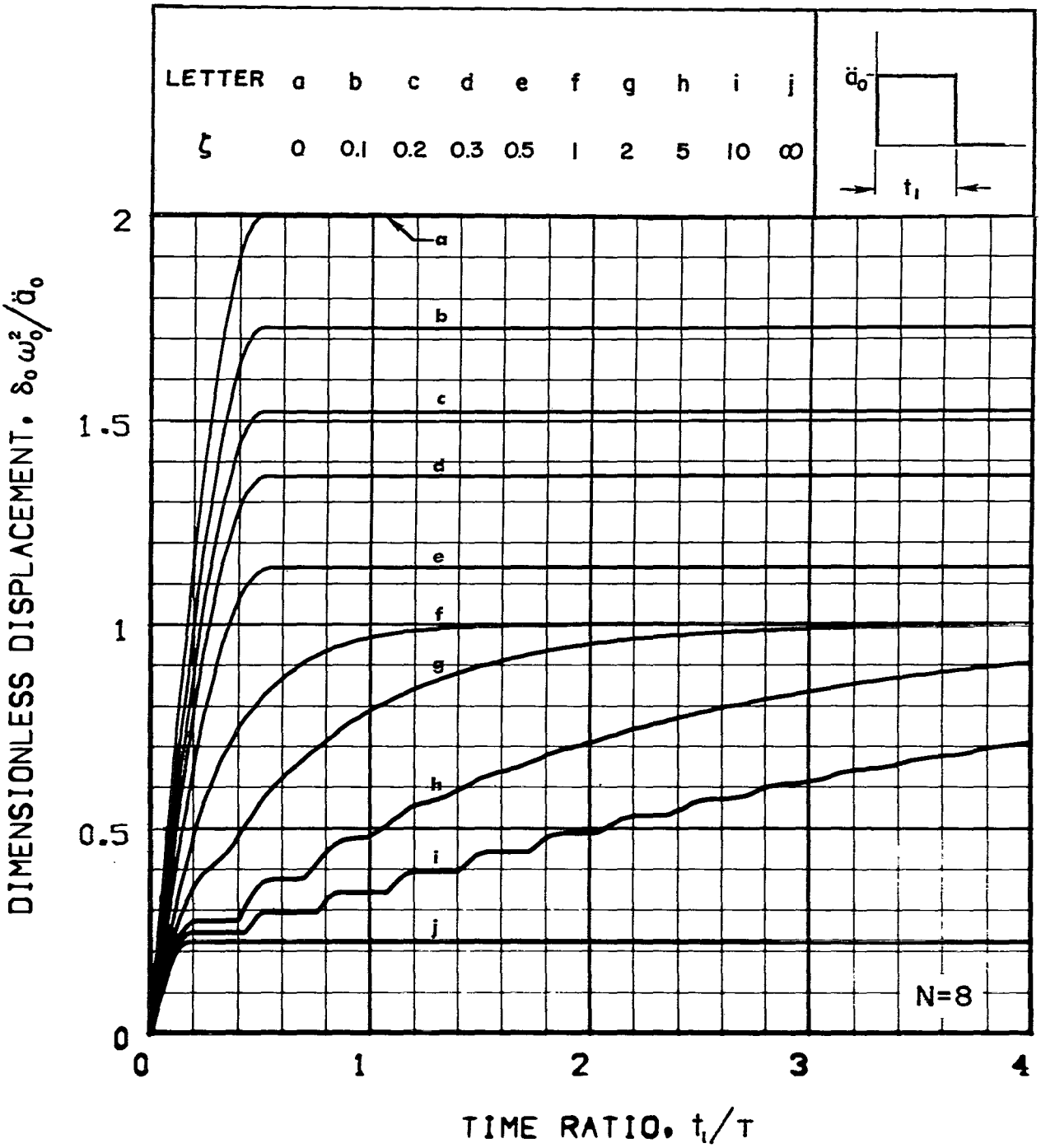

Figure 43.-Peak displacement response to an acceleration rectangular pulse input for the isolation system shown in Figure 1(a) with N = 8

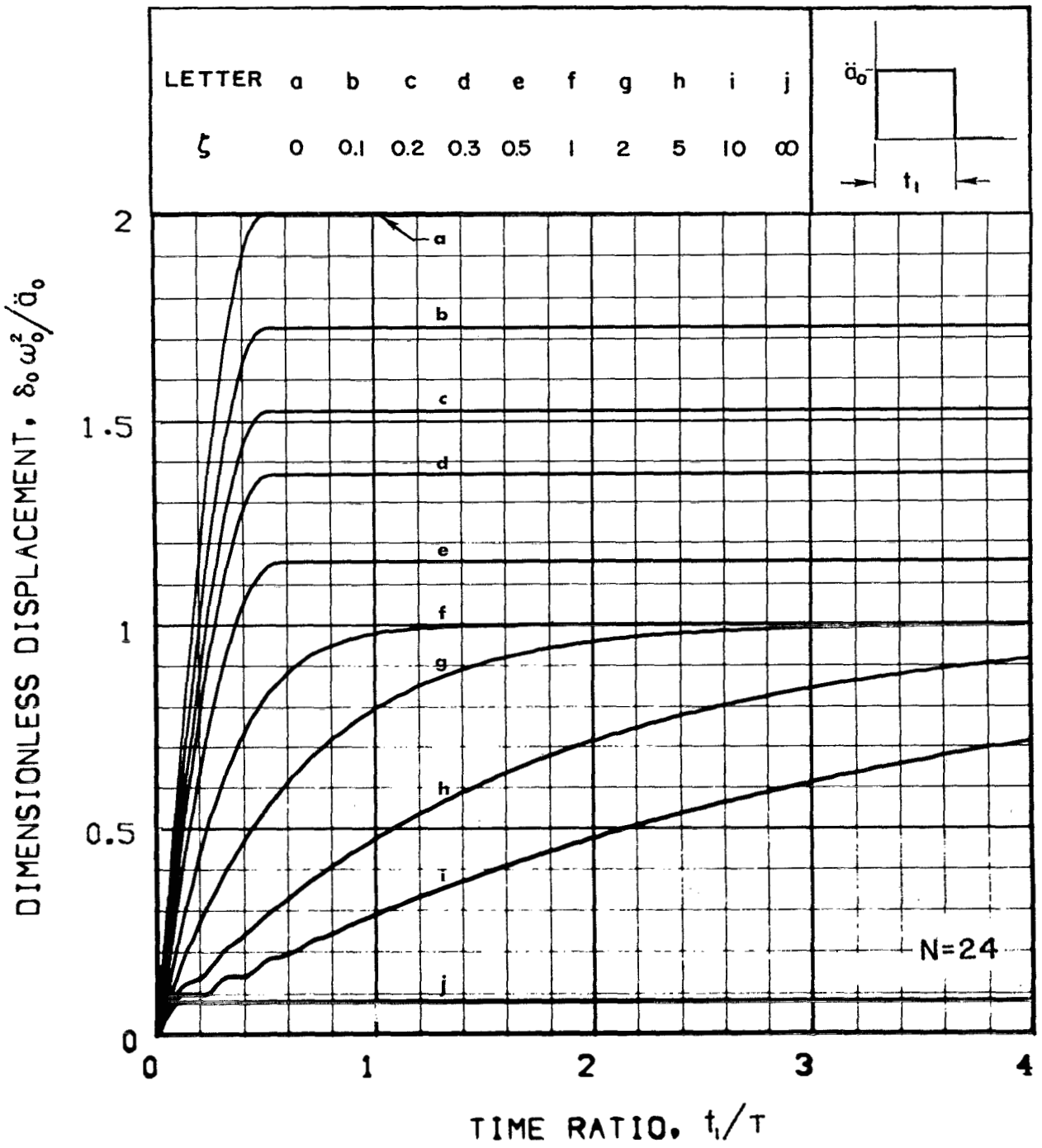

Figure 44.-Peak displacement response to an acceleration rectangular pulse input for the isolation system shown in Figure 1(a) with N = 24

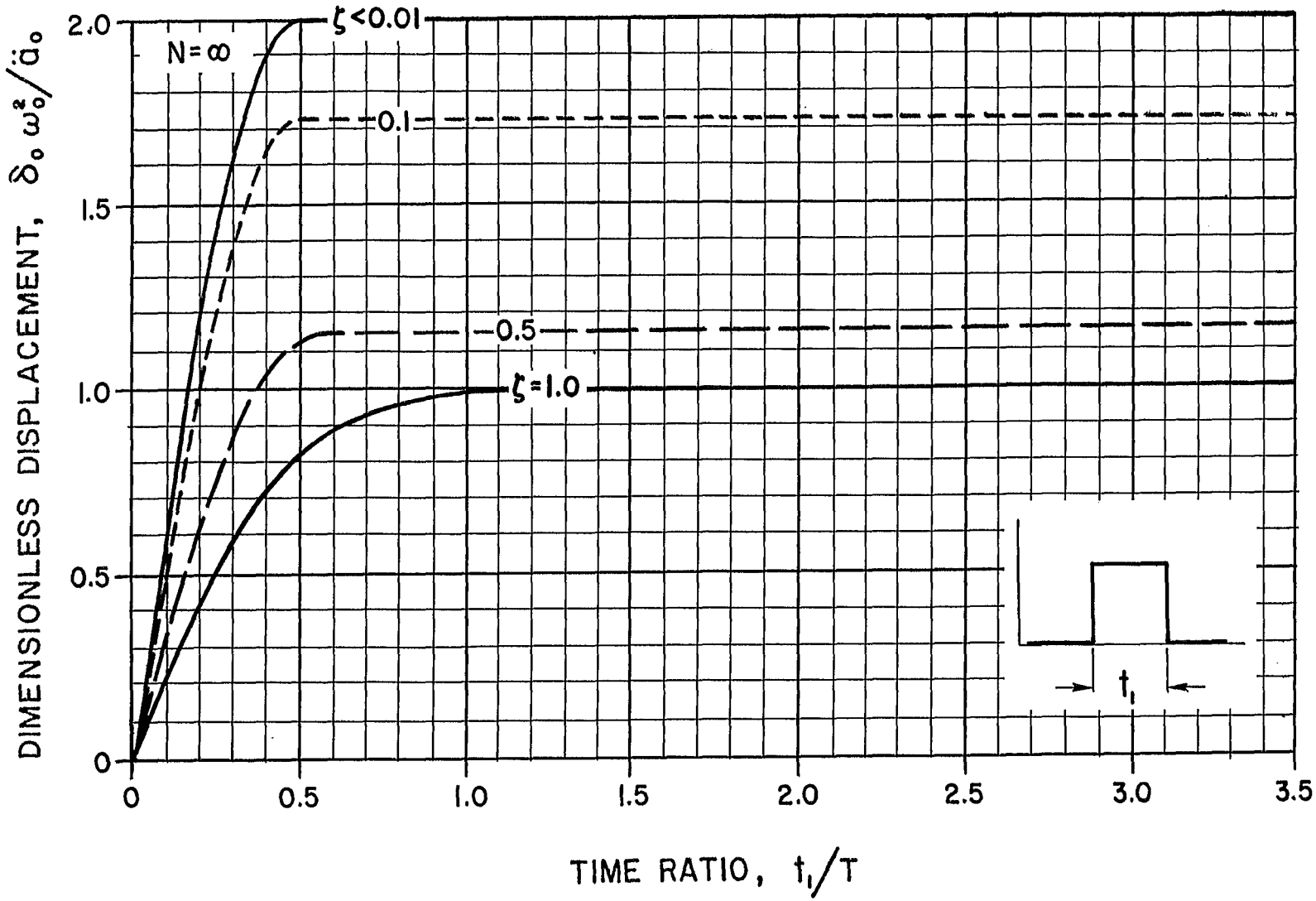

Figure 45.-Peak displacement response to an acceleration rectangular pulse input for the isolation system shown in Figure 1(a) with N = ∞

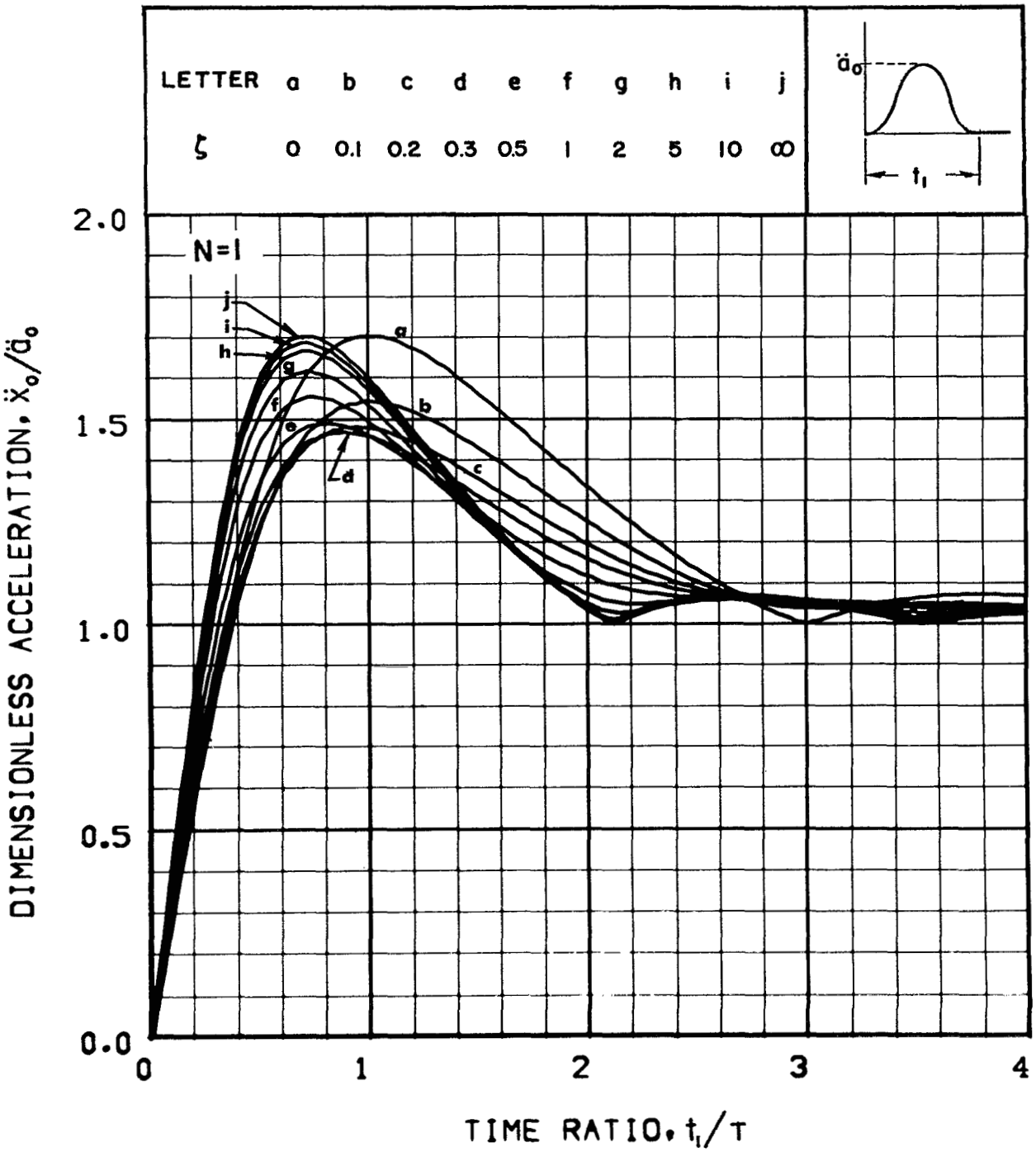

Figure 46.-Peak acceleration response to an acceleration versed-sine pulse input for the isolation system shown in Figure 1(a) with N = 1

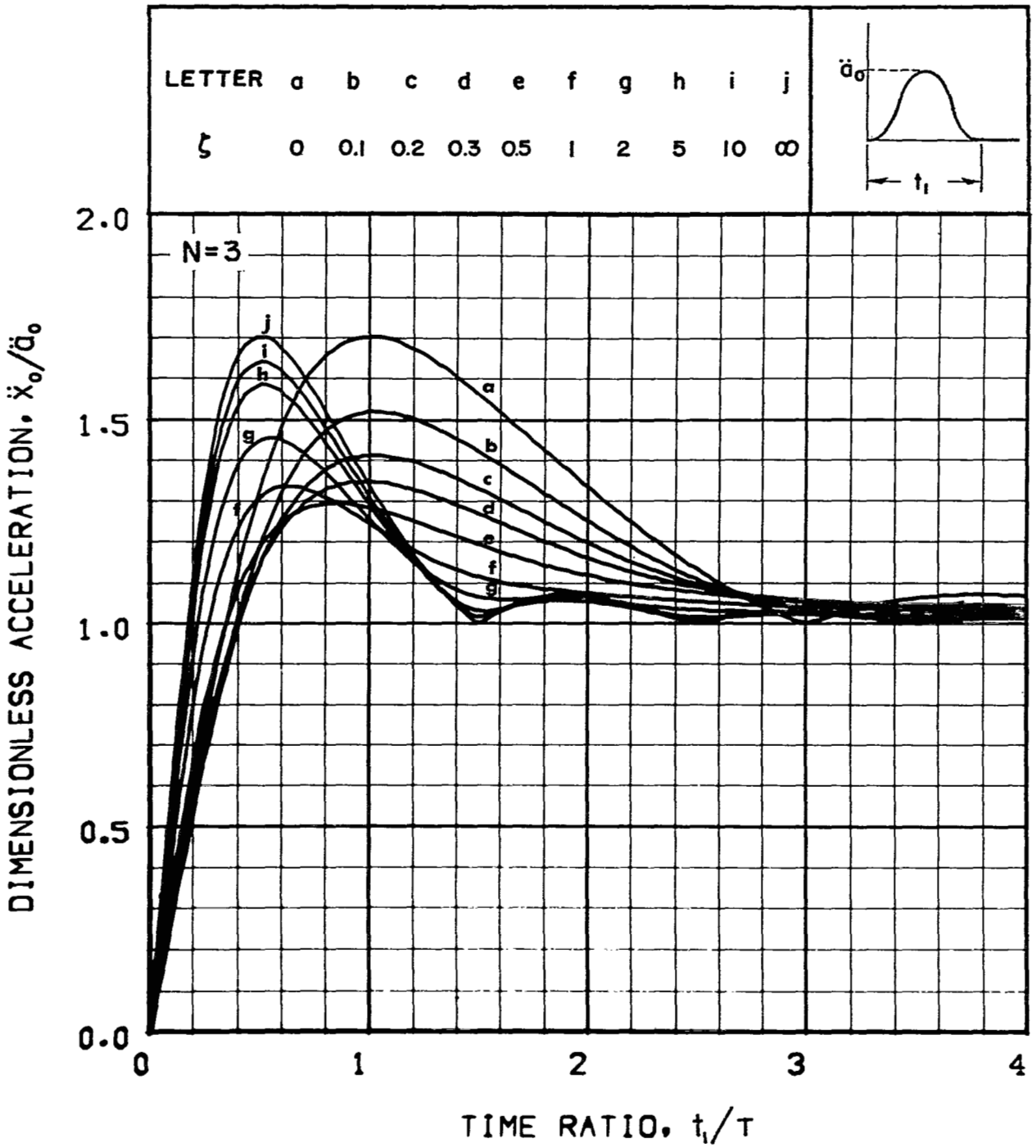

Figure 47.-Peak acceleration response to an acceleration versed-sine pulse input for the isolation system shown in Figure 1(a) with N = 3

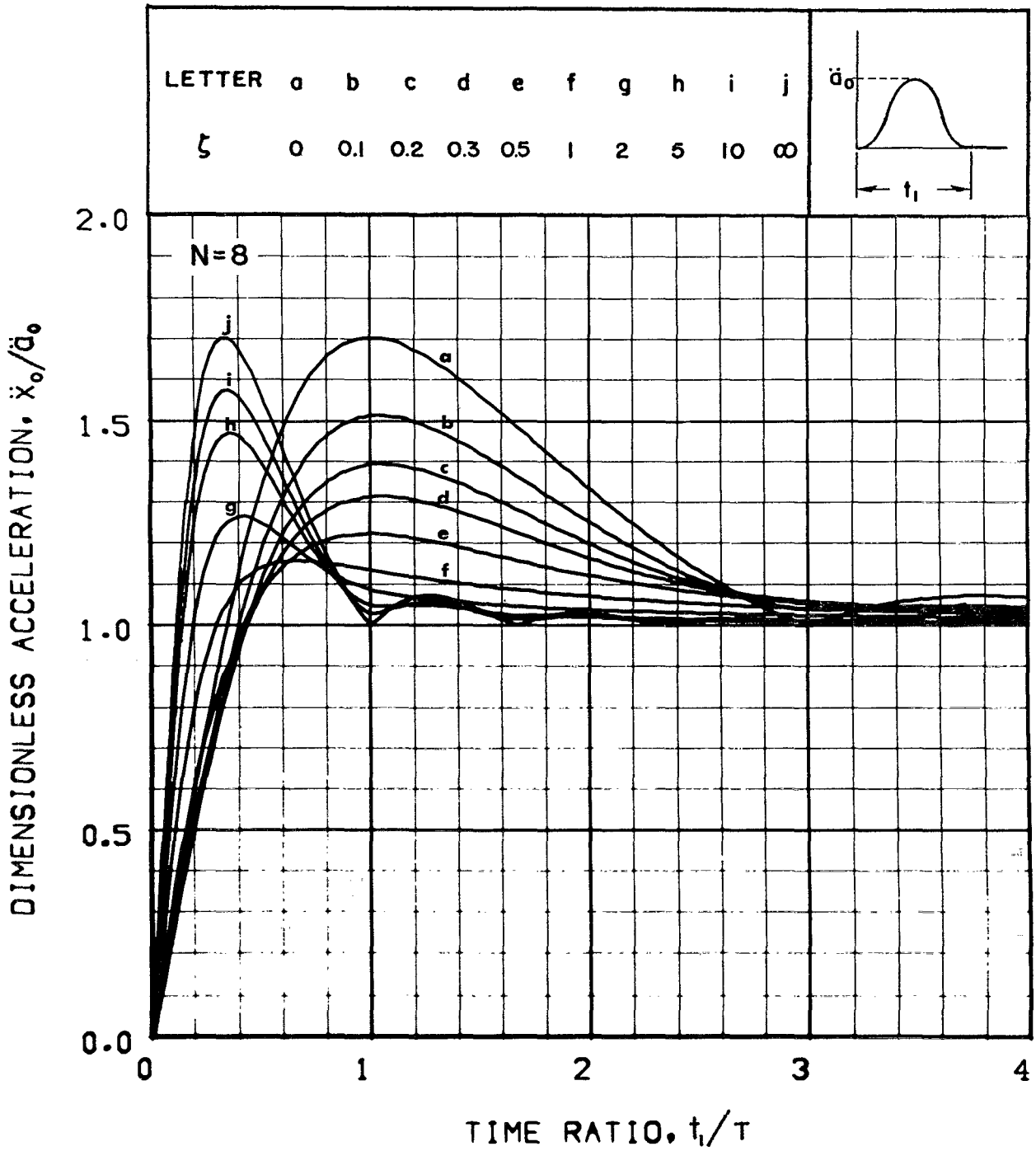

Figure 48.-Peak acceleration response to an acceleration versed-sine pulse input for the isolation system shown in Figure 1(a) with N = 8

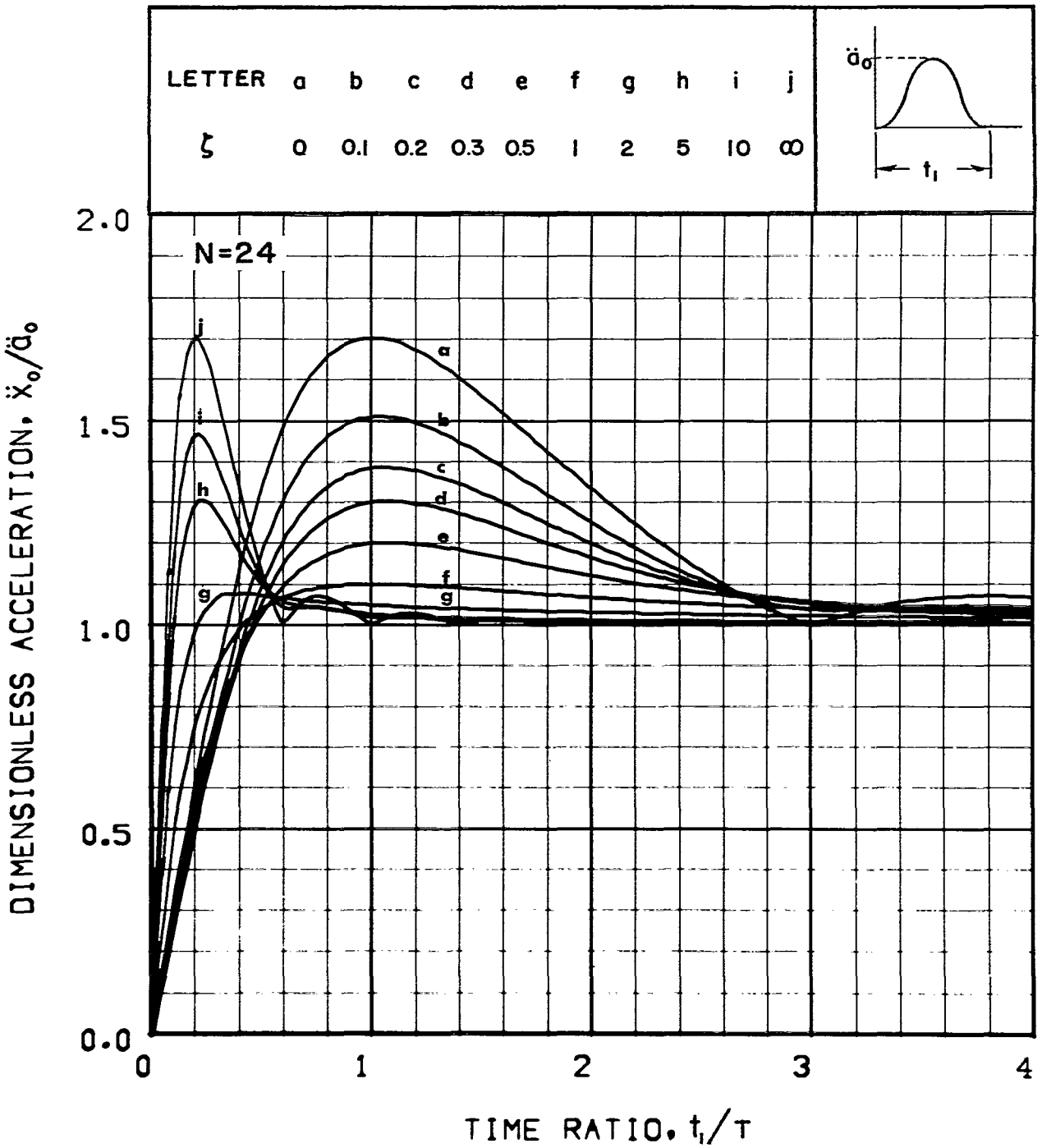

Figure 49.-Peak acceleration response to an acceleration versed-sine pulse input for the isolation system shown in Figure 1(a) with N = 24

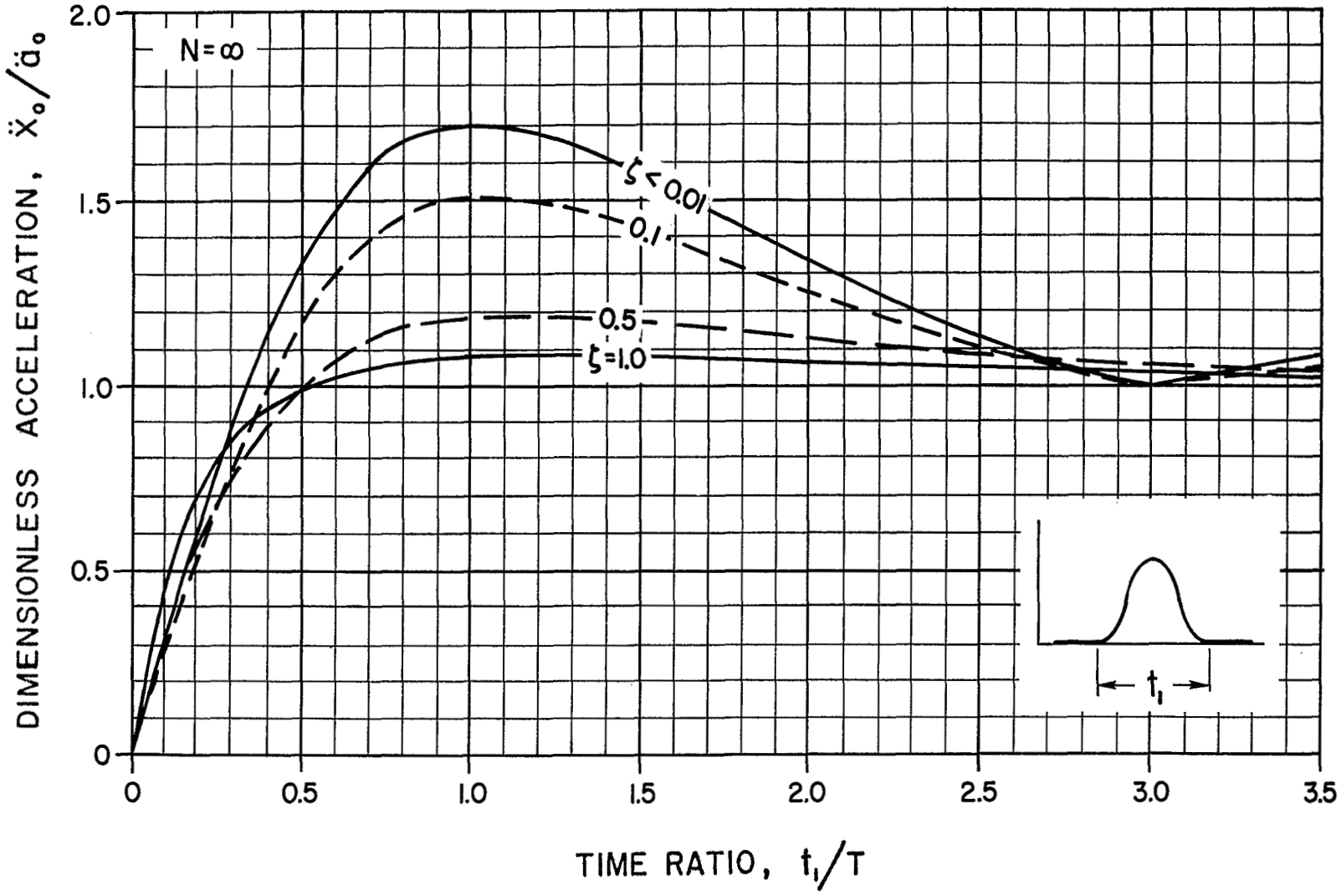

Figure 50.-Peak acceleration response to an acceleration versed-sine pulse input for the isolation system shown in Figure 1(a) with N = ∞

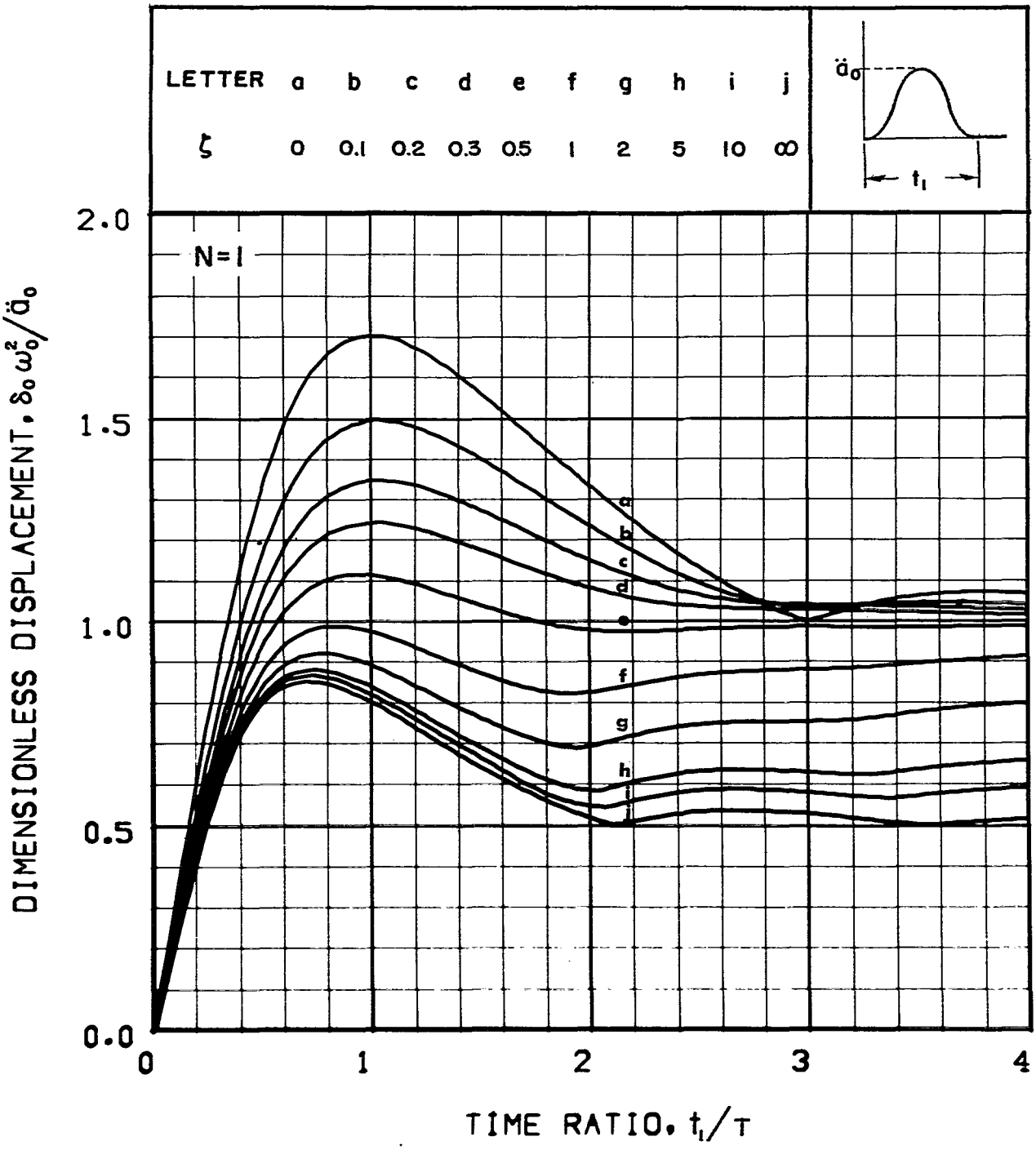

Figure 51.-Peak displacement response to an acceleration versed-sine pulse input for the isolation system shown in Figure 1(a) with N = 1

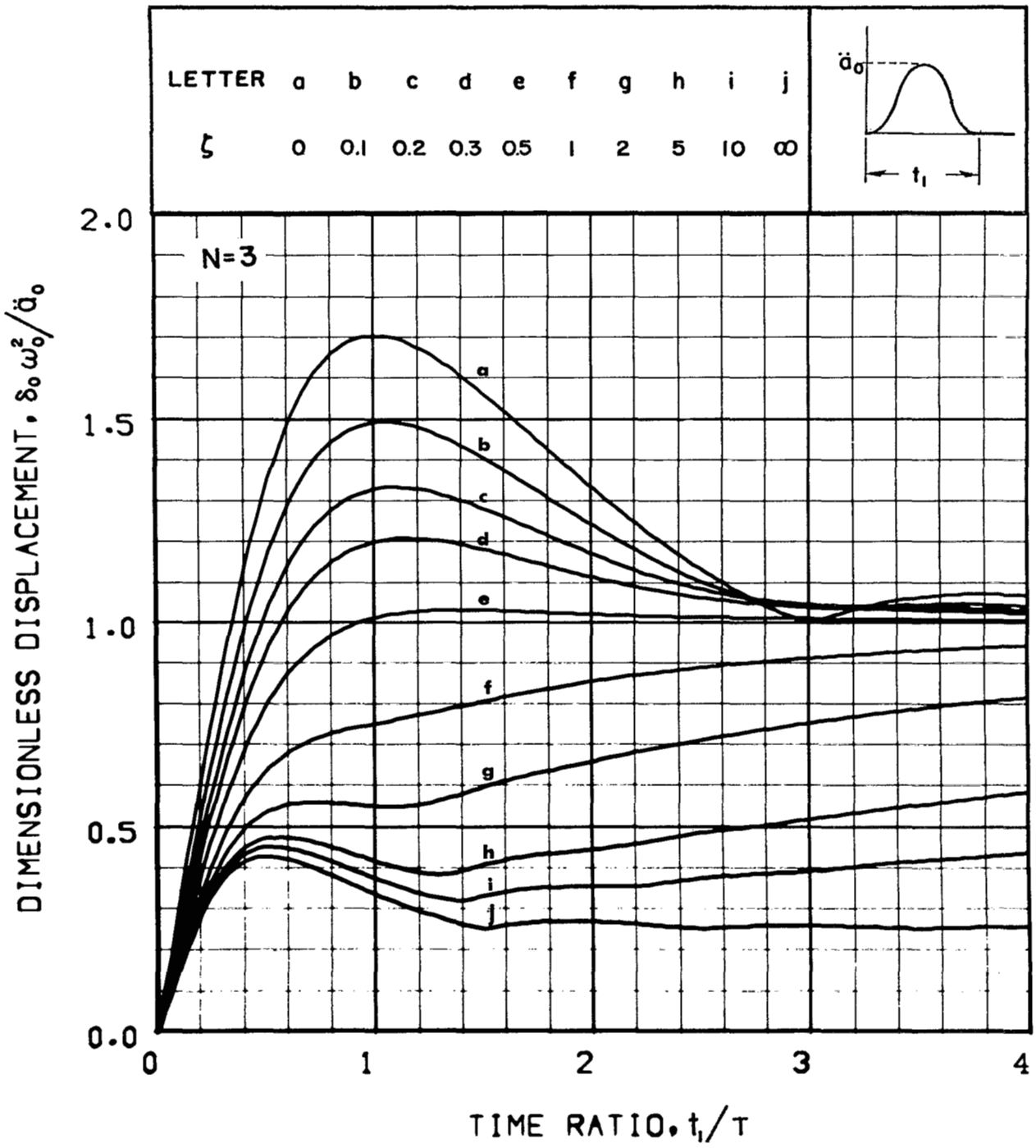

Figure 52.-Peak displacement response to an acceleration versed-sine pulse input for the isolation system shown in Figure 1(a) with N = 3

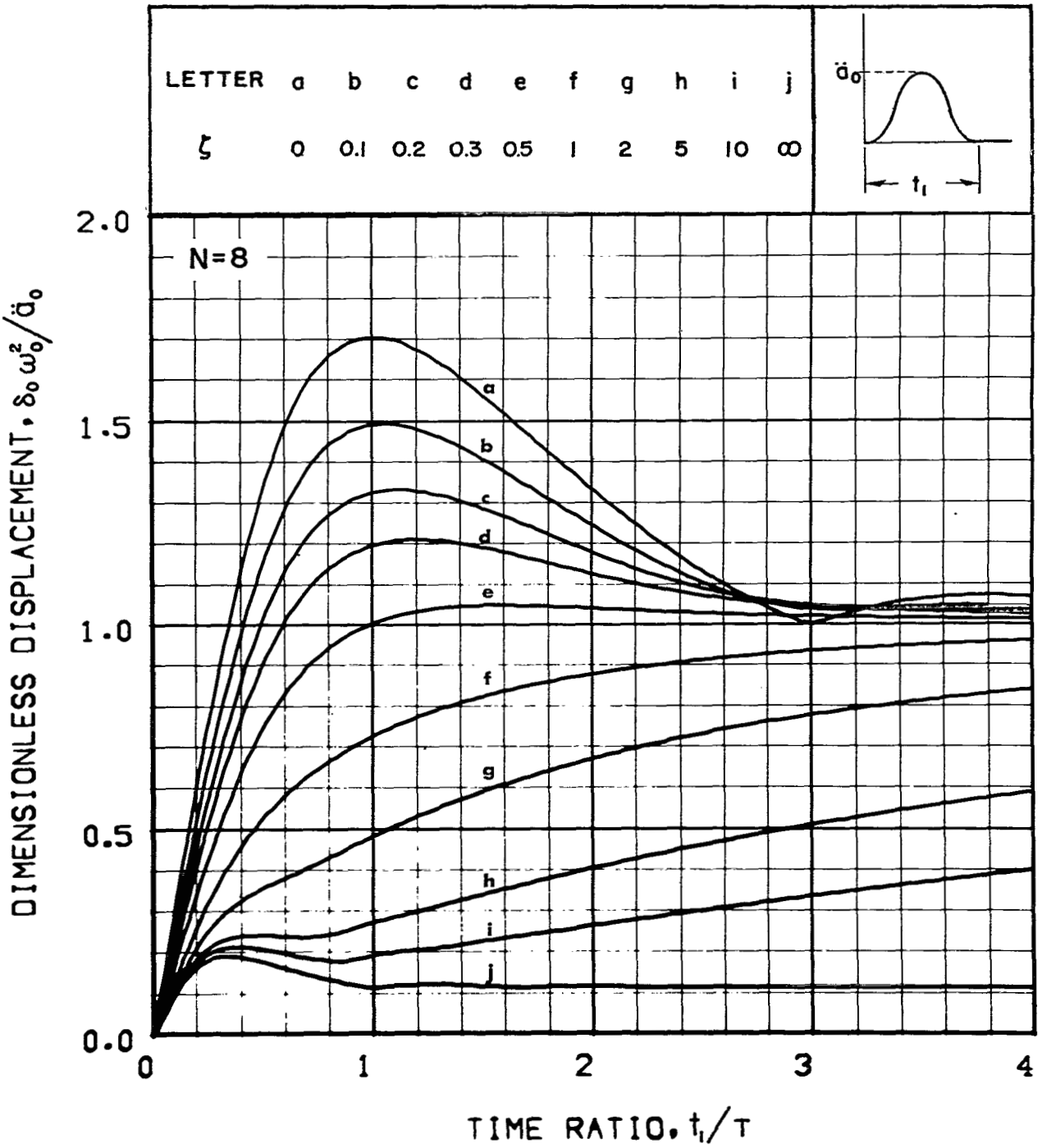

Figure 53.-Peak displacement response to an acceleration versed-sine pulse input for the isolation system shown in Figure 1(a) with N = 8

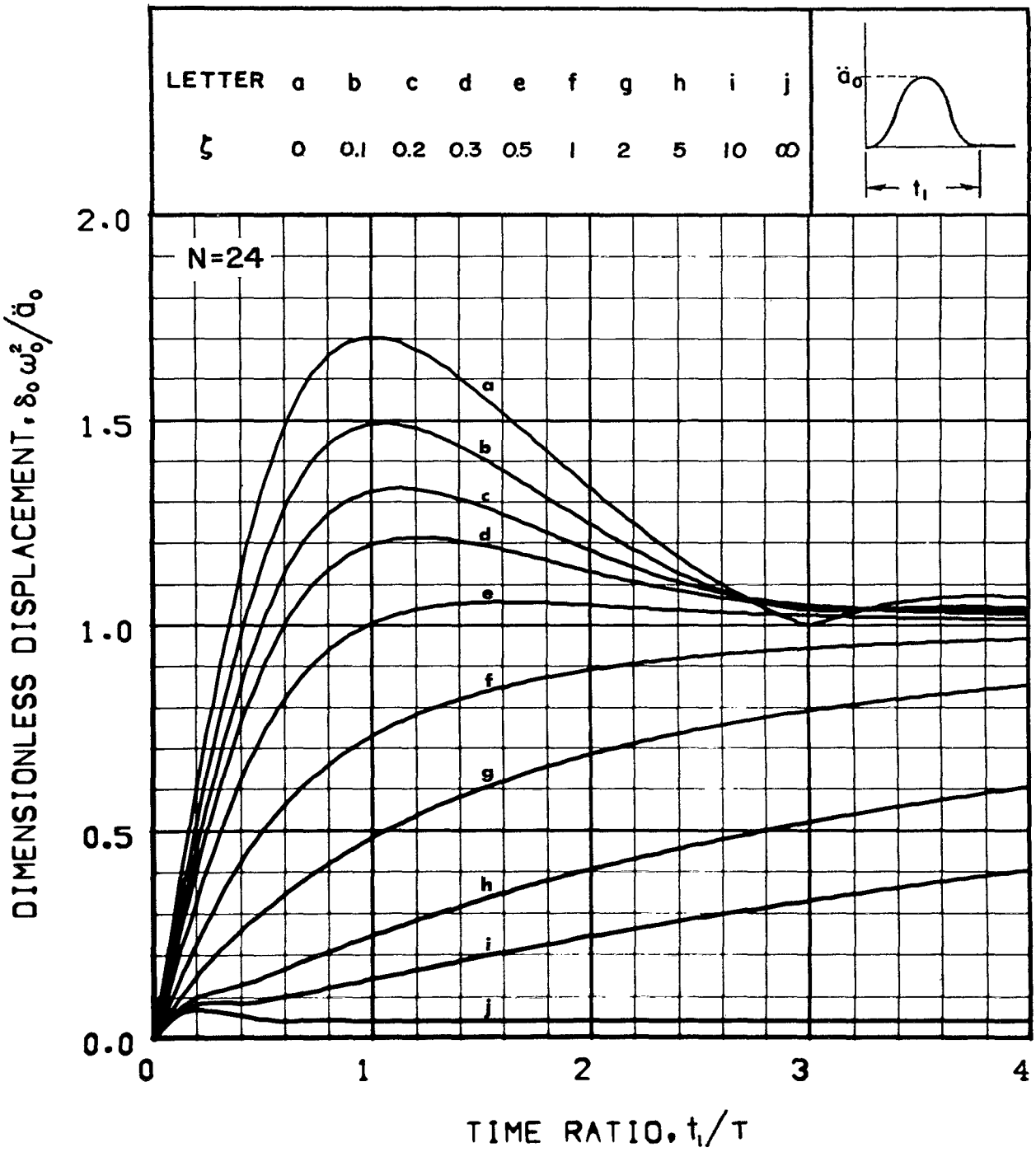

Figure 54.-Peak displacement response to an acceleration versed-sine pulse input for the isolation system shown in Figure 1(a) with N = 24

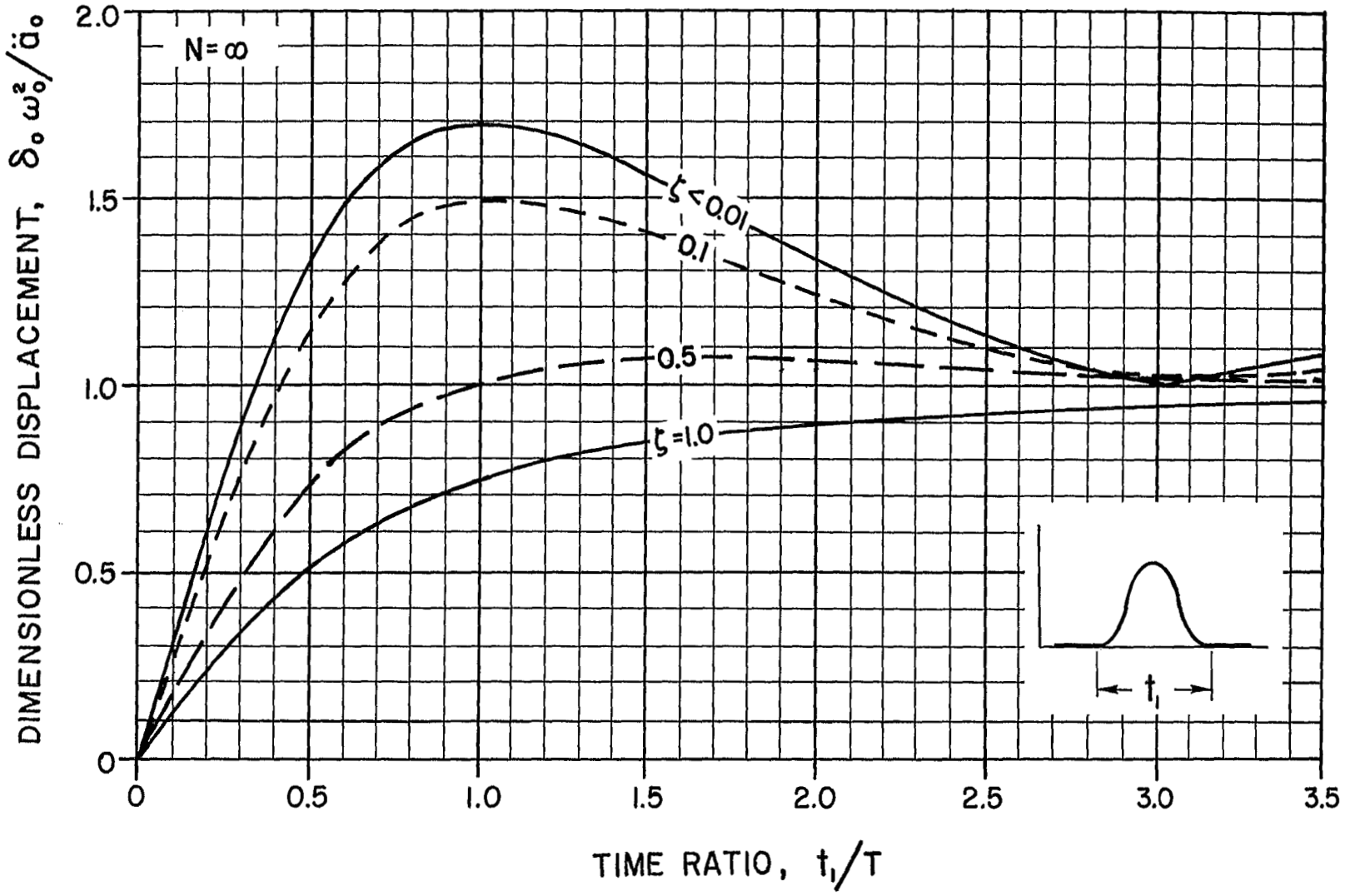

Figure 55.-Peak displacement response to an acceleration versed-sine pulse input for the isolation system shown in Figure 1(a) with N = ∞

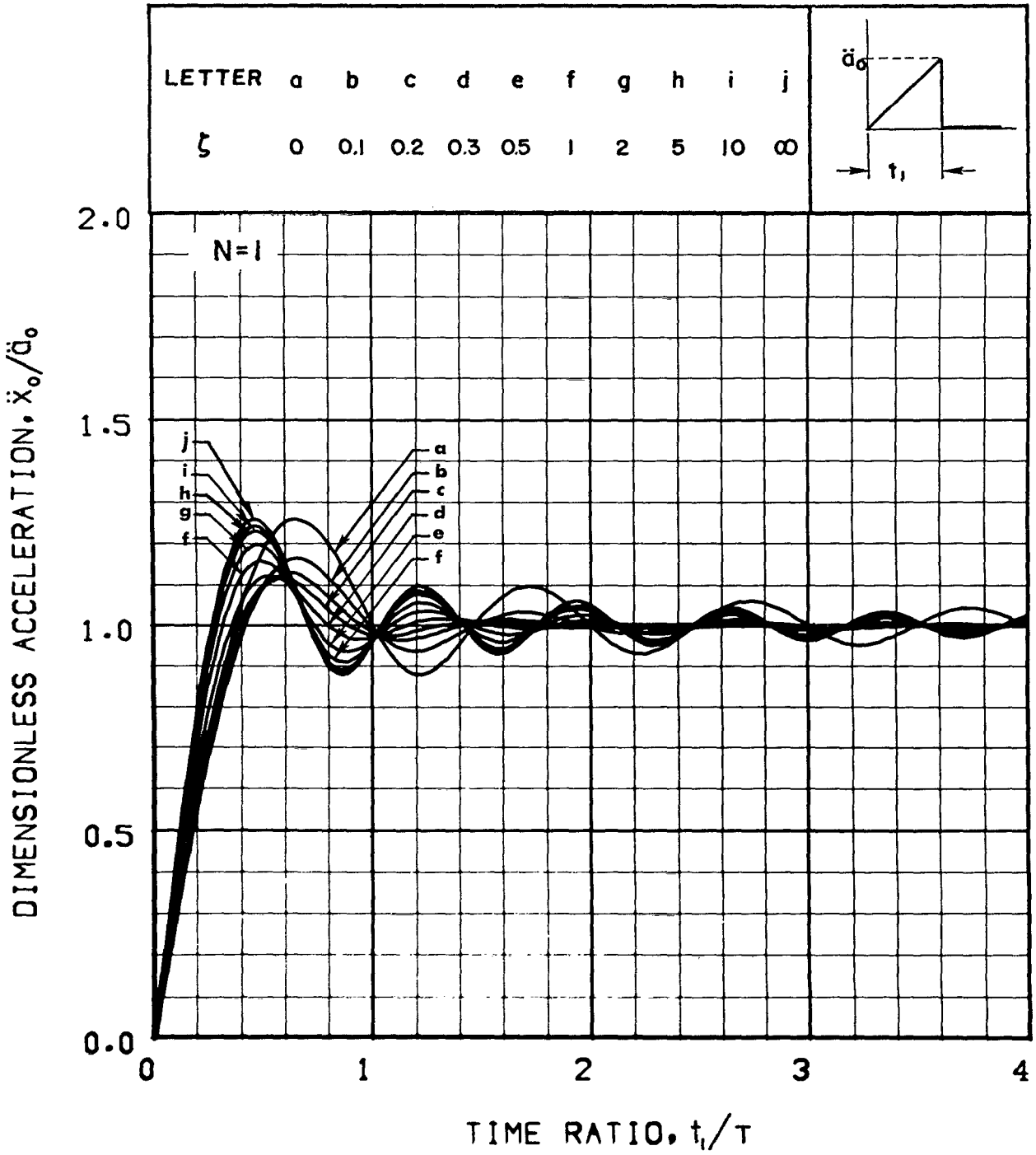

Figure 56.-Peak acceleration response to an acceleration terminal-peak saw-tooth pulse input for the isolation system shown in Figure 1(a) with N = 1

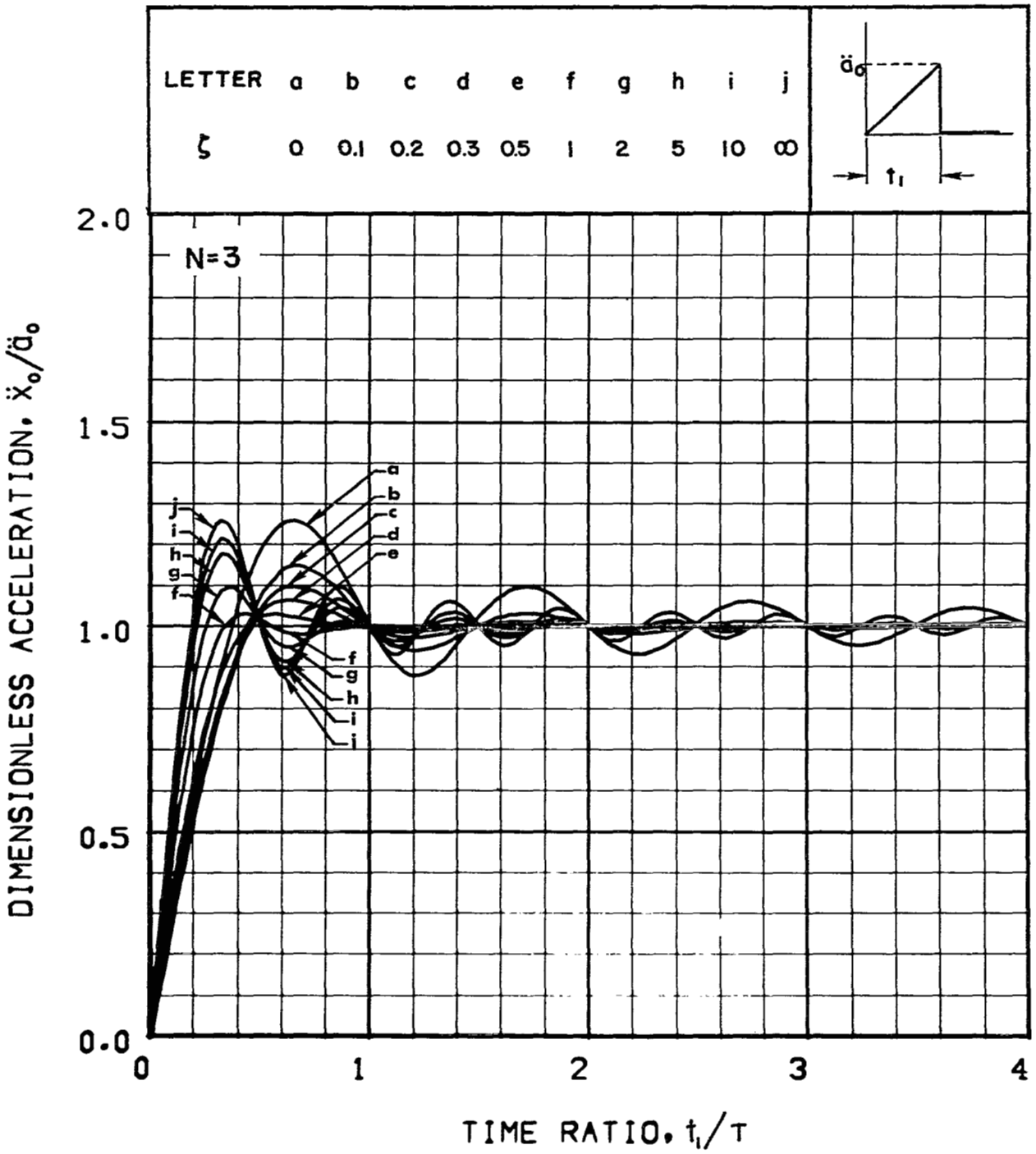

Figure 57.-Peak acceleration response to an acceleration terminal-peak saw-tooth pulse input for the isolation system shown in Figure 1(a) with N = 3

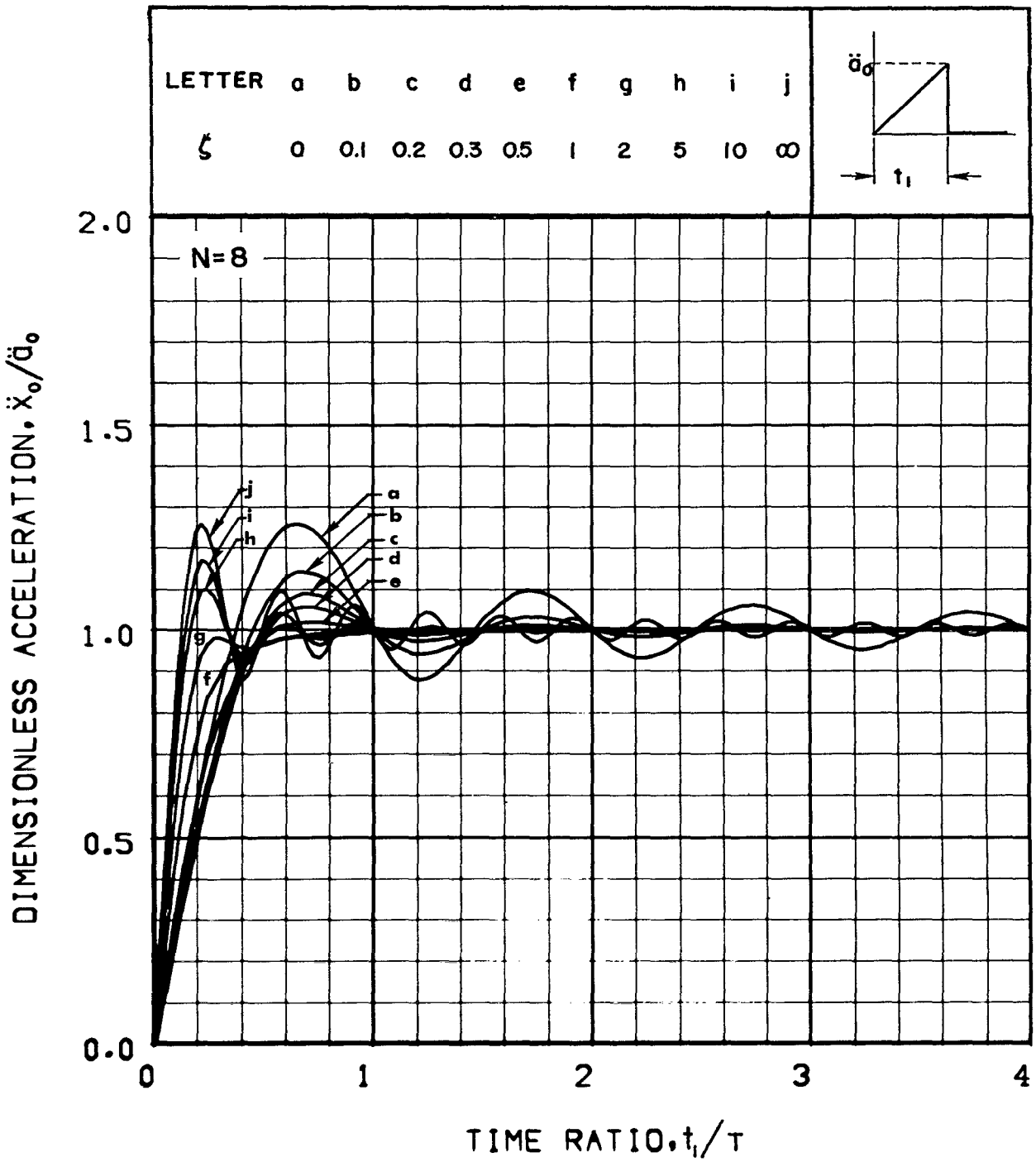

Figure 58.-Peak acceleration response to an acceleration terminal-peak saw-tooth pulse input for the isolation system shown in Figure 1(a) with N = 8

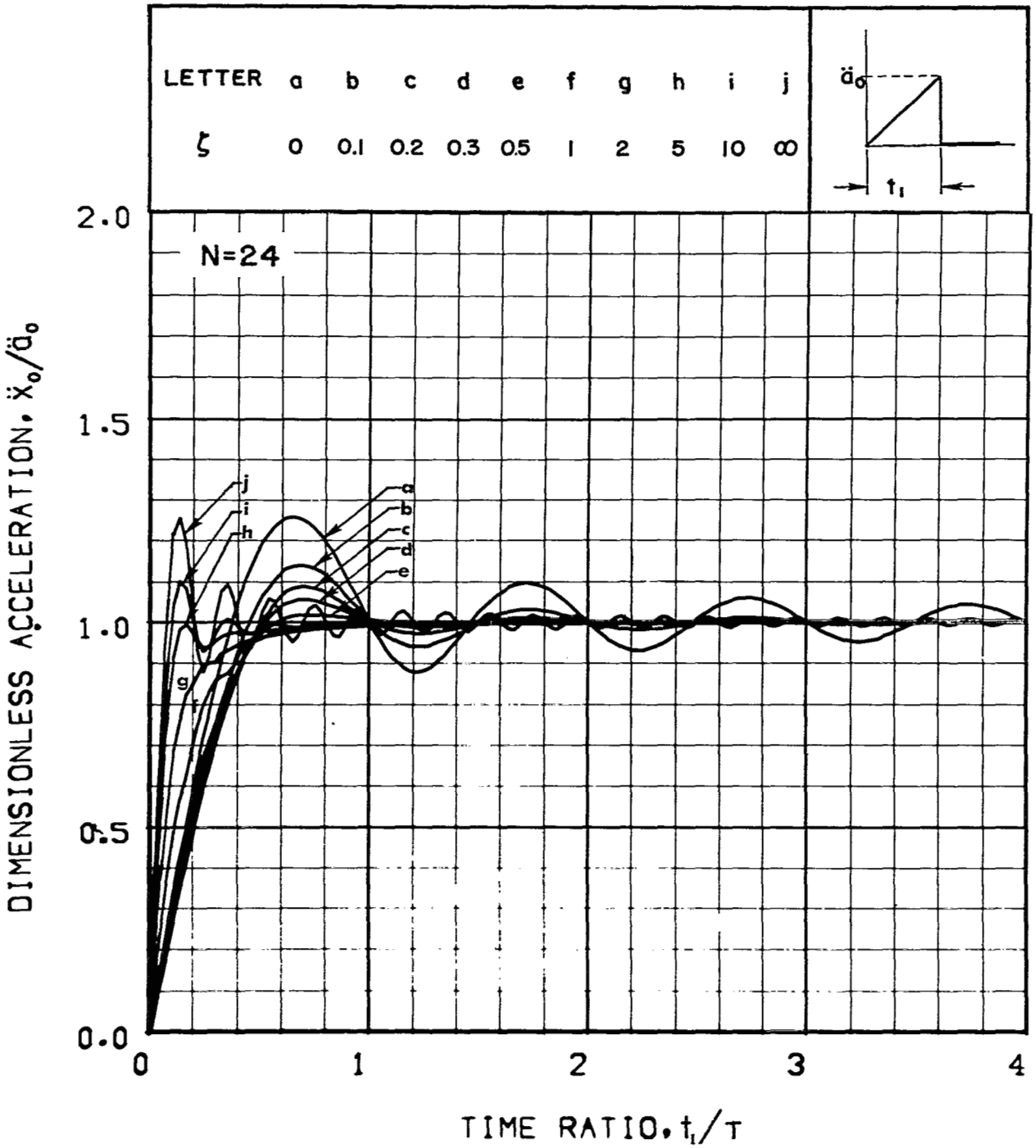

Figure 59.-Peak acceleration response to an acceleration terminal-peak saw-tooth pulse input for the isolation system shown in Figure 1(a) with N = 24

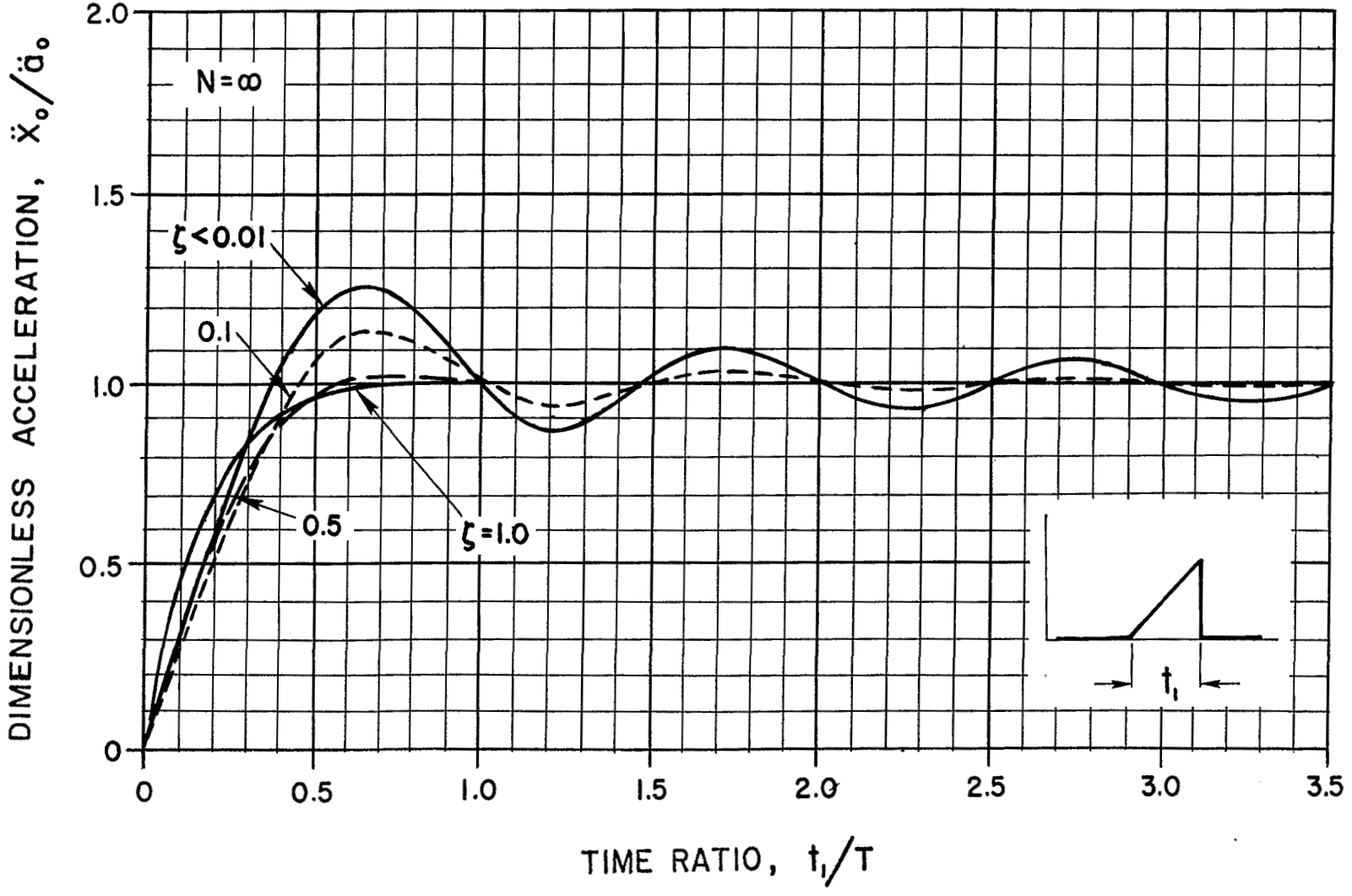

Figure 60.-Peak acceleration response to an acceleration terminal-peak saw-tooth pulse input for the isolation system shown in Figure 1(a) with N = ∞

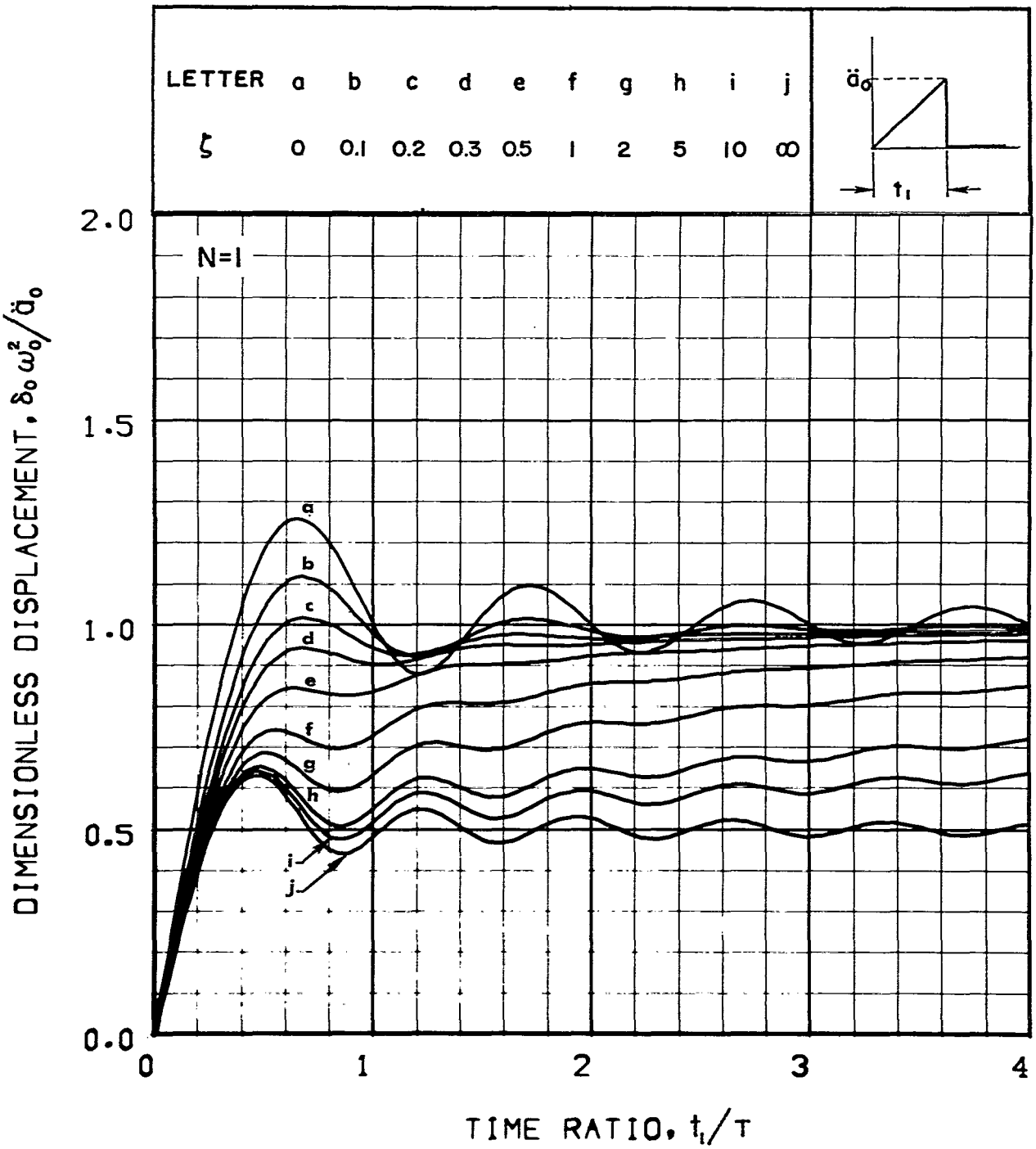

Figure 61.-Peak displacement response to an acceleration terminal-peak saw-tooth pulse input for the isolation system shown in Figure 1(a) with N = 1

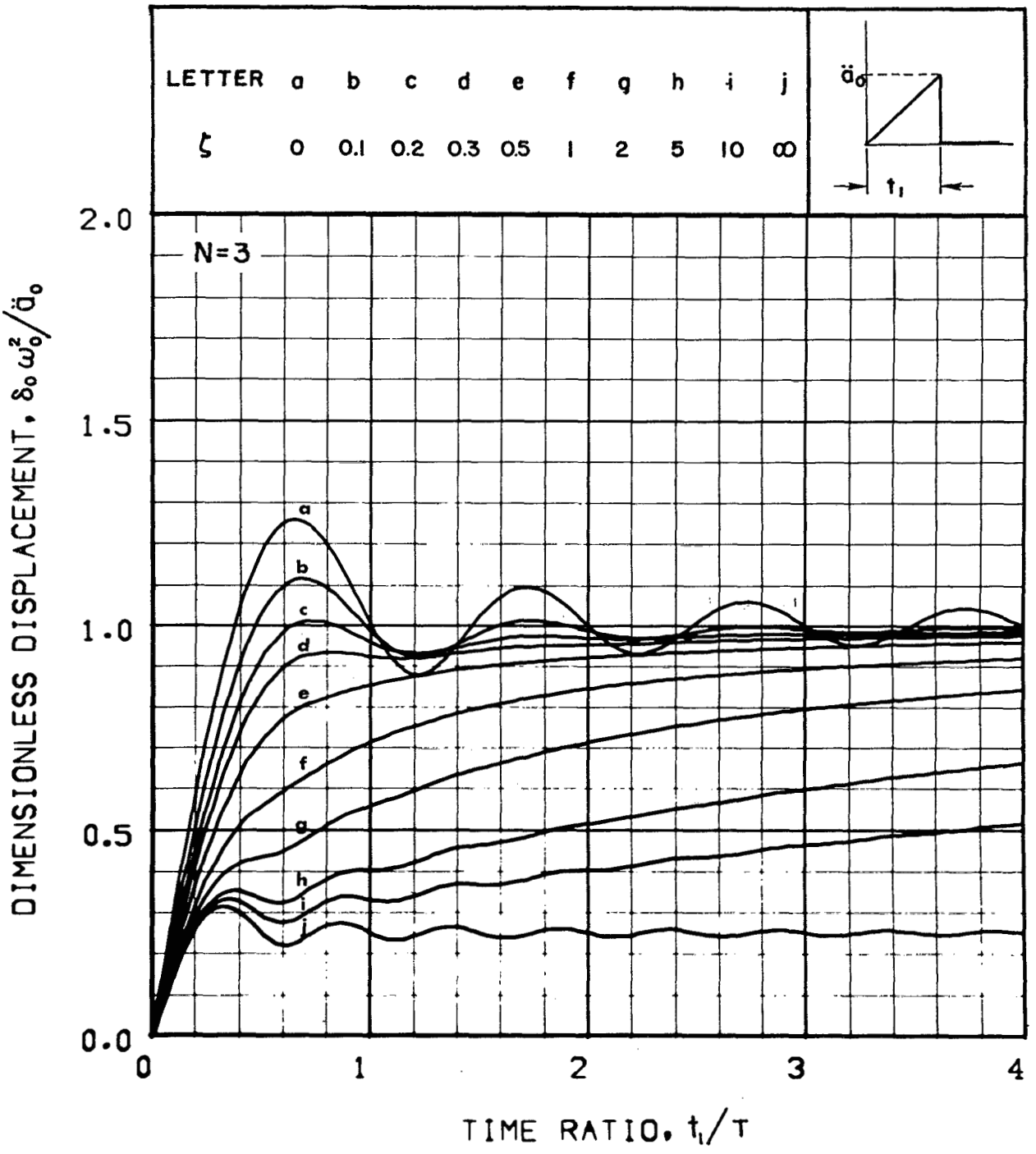

Figure 62.-Peak displacement response to an acceleration terminal-peak saw-tooth pulse input for the isolation system shown in Figure 1(a) with N = 3

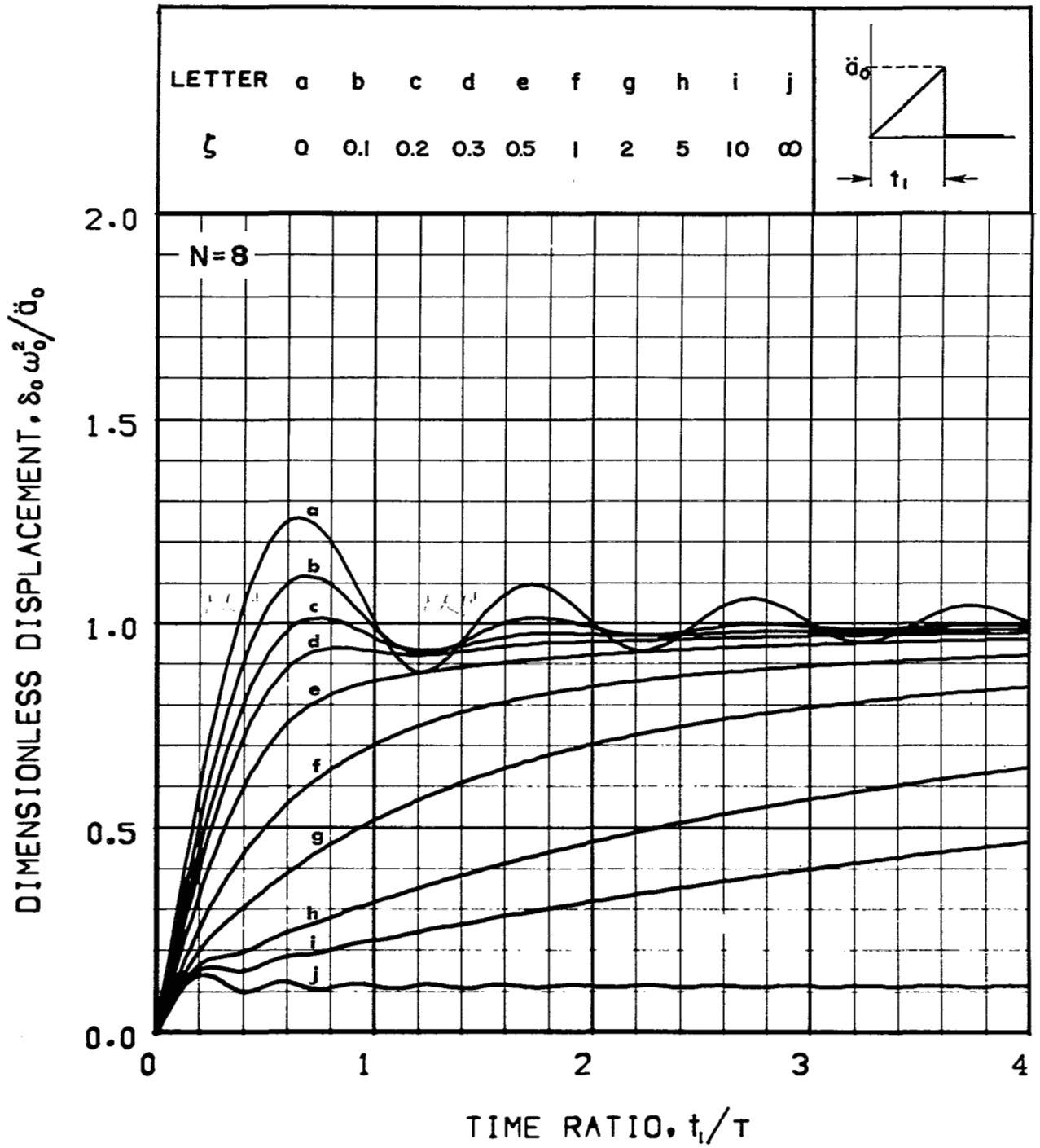

Figure 63.-Peak displacement response to an acceleration terminal-peak saw-tooth pulse input for the isolation system shown in Figure 1(a) with N = 8

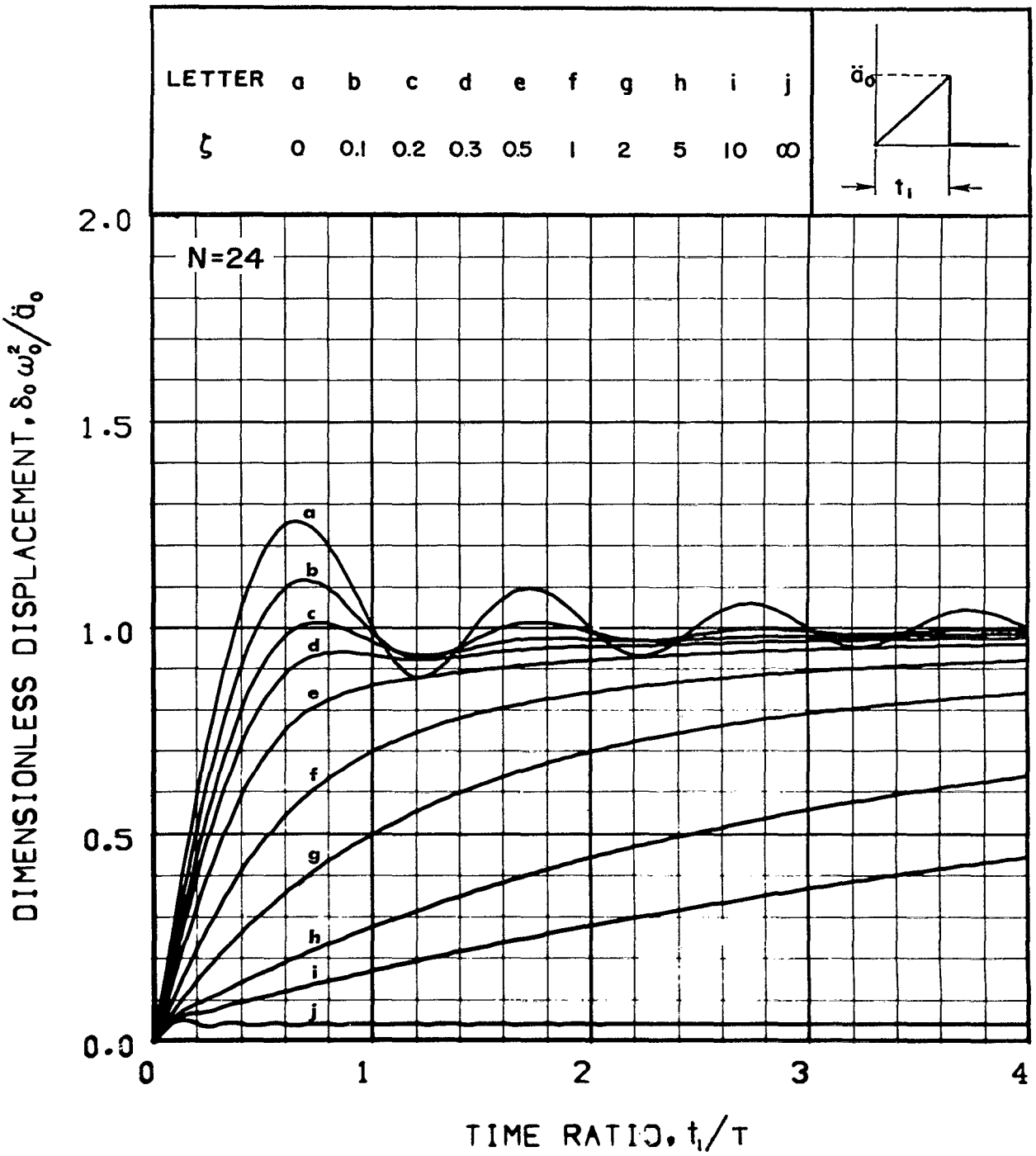

Figure 64.-Peak displacement response to an acceleration terminal-peak saw-tooth pulse input for the isolation system shown in Figure 1(a) with N = 24

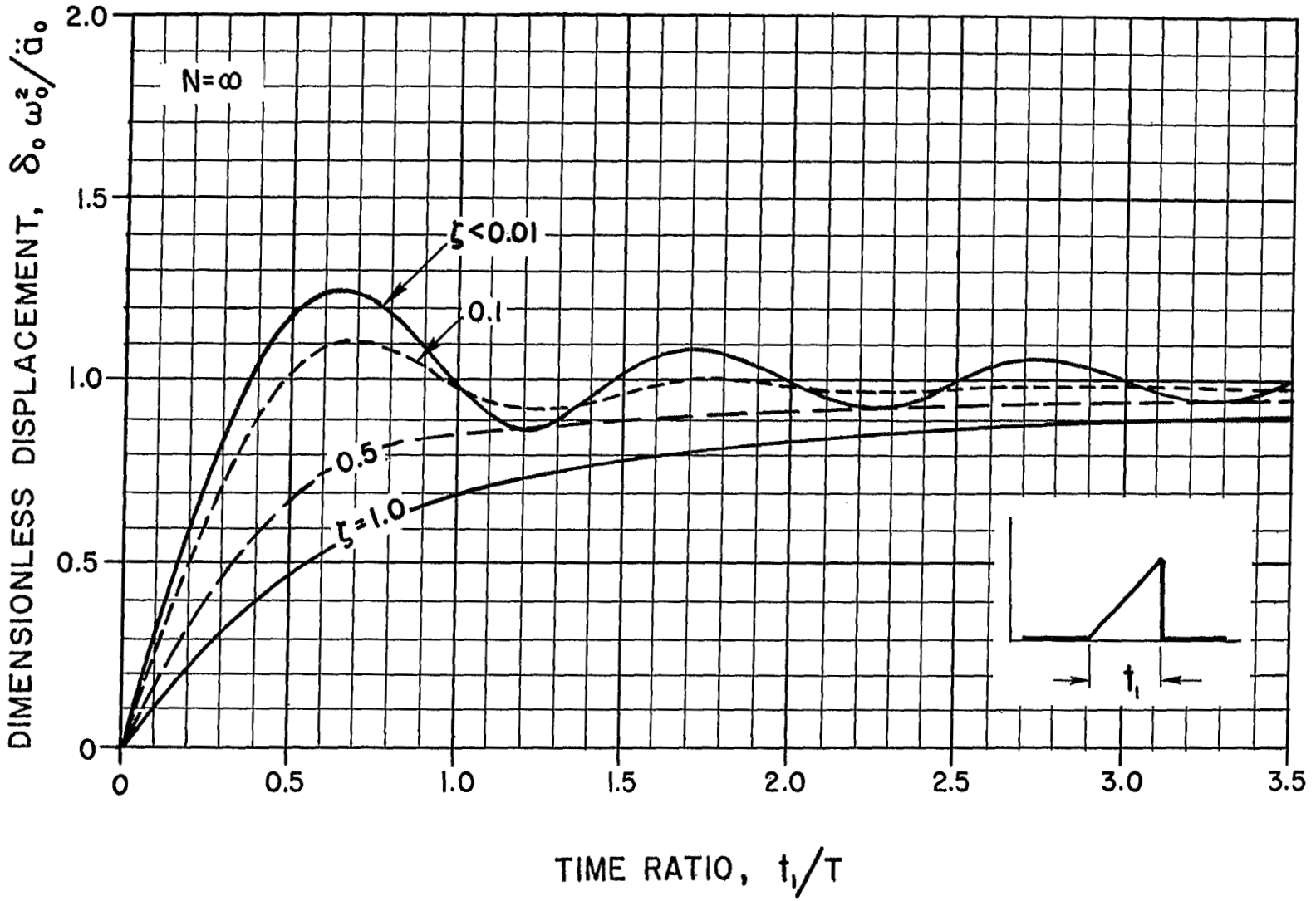

Figure 65.-Peak displacement response to an acceleration terminal-peak saw-tooth pulse input for the isolation system shown in Figure 1(a) with N = ∞

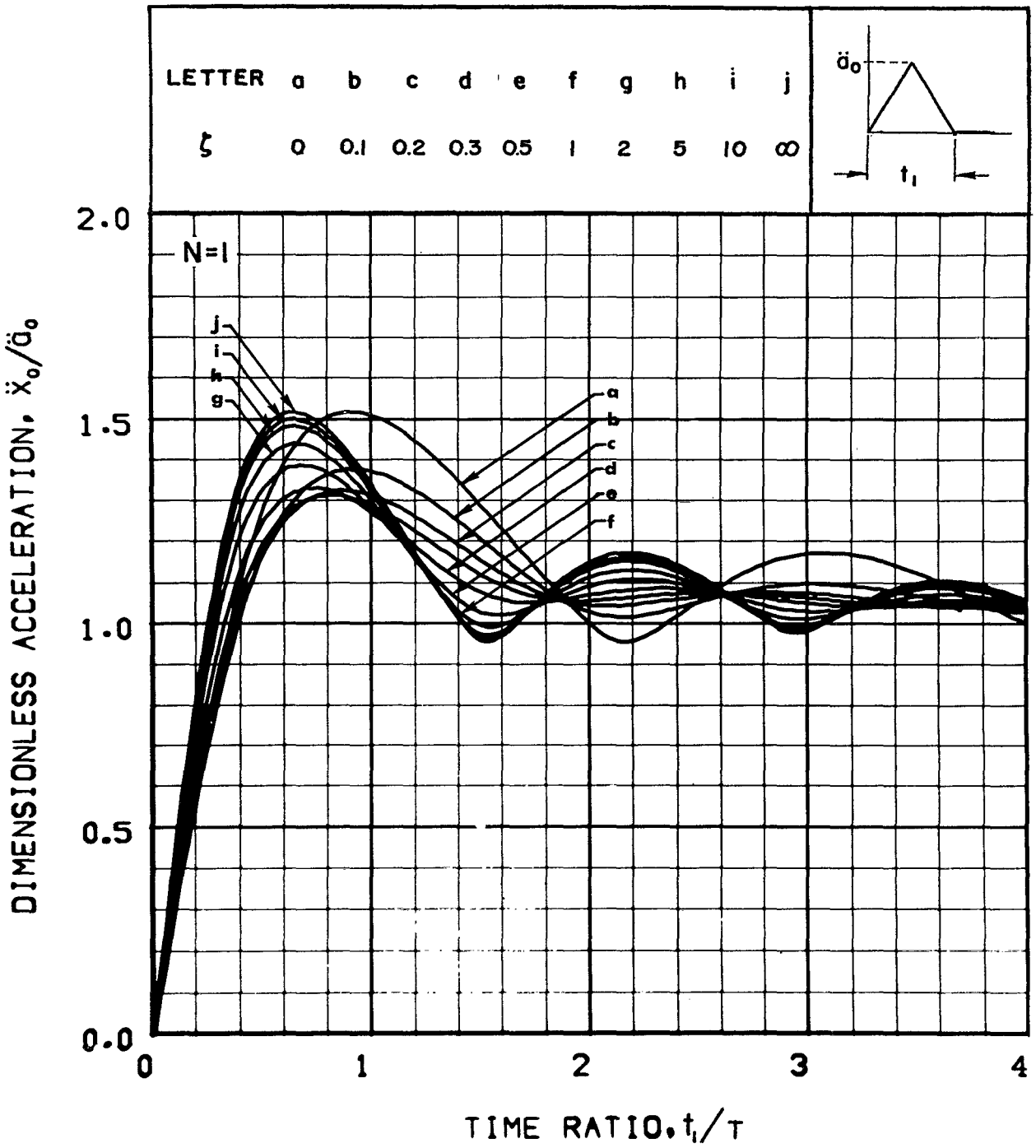

Figure 66.-Peak acceleration response to an acceleration symmetrical triangular pulse input for the isolation system shown in Figure 1(a) with N = 1

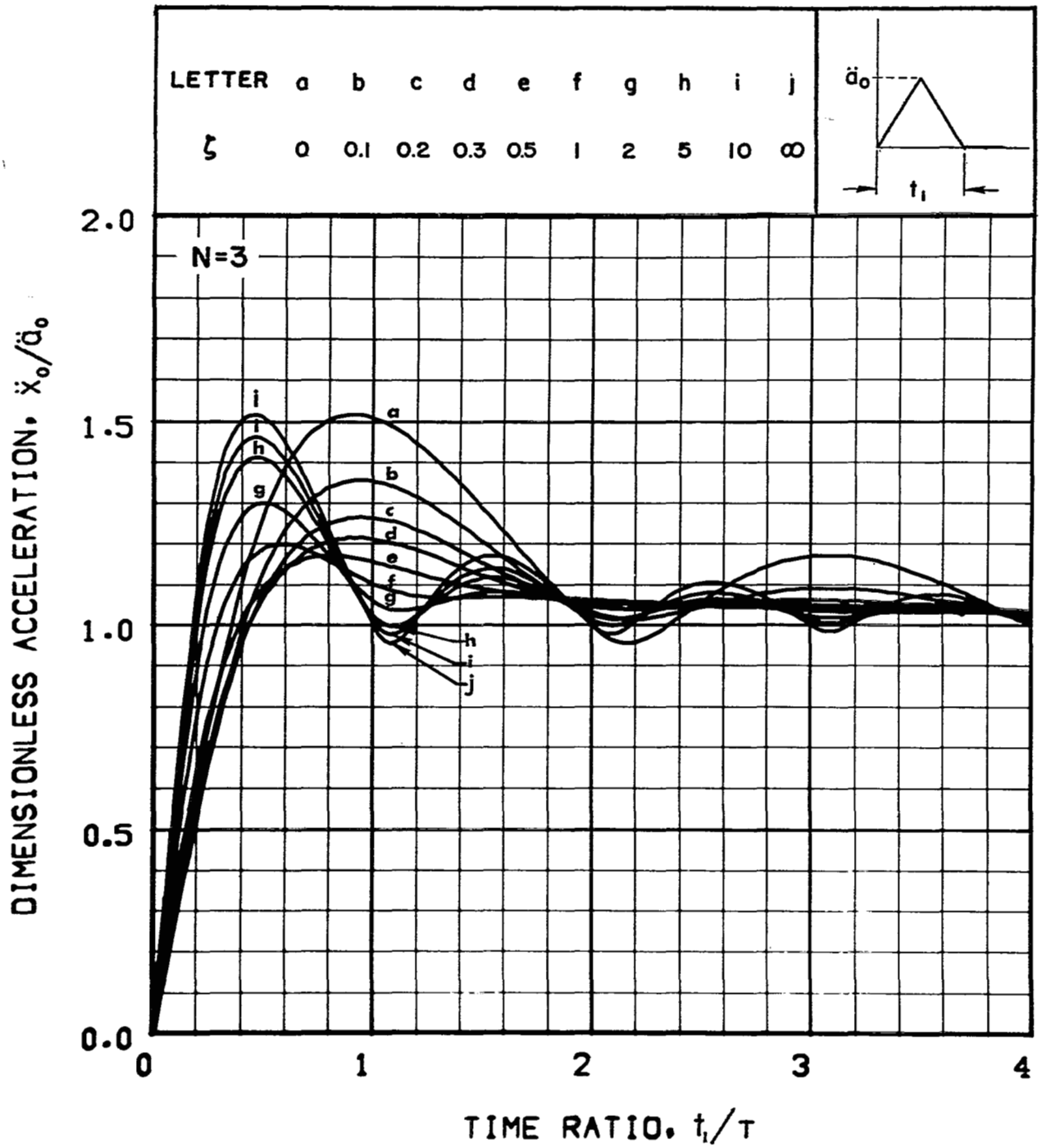

Figure 67.-Peak acceleration response to an acceleration symmetrical triangular pulse input for the isolation system shown in Figure 1(a) with N = 3

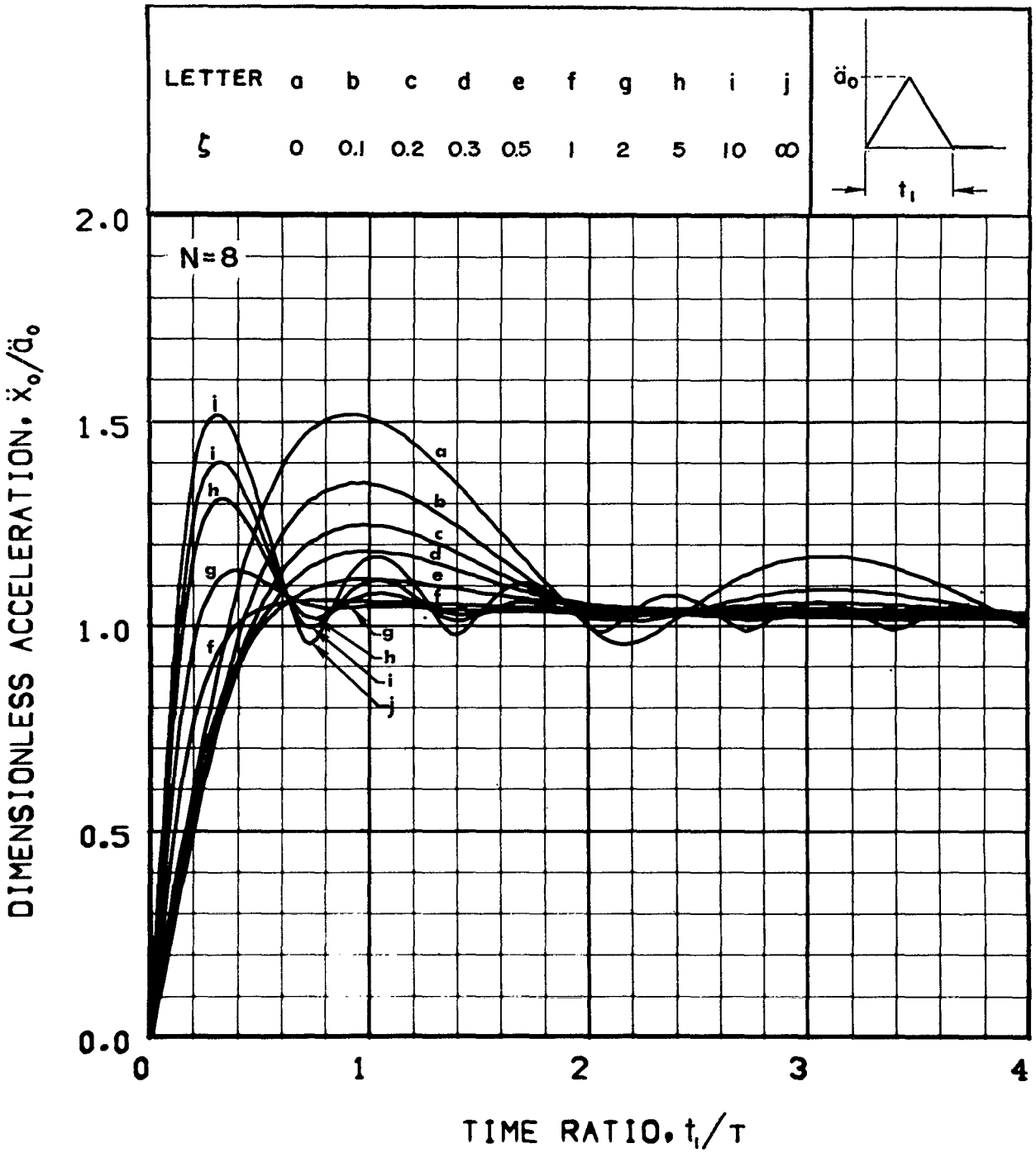

Figure 68.-Peak acceleration response to an acceleration symmetrical triangular pulse input for the isolation system shown in Figure 1(a) with N = 8

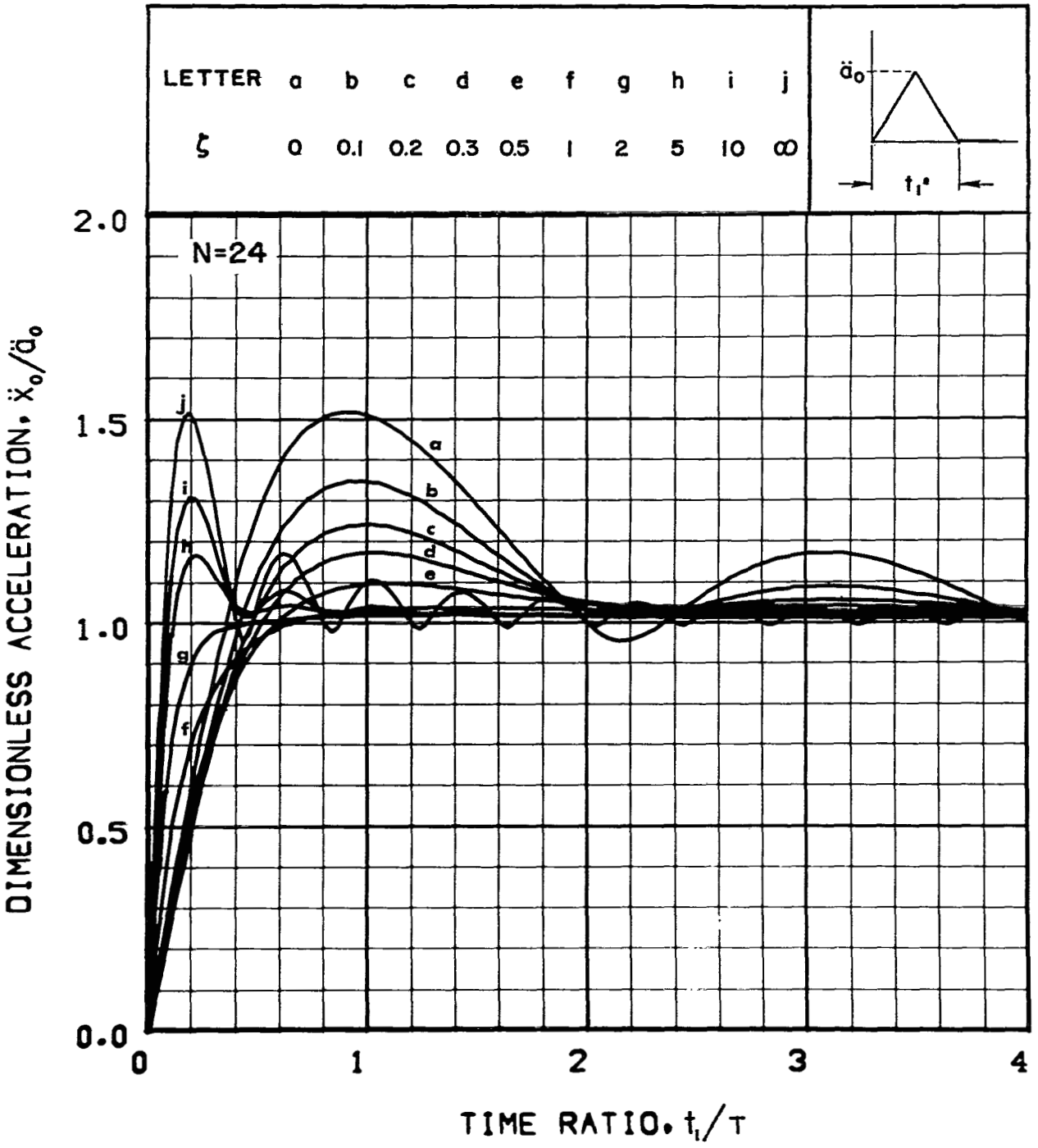

Figure 69.-Peak acceleration response to an acceleration symmetrical triangular pulse input for the isolation system shown in Figure 1(a) with N = 24

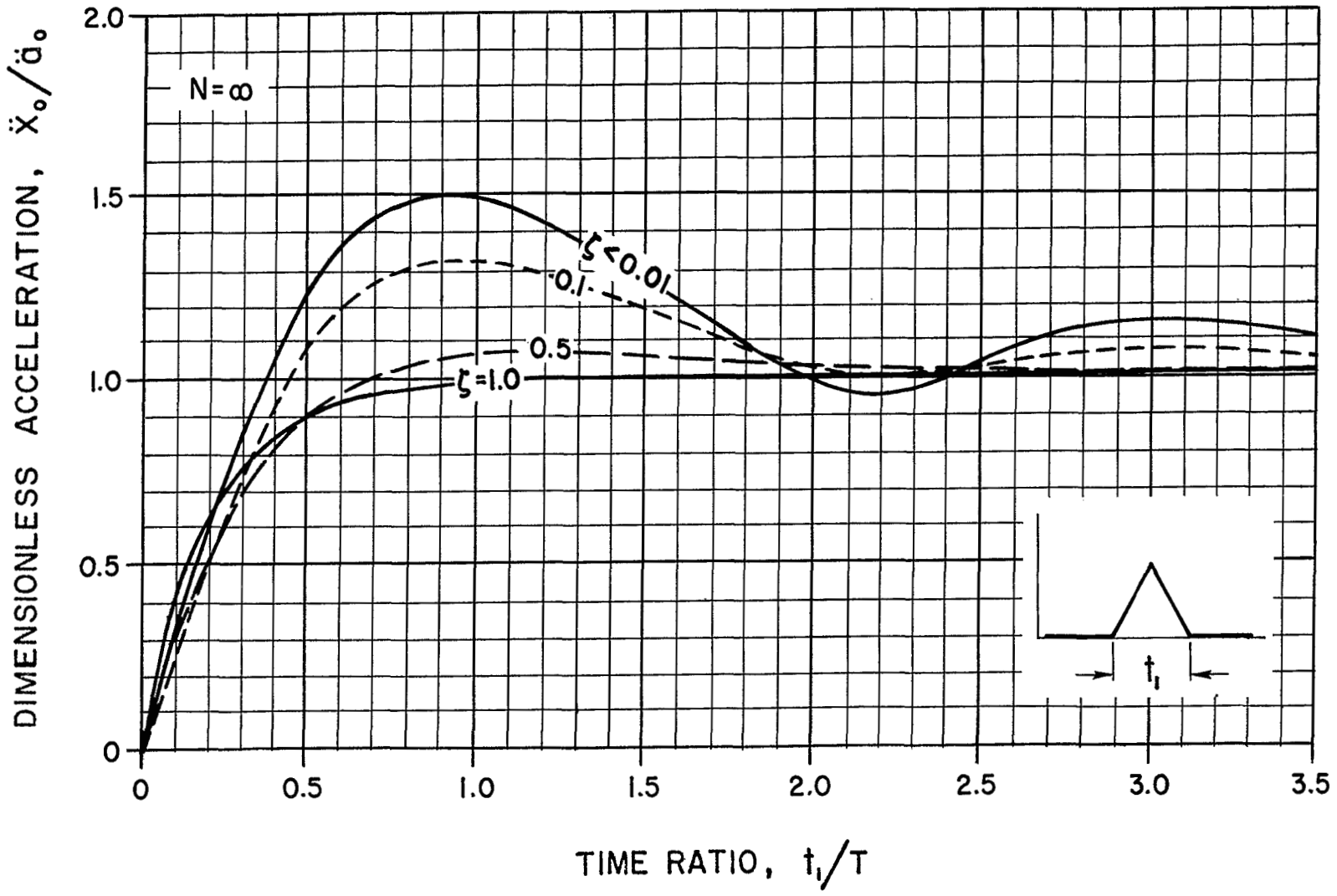

Figure 70.-Peak acceleration response to an acceleration symmetrical triangular pulse input for the isolation system shown in Figure 1(a) with N = ∞

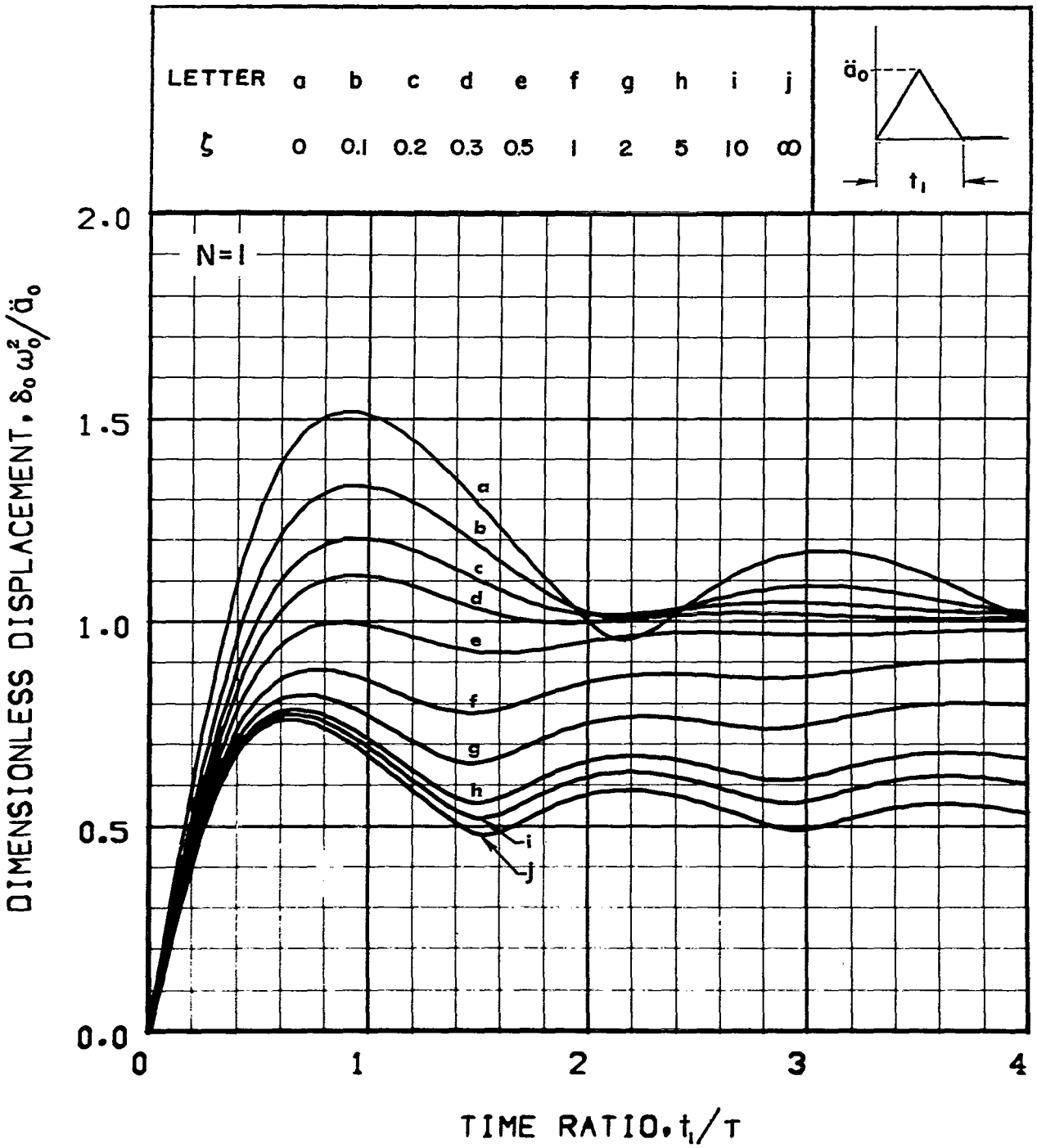

Figure 71.-Peak displacement response to an acceleration symmetrical triangular pulse input for the isolation system shown in Figure 1(a) with N = 1

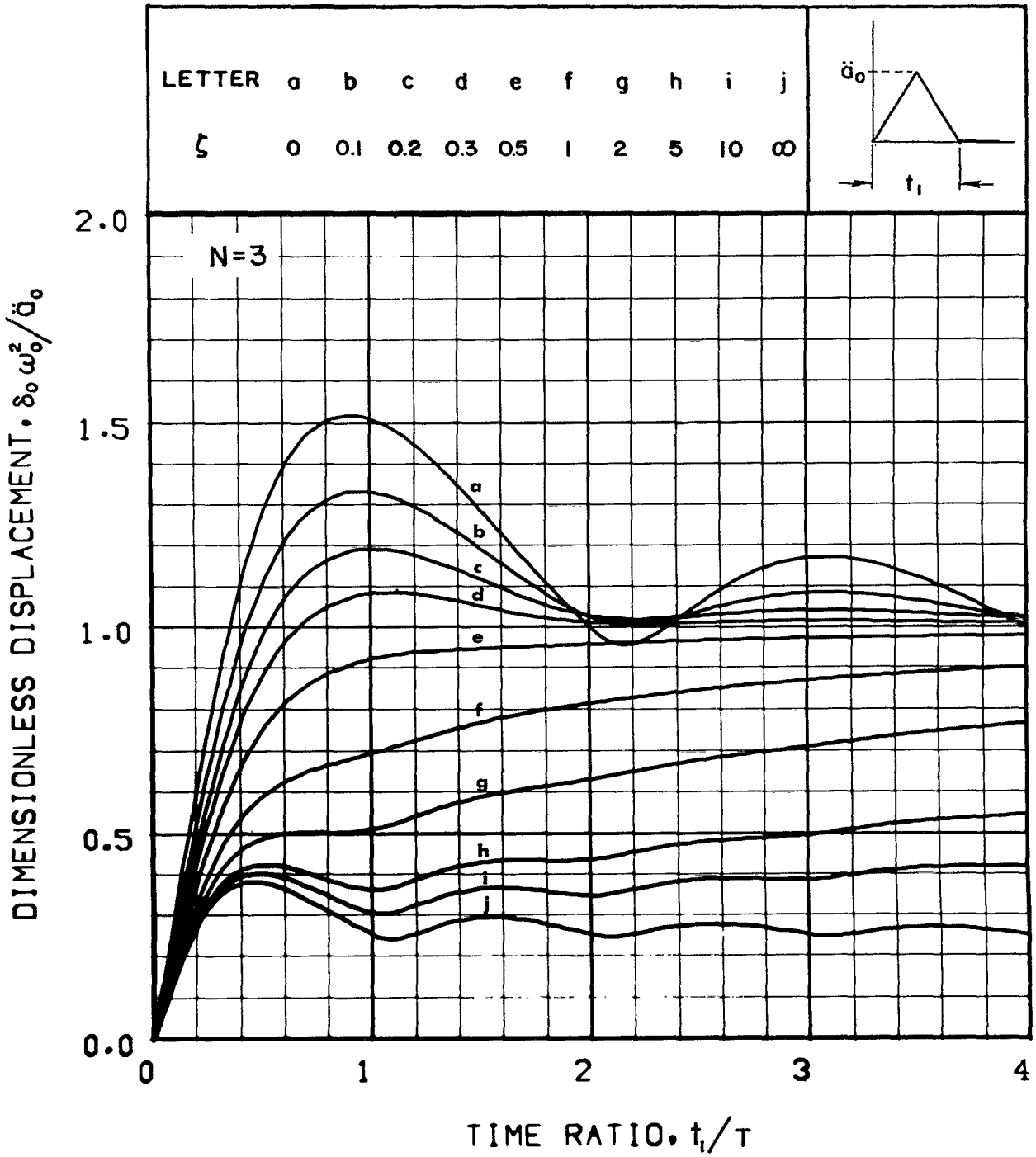

Figure 72.-Peak displacement response to an acceleration symmetrical triangular pulse input for the isolation system shown in Figure 1(a) with N = 3

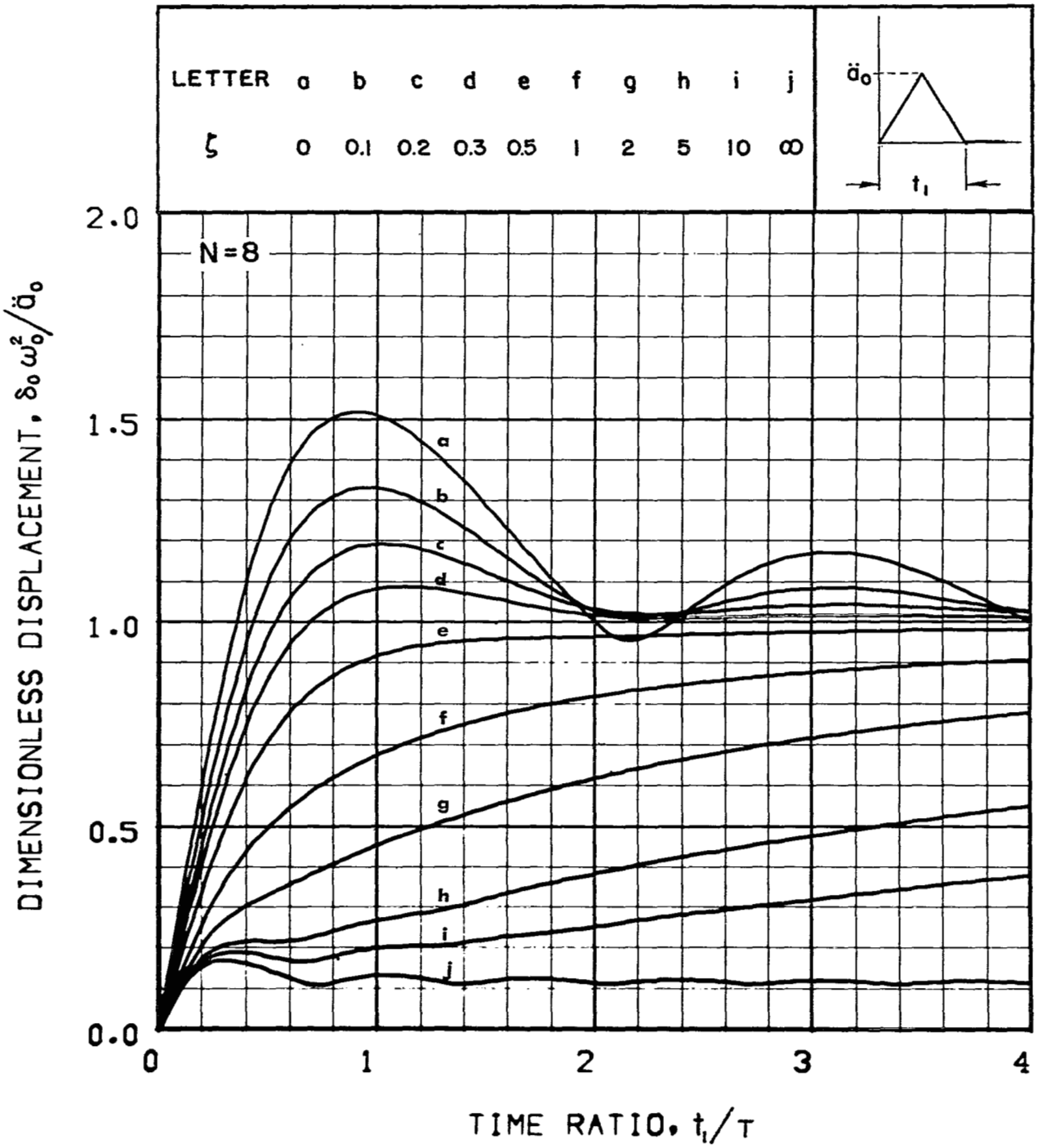

Figure 73.-Peak displacement response to an acceleration symmetrical triangular pulse input for the isolation system shown in Figure 1(a) with N = 8

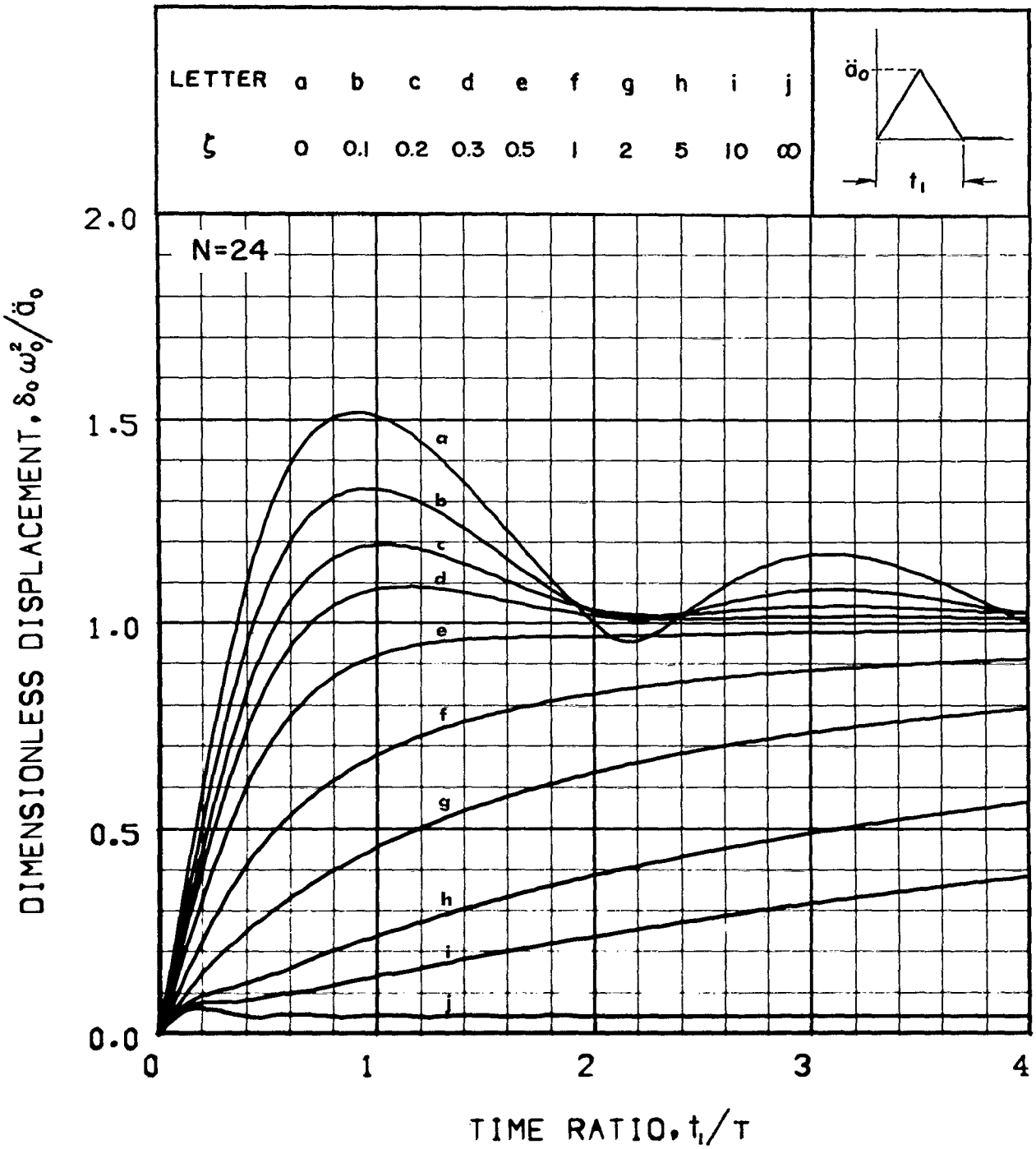

Figure 74.-Peak displacement response to an acceleration symmetrical triangular pulse input for the isolation system shown in Figure 1(a) with N = 24

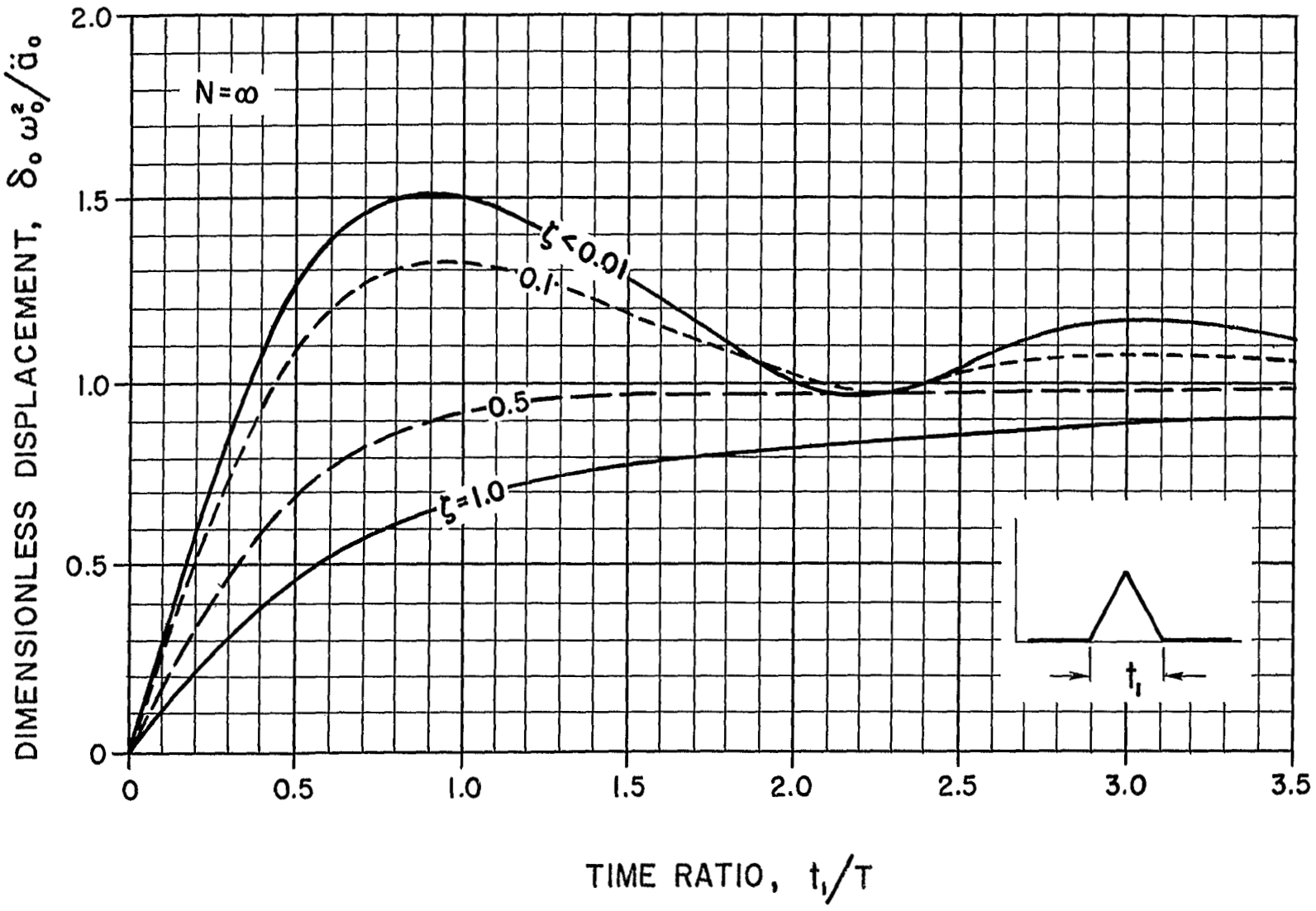

Figure 75.-Peak displacement response to an acceleration symmetrical triangular pulse input for the isolation system shown in Figure 1(a) with N = ∞

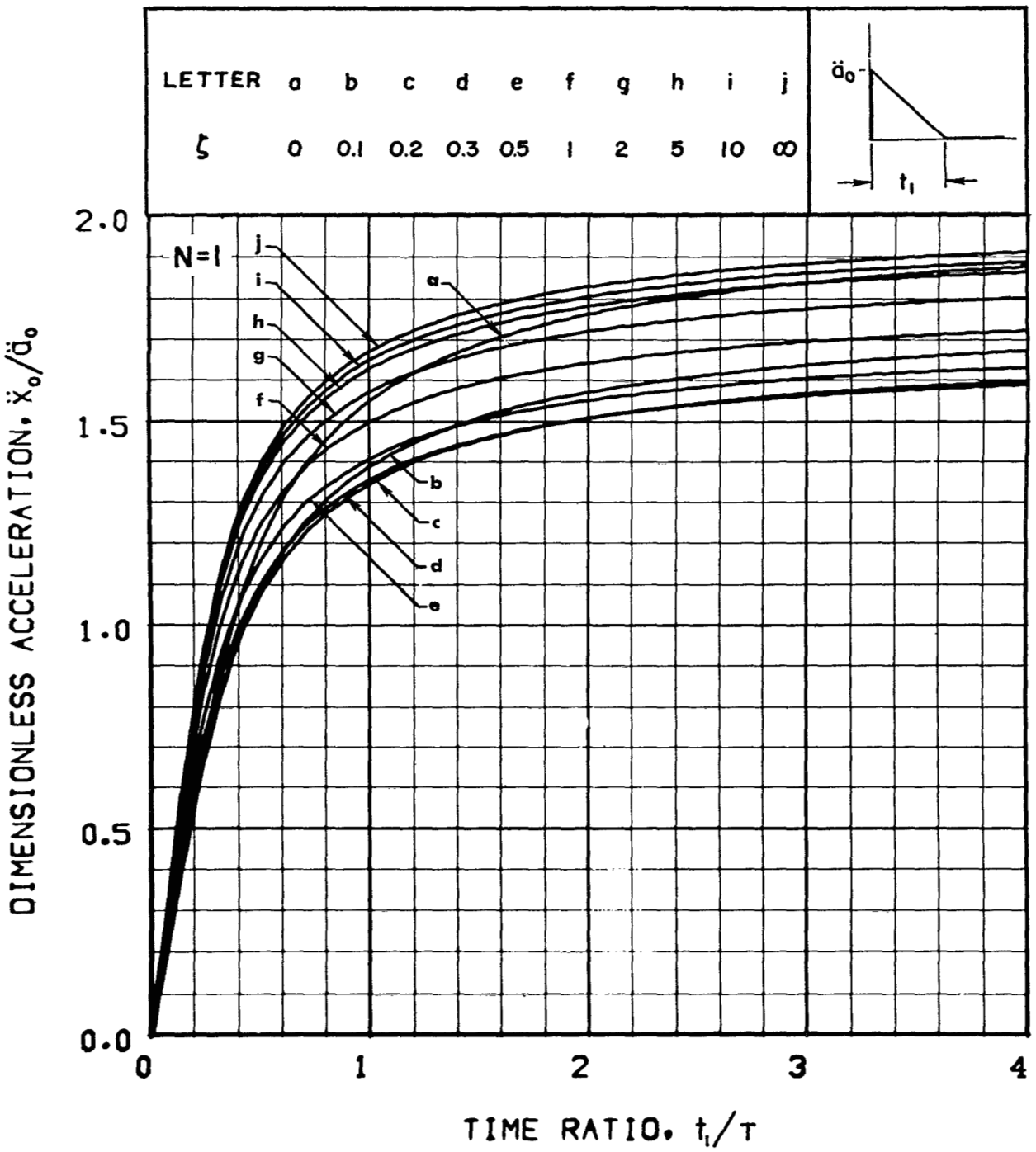

Figure 76.-Peak acceleration response to an acceleration initial-peak saw-tooth pulse input for the isolation system shown in Figure 1(a) with N = 1

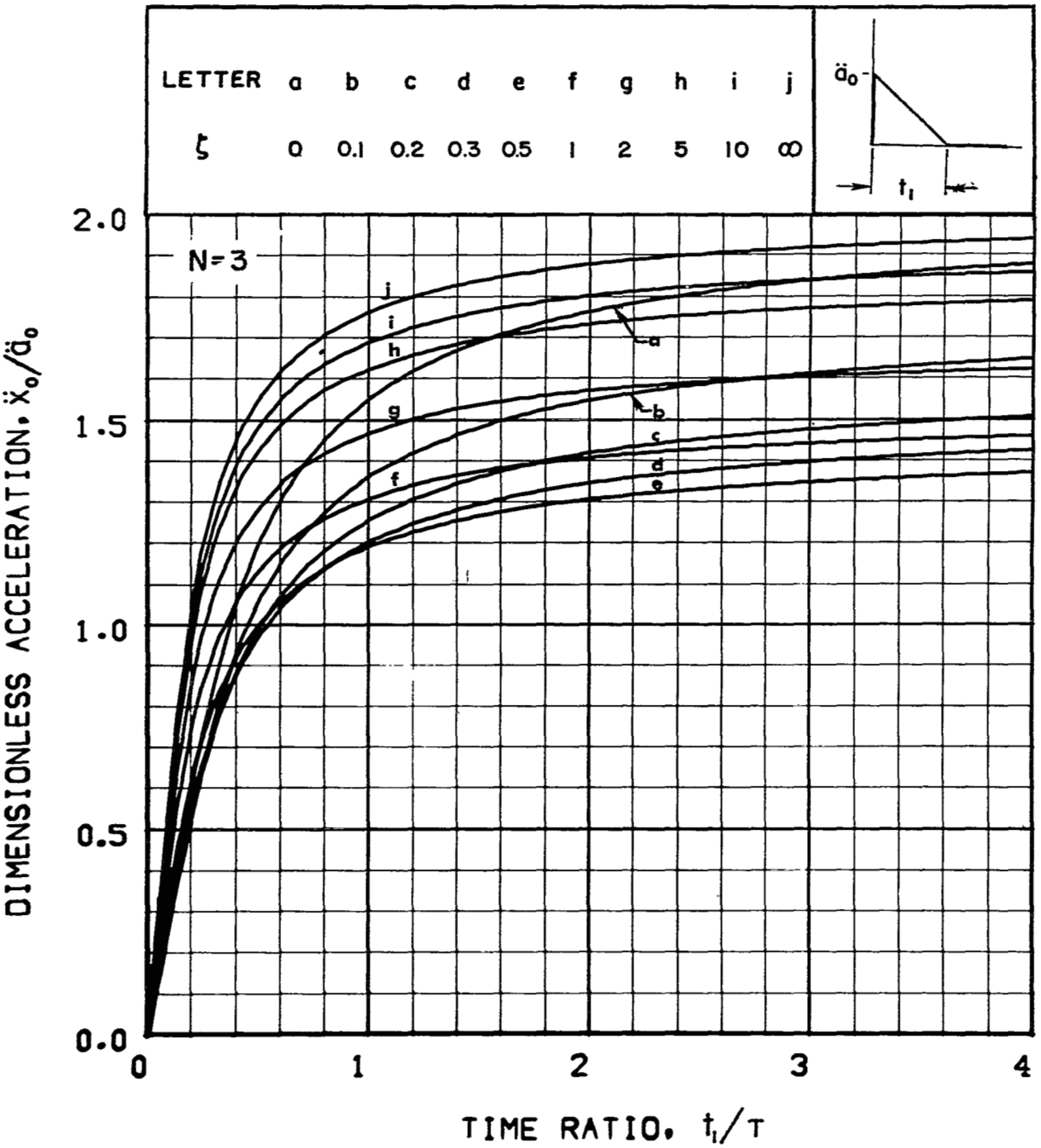

Figure 77.-Peak acceleration response to an acceleration initial-peak saw-tooth pulse input for the isolation system shown in Figure 1(a) with N = 3

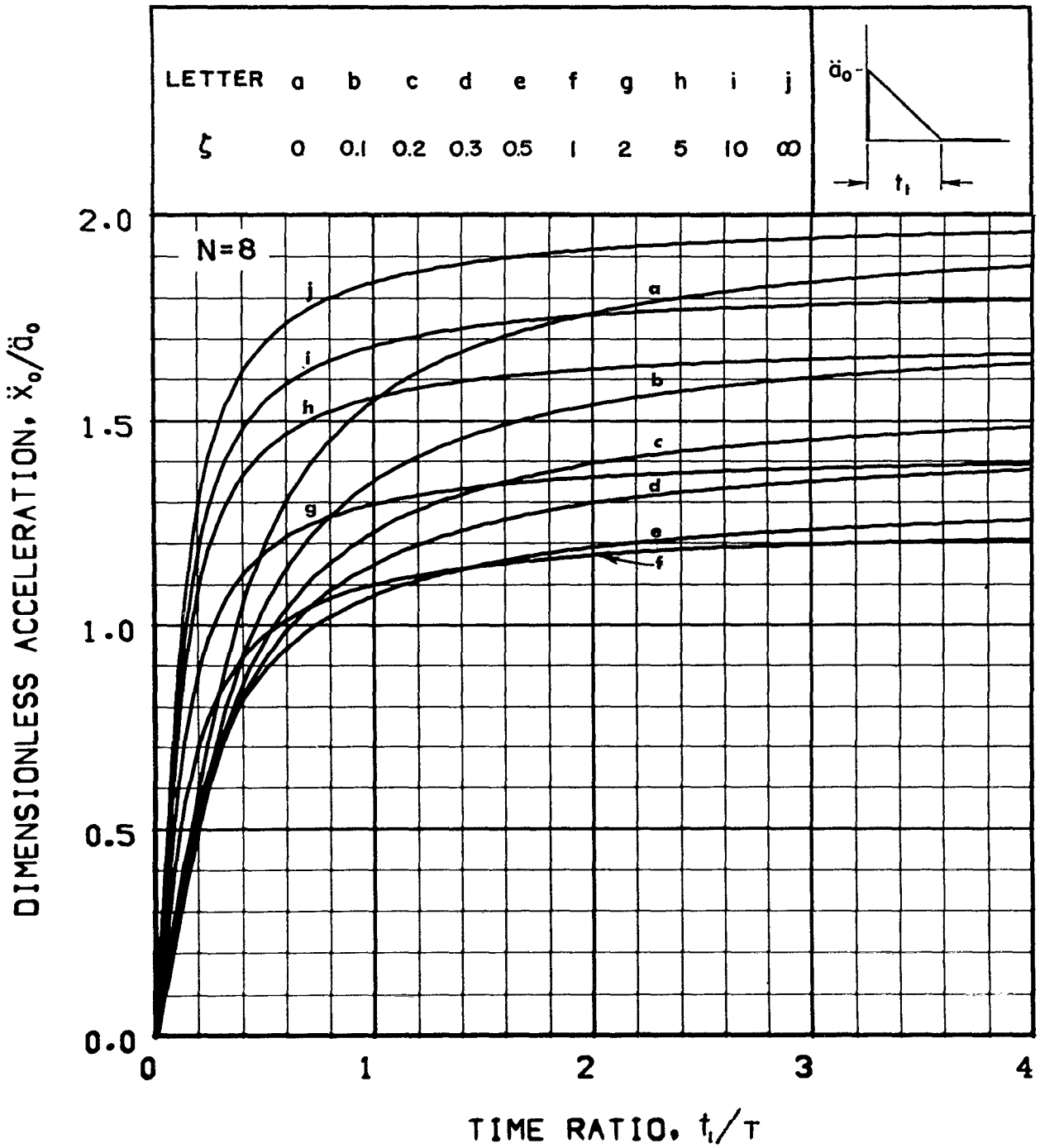

Figure 78.-Peak acceleration response to an acceleration initial-peak saw-tooth pulse input for the isolation system shown in Figure 1(a) with N = 8

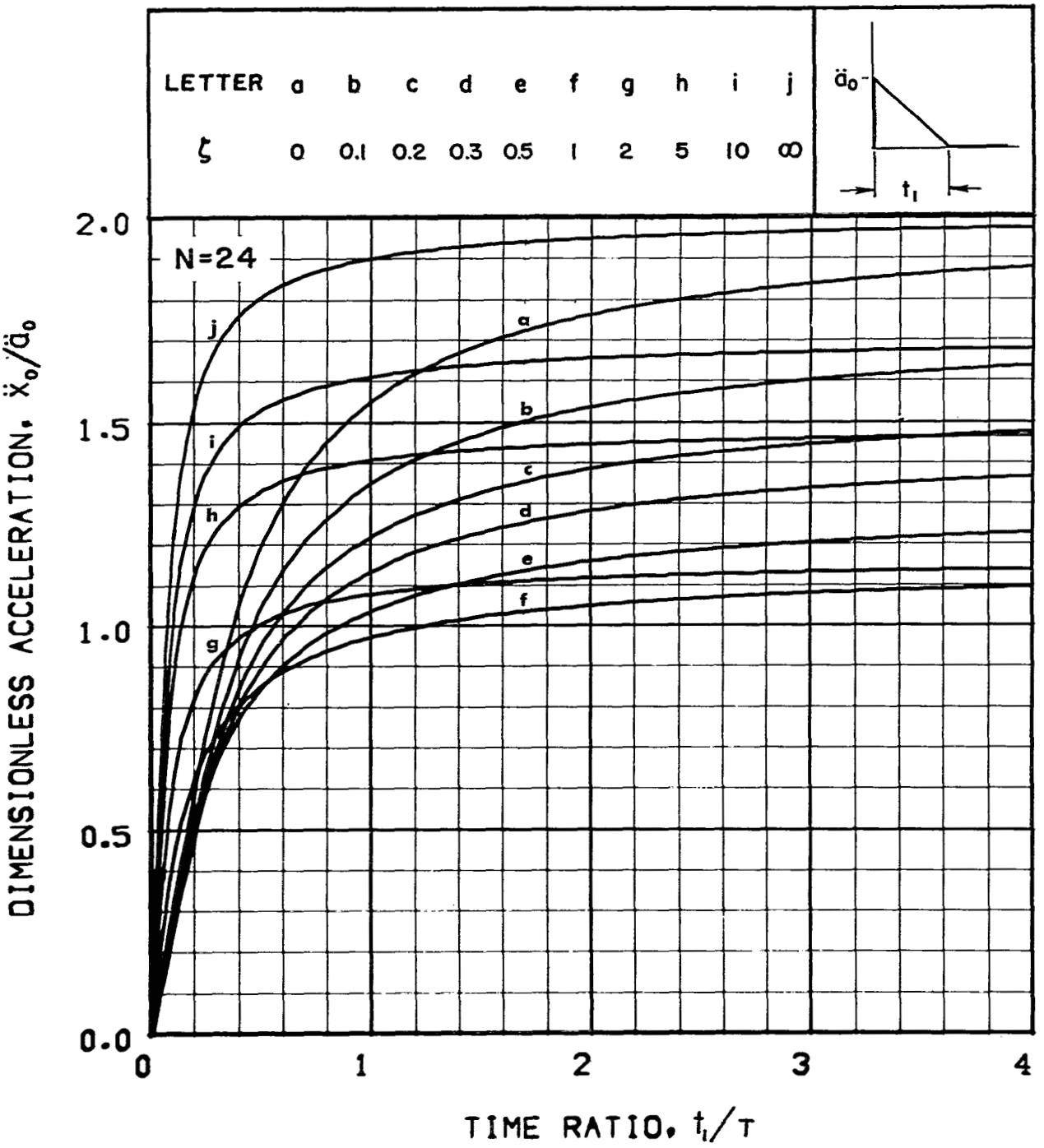

Figure 79.-Peak acceleration response to an acceleration initial-peak saw-tooth pulse input for the isolation system shown in Figure 1(a) with N = 24

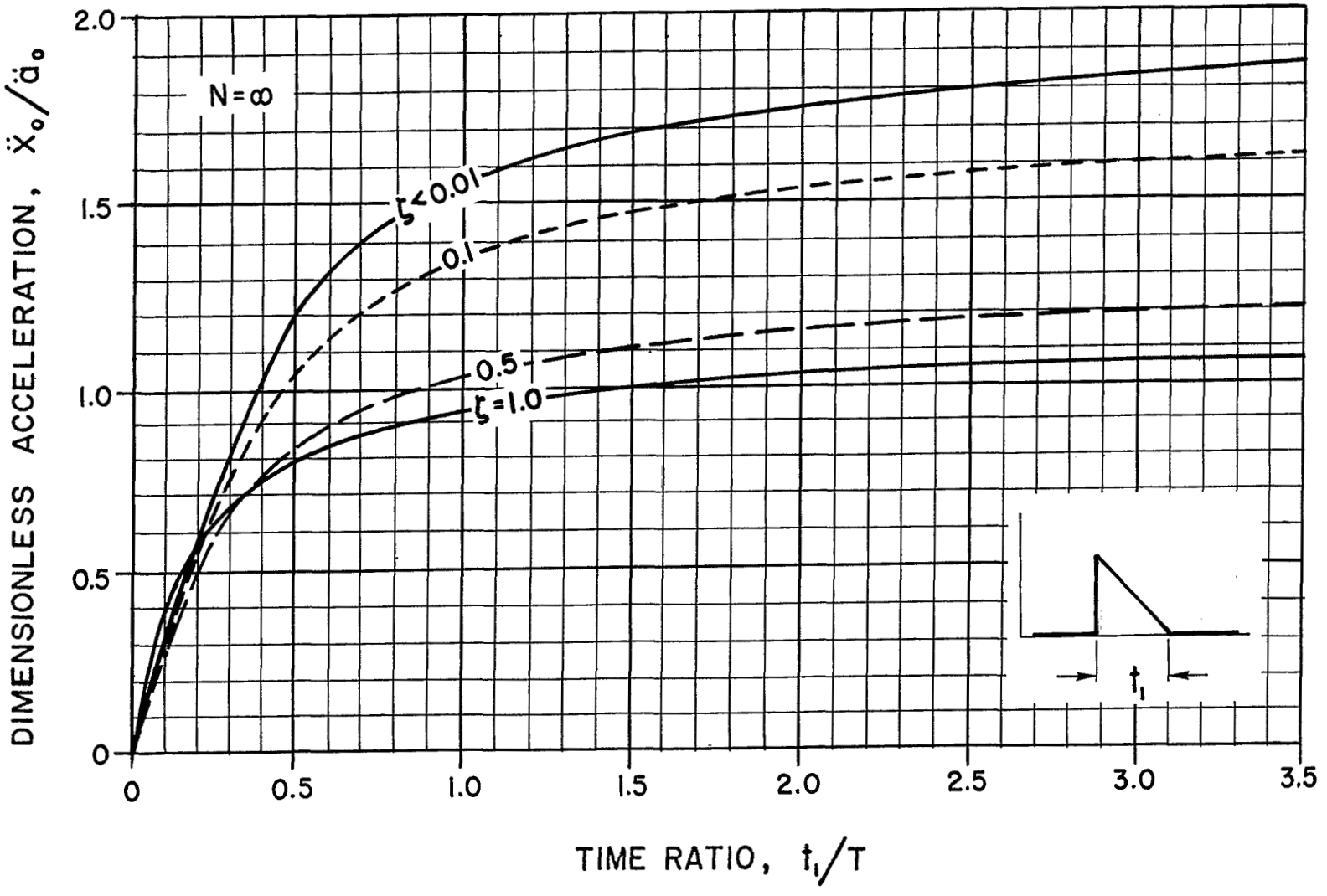

Figure 80.-Peak acceleration response to an acceleration initial-peak saw-tooth pulse input for the isolation system shown in Figure 1(a) with N = ∞

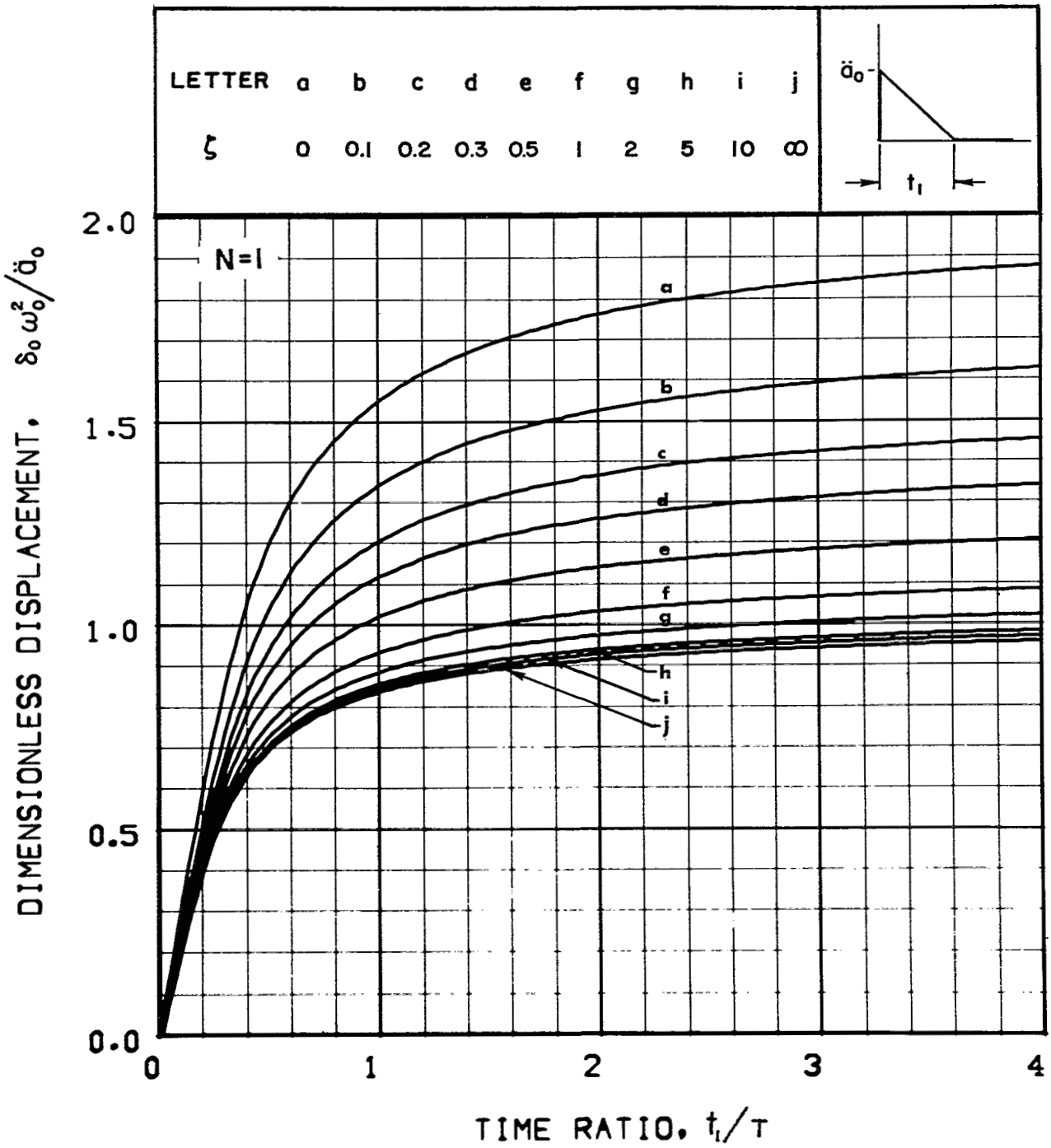

Figure 81.-Peak displacement response to an acceleration initial-peak saw-tooth pulse input for the isolation system shown in Figure 1(a) with N = 1

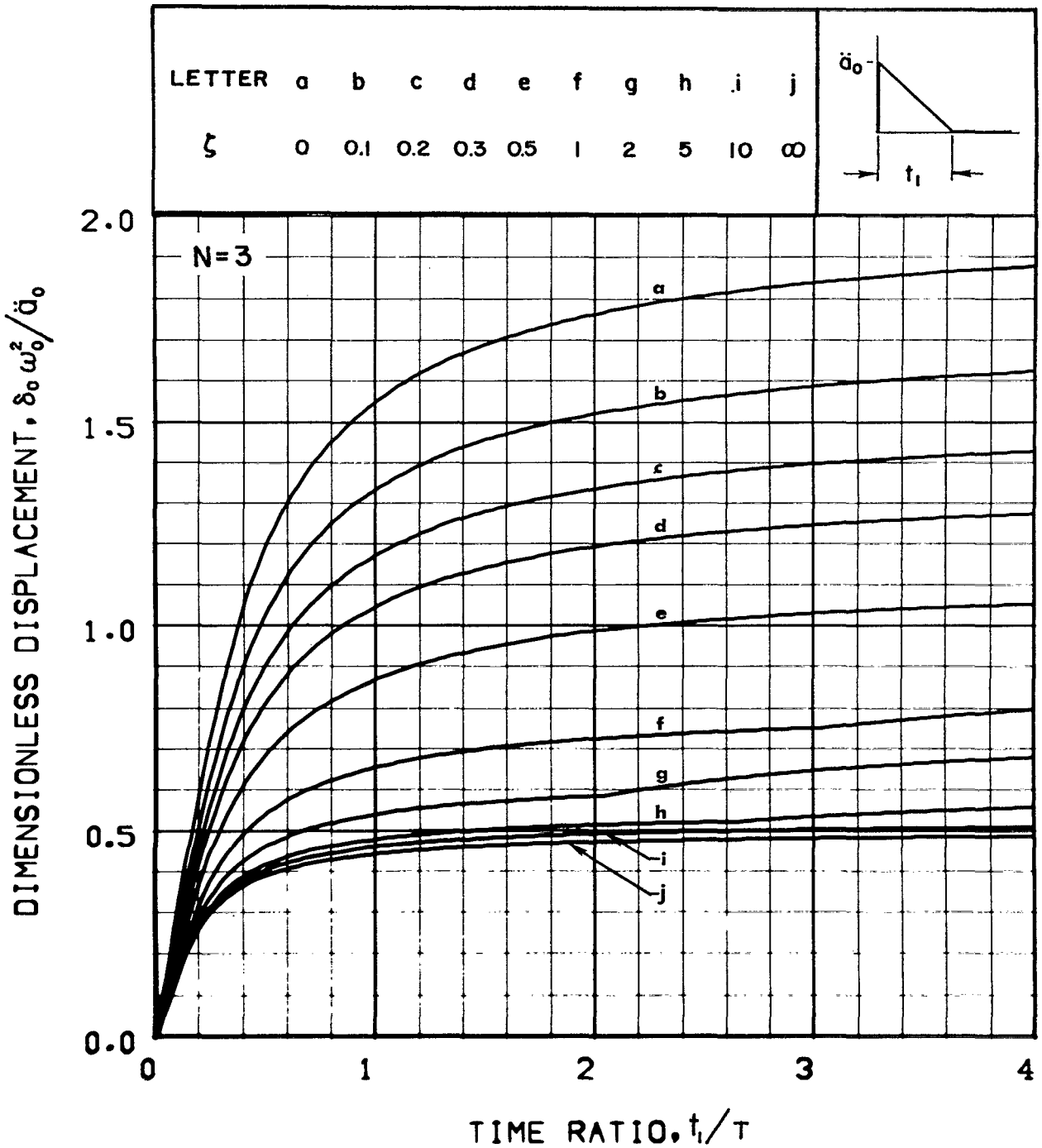

Figure 82.-Peak displacement response to an acceleration initial-peak saw-tooth pulse input for the isolation system shown in Figure 1(a) with N = 3

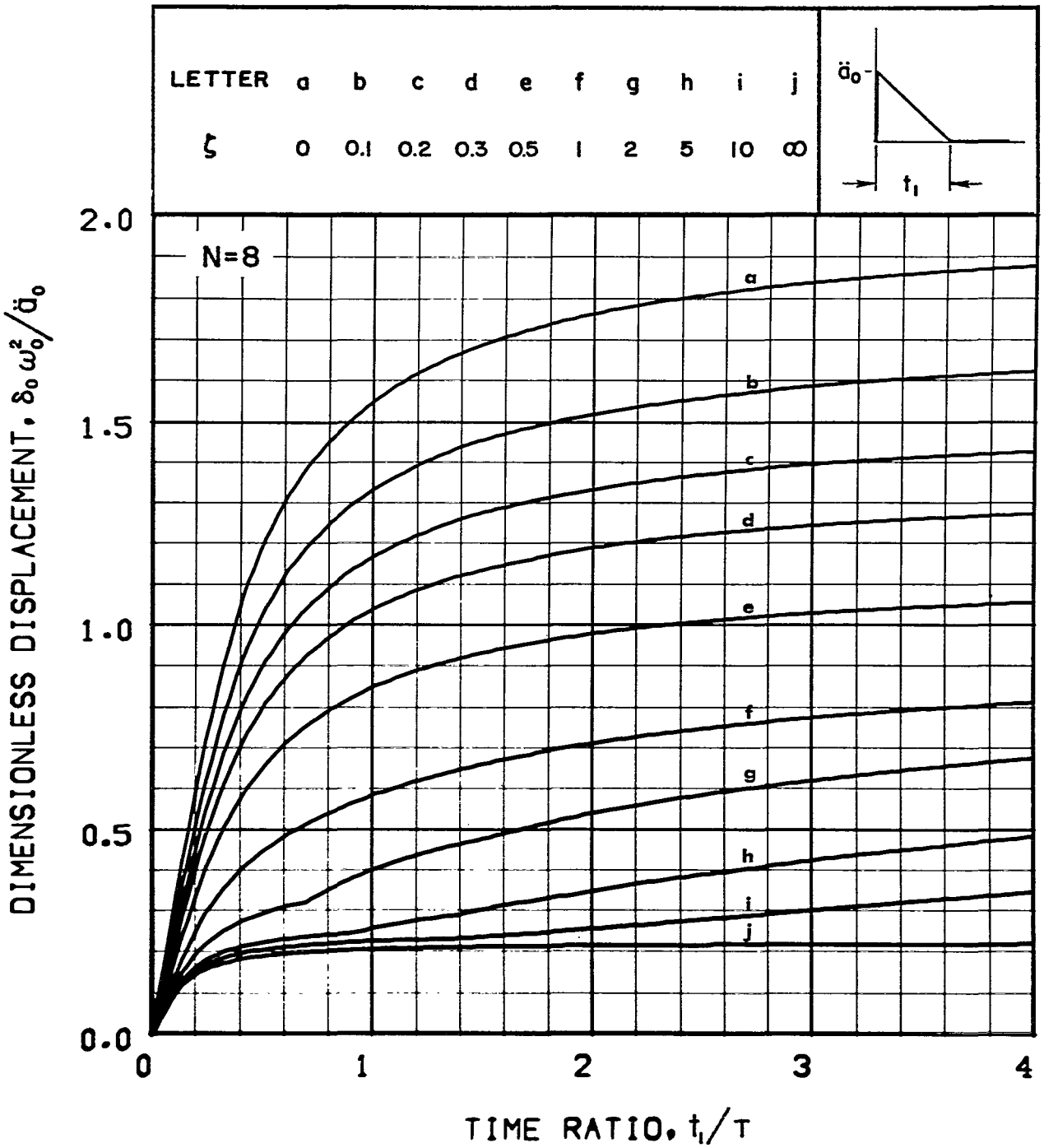

Figure 83.-Peak displacement response to an acceleration initial-peak saw-tooth pulse input for the isolation system shown in Figure 1(a) with N = 8

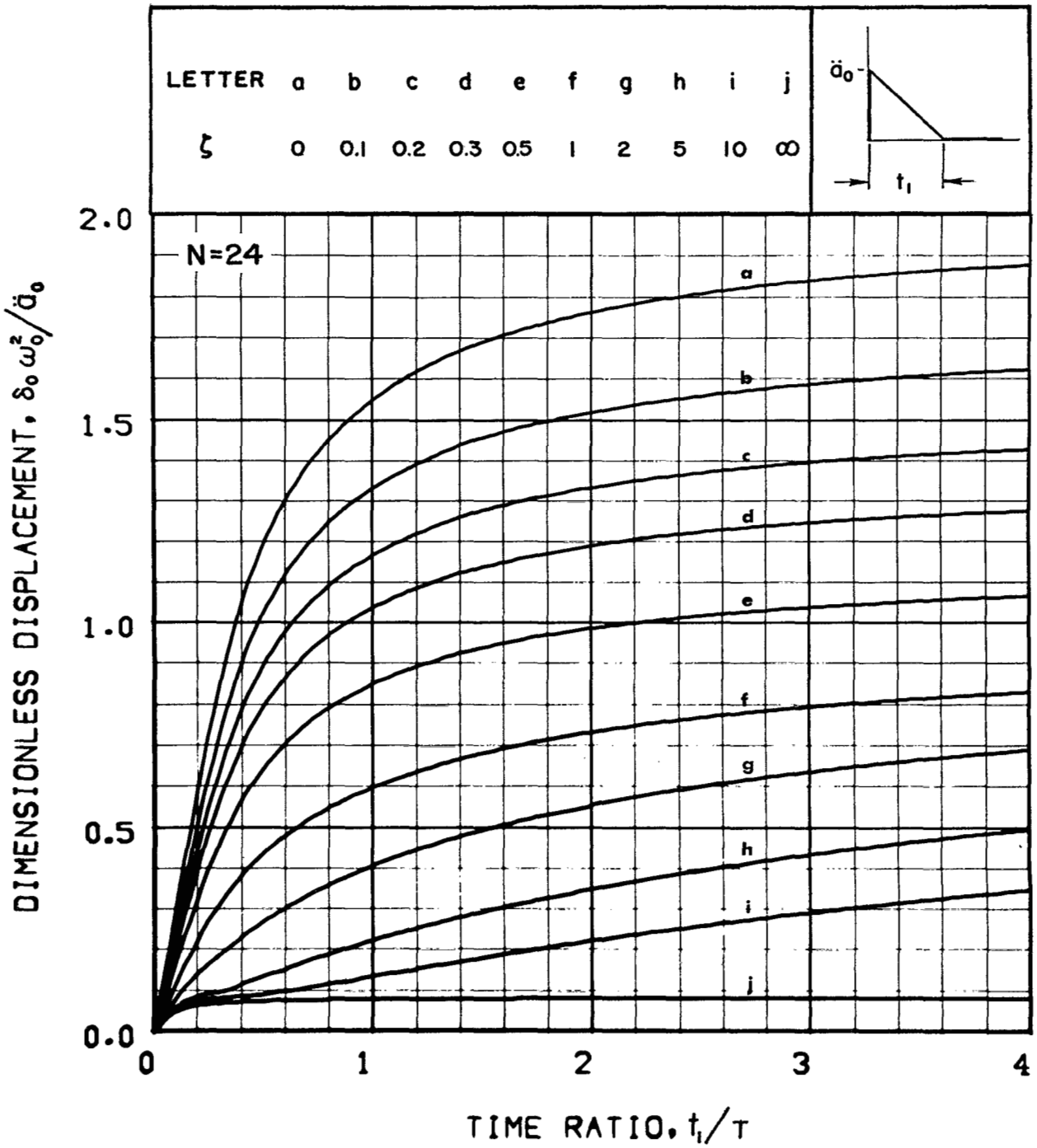

Figure 84.-Peak displacement response to an acceleration initial-peak saw-tooth pulse input for the isolation system shown in Figure 1(a) with N = 24

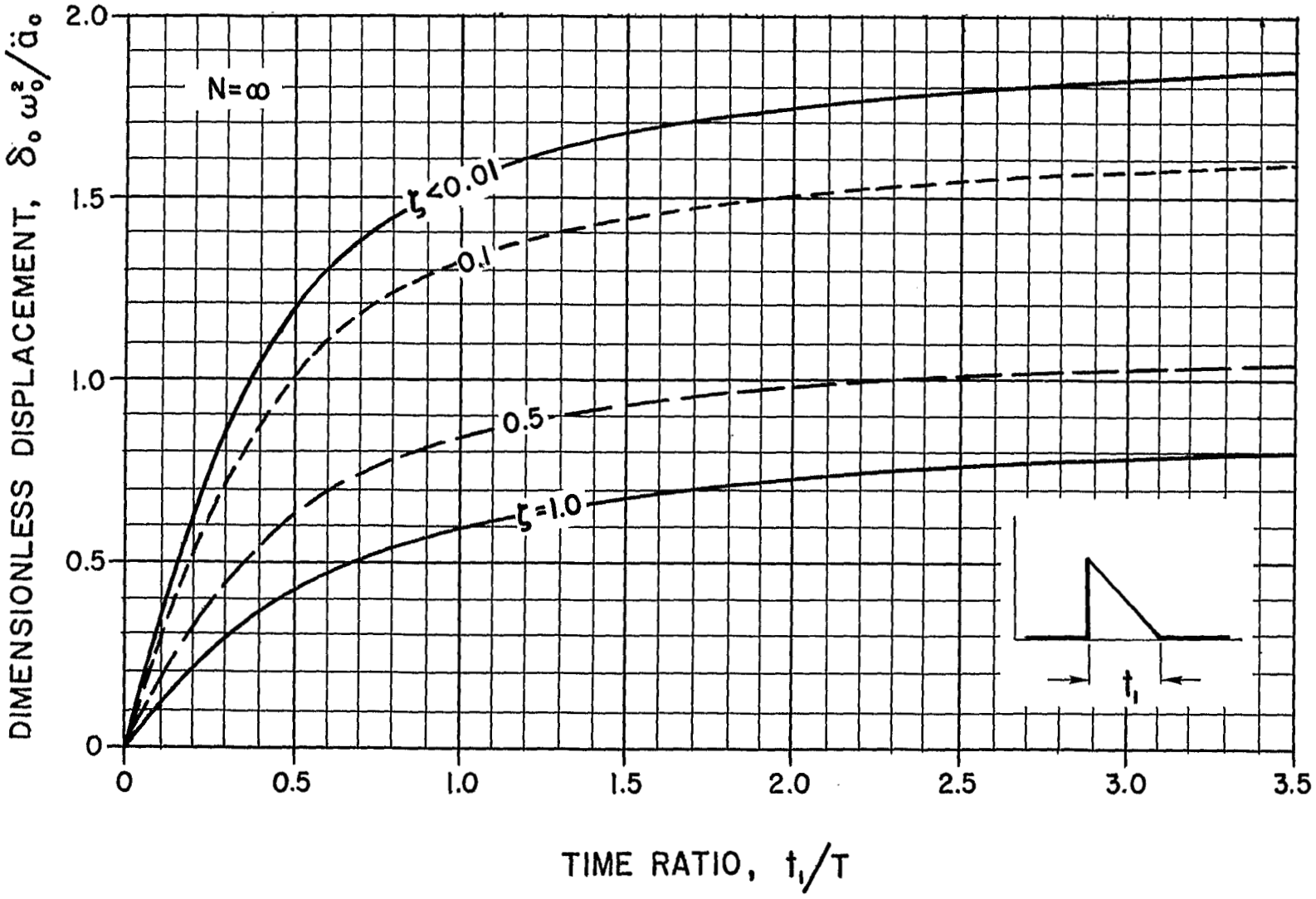

Figure 85.-Peak displacement response to an acceleration initial-peak saw-tooth pulse input for the isolation system shown in Figure 1(a) with N = ∞